lateral stability and curving performance, while vertical ride quality is independent of both of these criteria. To get a full picture of the EP-optimal set, several sets of weighting factors and corresponding optimizations are needed. The associated computational burden can be significantly reduced using parallel processing, for which the hybrid MDO method is ideally suited.

Chapter 8

Multidisciplinary Optimization of Combined Mechanical and Control Systems

8.1 Introduction

The purpose of this chapter is to show an extension to the research reported earlier in our paper [67] using the A-i-O multidisciplinary optimization method combining the A'GEM multibody dynamics package, the GA, LQG, and Kalman filter algorithms. To verify the efficacy of the integrated approach, it is used to resolve the conflicting requirements for ride comfort, suspension working spaces, and dynamic wheel loads in the optimization of quarter-vehicle models and half-vehicle models with active suspensions. Both deterministic and random track excitations are considered for both rigid and flexible vehicle body (for the half-vehicle models only) cases.

The integrated approach is implemented in a GA-A'GEM-MATLAB simulation environment in such a way that the linear mechanical vehicle models are generated in A'GEM, the controllers and Kalman filters are modelled in MATLAB, then the coupled mechanical and control subsystems are optimized simultaneously using the GA.

In the following sections, first, the vehicle and track models are described; second, the LQG and Kalman Filter algorithms are recalled briefly; third, the A-i-O method and

its implementation are outlined; finally, the numerical simulation results for the linear quarter-vehicle models and half-vehicle models are reported and discussed. For simplicity, in the following sections, we use the term 'A-i-O method' instead of the term 'integrated approach' to represent the A-i-O method combining the A'GEM package, the GA, LQG, and Kalman filter algorithms.

8.2 Vehicle and Track Models

8.2.1 Track Models

In vertical ride quality analyses for ground vehicles, the track profiles (excitations) are often modelled as displacement spectral density functions with the characteristics of filtered white noise or integrated white noise [61], as discussed below.

Integrated White Noise Track Excitation

The power spectral density (PSD) of an integrated white noise track displacement excitation can be taken from the approximate formula [129, 131]

$$S_w(\omega) = a_t V/\omega^2 \tag{8.1}$$

where ω is a temporal angular frequency, a_t is a track roughness constant, and V is the vehicle velocity.

For a linear vehicle system, given that $y_r(t)$ is the output for the random excitation and $y_s(t)$ is the corresponding output for a unit step input, the mean-square value of $y_r(t)$ is related to the integrated-squared value of $y_s(t)$ as follows:

$$E[y_r^2(t)] = a_t V \int_0^\infty y_s^2(t)dt \tag{8.2}$$

where $E[\cdot]$ denotes the expectation or average. Equation (8.2) is useful for computing the mean-square value of any output due to an integrated white noise input, since it is much simpler to generate a unit step function than a continuous random signal for the input. Moreover, based on equation (8.2), if a vehicle system is optimized for a unit step input, it will also be optimal for the corresponding integrated white noise track excitation as offered by equation (8.1) [129, 131].

Filtered White Noise Track Excitation

The PSD of a filtered white noise track displacement excitation can be formulated as [59, 60, 73]

$$S_w(\omega) = (\sigma_t/\pi)a_t V/(\omega^2 + a_t^2 V^2) \tag{8.3}$$

where σ_t is the variance of track irregularities. The process vector $\mathbf{w}$ with the PSD (8.3) can be generated from the pure white noise precess vector ξ using a shaping filter of the form

$$\dot{\mathbf{w}} = \mathbf{F}_w \mathbf{w} + \mathbf{D}_w \xi \tag{8.4}$$

where

$$\begin{cases} \mathbf{w} = \begin{bmatrix} w_1 & w_2 & ... & w_n \end{bmatrix}^T \\ \xi = \begin{bmatrix} \xi_1 & \xi_2 & ... & \xi_n \end{bmatrix}^T \\ \mathbf{F}_w = -a_t V \mathbf{I}_{n\times n} \\ \mathbf{D}_w = \mathbf{I}_{n\times n} \end{cases} \tag{8.5}$$

and $\mathbf{I}_{n\times n}$ is identity matrix of dimension $n \times n$, $\xi_1, \xi_2, ..., \xi_n$ are zero mean white noise processes, and $w_1, w_2, ..., w_n$ are the corresponding track inputs with the PSD described by equation (8.3).

For simplicity, we assume that there are only 2 inputs, i.e. w_1 and w_2, and the track inputs to a vehicle traveling at a constant speed, V, and separated by a fixed length, l, are related by

$$\begin{cases} w_1(t) = w_2(t + D) \\ D = l/V \end{cases} \tag{8.6}$$

Accordingly we have the relation between ξ_1 and ξ_2 as follows:

$$\xi_1(t) = \xi_2(t + D) \tag{8.7}$$

Therefore, the Gaussian white noise process vector $\xi(\mathbf{t})$, i.e. $\left[\begin{array}{cc} \xi_1(t) & \xi_2(t) \end{array}\right]^T$, has the covariance matrix taking the form as

$$\left\{\begin{array}{l} E[\xi(\mathbf{t})\xi^{\mathbf{T}}(\tau)] = Q_0 \left[\begin{array}{cc} \delta(t-\tau) & \delta(t-\tau+D) \\ \delta(t-\tau-D) & \delta(t-\tau) \end{array}\right] \\ Q_0 = 2\sigma_t a_t V \end{array}\right. \tag{8.8}$$

where $\delta(\cdot)$ stands for the Dirac δ function. If the correlation between ξ_1 and ξ_2 is neglected, the covariance matrix can be rewritten as

$$\left\{\begin{array}{l} E[\xi(\mathbf{t})\xi^{\mathbf{T}}(\tau)] = \mathbf{Q}\delta(t-\tau) \\ \mathbf{Q} = 2\sigma_t a_t V \mathbf{I}_{2\times 2} \end{array}\right. \tag{8.9}$$

8.2.2 Quarter-Vehicle (2 DOF) Model

The linear 2 DOF vehicle model to be optimized with passive and active suspension components is shown in Figure 8.1. In the model, the sprung mass and unsprung mass are represented by rigid bodies of masses m_2 and m_1 that are permitted to move in the vertical direction. The motions of masses m_2 and m_1 are described by the independent generalized coordinates x_2 and x_1, respectively. These coordinates are measured from the static equilibrium position. The coordinate w denotes track displacement irregularities in the vertical direction. In the secondary suspension, the passive spring and damping elements are modelled as a linear spring and a linear damper with stiffness and damping coefficients of k_2 and c_2, respectively. In the primary suspension, the spring and damping elements are modelled as a linear spring and linear damper with the stiffness and damping coefficients of k_1 and c_1, respectively. The actuator force, u, is the control variable that acts independently of the forces in the passive elements. It is assumed that the wheel follows the track exactly at all times.

The 2 DOF vehicle model shown in Figure 8.1 is optimized in two different cases: the deterministic track excitation case, i.e. a unit step input corresponding to the integrated white noise track excitation, and the random track excitation case, i.e. the filtered white noise track excitation. To compare the simulation results from the research with published results, for the deterministic track excitation case, the nominal parameter values denoted as parameter set 1 shown in Figure 8.1 are based on those used by Thompson [129].

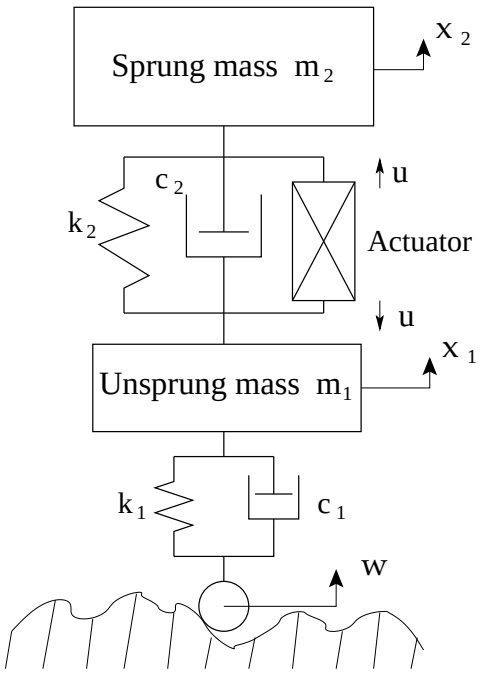

Parameter Set 1:
m_1=28.58 [kg];
m_2=288.9 [kg];
k_1 =155900 [N/m];
c_1 =0.0 [N/m/s];
k_2=19960 [N/m];
c_2=1861 [N/m/s].

Parameter Set 2:
m_1=100 [kg];
m_2=500 [kg];
k_1 =200000 [N/m];
c_1 =0.0 [N/m/s];
k_2=5000 [N/m];
c_2=1000 [N/m/s].

Random Track Characteristics :
a_t=0.45 [1/m];
σ_t=9.0E−6 [1/m^2].

Figure 8.1: 2 DOF quarter-vehicle models

For the filtered white noise track excitation case, the nominal parameter values denoted as parameter set 2 together with the random track characteristics parameters shown in Figure 8.1 are based on those used by Hac [59]. Note that the primary suspension damping coefficient, c_1, takes the value of zero in both cases.

For the two track excitation cases, the governing equations of motion of the vehicle model are described separately in the following subsections.

Deterministic Track Excitation Case

The state variable vector $\mathbf{x}$ is assumed to take the following form:

$$\mathbf{x} = \begin{bmatrix} x_1 - w & x_2 - w & \dot{x}_1 & \dot{x}_2 \end{bmatrix}^T \tag{8.10}$$

Thus, the governing equations of motion of the 2 DOF model can be written in state space form as

$$\begin{cases} \dot{\mathbf{x}} = \mathbf{A}\mathbf{x} + \mathbf{B}\mathbf{u} + \mathbf{D}\dot{\mathbf{w}} \\ \mathbf{y} = \mathbf{C}\mathbf{x} \end{cases} \tag{8.11}$$

where $\mathbf{u}$ is the actuator force vector of dimension 1×1, $\dot{\mathbf{w}}$ is the track velocity excitation vector of dimension 1×1, $\mathbf{y}$ is the output vector of dimension 2×1, $\mathbf{A}$, $\mathbf{B}$, $\mathbf{C}$, and $\mathbf{D}$ are the system matrix, control matrix, output matrix, and disturbance matrix, respectively, which are as follows:

$$\begin{cases} \mathbf{A} = \begin{bmatrix} 0 & 0 & 1 & 0 \\ 0 & 0 & 0 & 1 \\ -\frac{k_1+k_2}{m_1} & \frac{k_2}{m_1} & -\frac{c_1+c_2}{m_1} & \frac{c_2}{m_1} \\ \frac{k_2}{m_2} & -\frac{k_2}{m_2} & \frac{c_2}{m_2} & -\frac{c_2}{m_2} \end{bmatrix} \\ \mathbf{B} = \begin{bmatrix} 0 & 0 & -\frac{1}{m_1} & \frac{1}{m_2} \end{bmatrix}^T \\ \mathbf{C} = \begin{bmatrix} 1 & 0 & 0 & 0 \\ 0 & 1 & 0 & 0 \end{bmatrix} \\ \mathbf{D} = \begin{bmatrix} -1 & -1 & \frac{c_1}{m_1} & 0 \end{bmatrix}^T \end{cases} \tag{8.12}$$

Random Track Excitation Case

Assume that the state variable vector $\mathbf{x}$ is as follows:

$$\mathbf{x} = \begin{bmatrix} x_1 & x_2 & \dot{x}_1 & \dot{x}_2 \end{bmatrix}^T \tag{8.13}$$

Then the governing equations of the 2 DOF vehicle model can be written as

$$\dot{\mathbf{x}} = \mathbf{A}\mathbf{x} + \mathbf{B}\mathbf{u} + \mathbf{D}_1\mathbf{w} + \mathbf{D}_2\dot{\mathbf{w}} \tag{8.14}$$

where $\mathbf{w}$, $\dot{\mathbf{w}}$, and $\mathbf{u}$ are the track displacement excitation vector, track velocity excitation vector, and actuator force vector. All these vectors have dimension of 1×1. The matrices

$\mathbf{A}$ and $\mathbf{B}$ are the same as those offered in equation set (8.12). The matrices $\mathbf{D}_1$ and $\mathbf{D}_2$ take the forms

$$\begin{cases} \mathbf{D}_1 = \begin{bmatrix} 0 & 0 & \frac{k_1}{m_1} & 0 \end{bmatrix}^T \\ \\ \mathbf{D}_2 = \begin{bmatrix} 0 & 0 & \frac{c_1}{m_1} & 0 \end{bmatrix}^T \end{cases} \tag{8.15}$$

If the augmented state vector $\mathbf{x_a}$ takes the form

$$\mathbf{x_a} = \begin{bmatrix} \mathbf{x^T} & \mathbf{w^T} \end{bmatrix}^T \tag{8.16}$$

then based on equations (8.4), (8.13), (8.16), and (8.14), we have the augmented state space equations

$$\begin{cases} \dot{\mathbf{x}}_a = \mathbf{A}_a \mathbf{x}_a + \mathbf{B}_a u + \mathbf{D}_a \xi \\ \mathbf{y}_a = \mathbf{C}_a \mathbf{x}_a \end{cases} \tag{8.17}$$

where the matrices $\mathbf{A}_a$, $\mathbf{B}_a$, and $\mathbf{D}_a$ are given as

$$\begin{cases} \mathbf{A}_a = \begin{bmatrix} \mathbf{A} & \mathbf{D}_1 + \mathbf{D}_2 \mathbf{F}_w \\ \mathbf{0}_{1\times 4} & \mathbf{F}_w \end{bmatrix} \\ \\ \mathbf{B}_a = \begin{bmatrix} \mathbf{B}^T & \mathbf{0}_{1\times 1} \end{bmatrix}^T \\ \\ \mathbf{D}_a = \begin{bmatrix} \mathbf{D}_w^T \mathbf{D}_2^T & \mathbf{D}_w^T \end{bmatrix}^T \end{cases} \tag{8.18}$$

where both $\mathbf{F}_w$ and $\mathbf{D}_w$ are of dimension 1×1 and can be calculated based on equation set (8.5).

It is assumed that either all the state variables are available or just the sprung mass and unsprung mass velocities are available. Therefore, the output matrix $\mathbf{C}_a$ takes the form of $\mathbf{I}_{5\times 5}$ or

$$\mathbf{C}_a = \begin{bmatrix} 0 & 0 & 1 & 0 & 0 \\ 0 & 0 & 0 & 1 & 0 \end{bmatrix} \tag{8.19}$$

correspondingly.

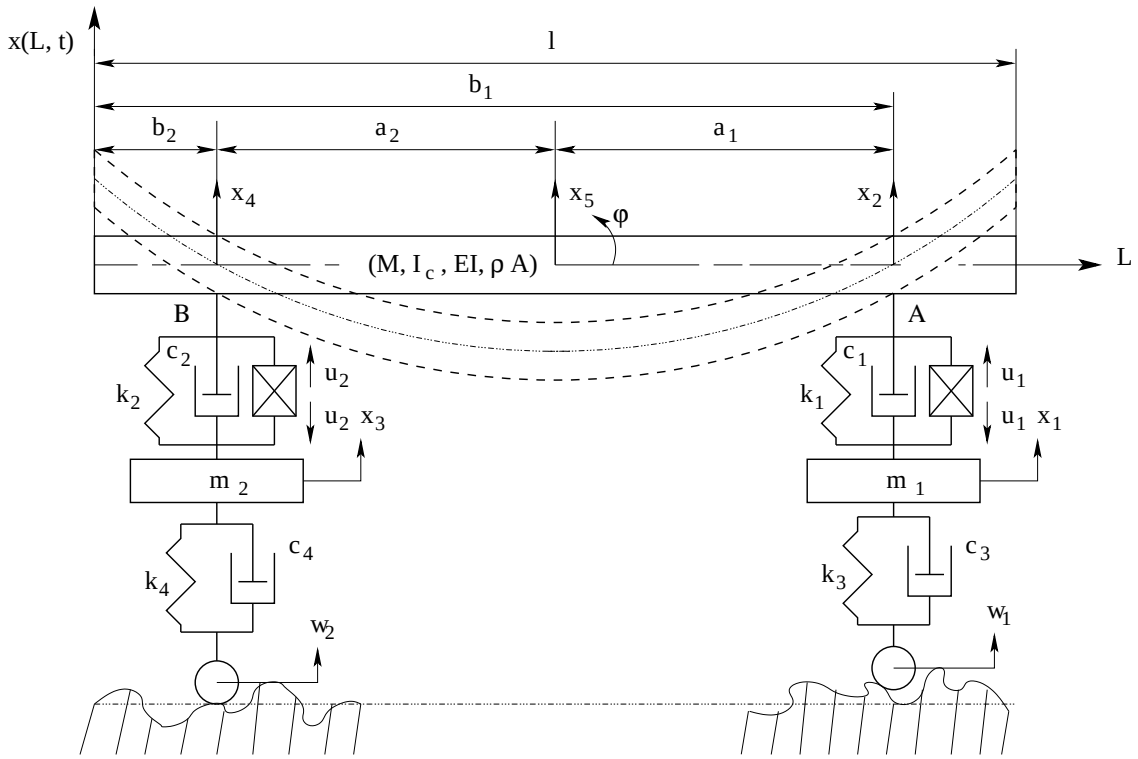

Figure 8.2: Half-vehicle models

8.2.3 Half-Vehicle Models

In the analytical design of active vehicle suspensions, researchers usually use lumped vehicle models [96, 130, 131]. This approach is justified for compact vehicles like cars. However, for vehicles with a long wheelbase like rail vehicles and truck-trailers, because of the large deflections of the vehicle body, researchers often introduce an elastic element into the vehicle model [47, 52, 60]. Thus, in the thesis, the half-vehicle models both with and without vehicle body flexibility are taken into account.

Shown in Figure 8.2 are the half-vehicle models with the rigid vehicle body represented by solid lines and the flexible vehicle body represented by curved dashed lines, respectively. The vehicle is considered to have a longitudinal central plane of symmetry, so that M is half the body mass and I_c is half the pitch moment of inertia about the center of gravity

of the vehicle body. For the rigid vehicle body, the motions considered are the body heave (x_5) and pitch (φ) (measured from the static equilibrium position of the center of the vehicle body). In addition to the rigid vehicle body modes, for the flexible vehicle body case, the body structure is described by its first 3 bending modes. The natural frequencies and approximating functions of mode shapes are based on those used by Hac [60]. Thus, the flexible vehicle body is approximately modeled as a beam of stiffness EI, body cross section area A, and mass density ρ. The front and rear unsprung masses are represented by rigid bodies of masses m_1 and m_2; they have a vertical DOF represented by x_1 and x_3. The actuator forces u_1 and u_2 are assumed to be applied between the unsprung masses and the vehicle body, at point A and B respectively. In the secondary suspensions, k_1, k_2, c_1, and c_2 represent stiffness and damping ratios of passive front and rear elements; in the primary suspensions, k_3, k_4, c_3, and c_4 denote stiffness and damping ratios of passive front and rear elements. In motion, the front and rear primary suspensions are submitted respectively to the track displacement excitations w_1 and w_2.

The nominal vehicle system parameters are listed in Tables B.1 and B.2 in Appendix B for both the half-vehicle models with rigid vehicle body and with the flexible vehicle body, respectively.

In the following subsections, the governing equations of motion for the half-vehicle model with rigid vehicle body are provided, then those for the half-vehicle model with flexible vehicle body are shown.

Rigid Vehicle Body Case

The dynamic equations of motion for the controlled vehicle model can be written in the same form as equation set (8.11). However, the state variable vector $\mathbf{x}$, actuator force vector $\mathbf{u}$, and track velocity excitation vector $\dot{\mathbf{w}}$ are as follows

$$\begin{cases} \mathbf{x} = \begin{bmatrix} x_1 - w_1 & x_2 - w_1 & x_3 - w_2 & x_4 - w_2 & \dot{x}_1 & \dot{x}_2 & \dot{x}_3 & \dot{x}_4 \end{bmatrix}^T \\ \mathbf{u} = \begin{bmatrix} u_1 & u_2 \end{bmatrix}^T \\ \dot{\mathbf{w}} = \begin{bmatrix} \dot{w}_1 & \dot{w}_2 \end{bmatrix}^T \end{cases} \tag{8.20}$$

The system matrix $\mathbf{A}$, control matrix $\mathbf{B}$, disturbance matrix $\mathbf{D}$, and output matrix $\mathbf{C}$ are provided in Appendix B.

Flexible Vehicle Body Case

Once the vehicle body flexibility is considered, in addition to the rigid body motions described in the last subsection, the bending modes are included. As shown in Figure 8.2, the flexible deformation of the vehicle body beam can be described by $\bar{x}(L,t)$, where L represents the distance along the beam and t stands for the time [52, 60, 99]. At a certain natural frequency ω_i, the deformation can be expressed as

$$\bar{x}_i(L,t) = Z_i(L)\Phi_i(t) \tag{8.21}$$

where $\Phi_i(t)$ is a function of t alone and $Z_i(L)$ is an eigenfunction, which describes the mode shape of the beam at the frequency ω_i. Because the beam's mass is distributed, the elastic body has an infinite number of vibration modes; its dynamic response may be calculated as the sum of principal mode contributions. Since the system is linear, the total deformation of the vehicle body beam is the superposition of the principal modes, that is,

$$\bar{x}(L,t) = \sum_{i=1}^{\infty} Z_i(L)\Phi_i(t) \tag{8.22}$$

Based on equation (8.22) and the partial differential equations of the vehicle body beam, using the orthogonal properties of principal modes, we can obtain the following equation

$$M_i\ddot{\Phi}_i(t) + \vartheta\gamma_i\dot{\Phi}_i(t) + \gamma_i\Phi_i(t) = f_A Z_i(b_1) + f_B Z_i(b_2) \tag{8.23}$$

where ϑ is a damping coefficient, M_i and γ_i are the modal mass and modal stiffness coefficient, which can be further described as

$$\begin{cases} M_i = \int_0^l \rho A Z_i^2(L)dL \\ \gamma_i = M_i\omega_i^2 \end{cases} \tag{8.24}$$

where ρA is mass per unit length, and ω_i is the i^{th} mode frequency of the vehicle body beam. In equation (8.23), f_A and f_B are suspension forces applied at points A and B, respectively. They can be formulated as

$$\begin{cases} f_A = -k_1(x_2 - x_1) - c_1(\dot{x}_2 - \dot{x}_1) + u_1 \\ f_B = -k_2(x_4 - x_3) - c_2(\dot{x}_4 - \dot{x}_3) + u_2 \end{cases} \tag{8.25}$$

where x_2 and x_4 are the total displacements including the contributions from both rigid and flexible vehicle body modes. The displacement of the vehicle body at a point, which is measured from the left end to a distance L, can be formulated as

$$x(L,t) = x_5 + (L - a_2 - b_2)\varphi + \sum_{i=1}^{\infty} Z_i(L)\Phi_i(t) \tag{8.26}$$

In the following description, the first three bending modes of the flexible vehicle beam are considered, but more can be incorporated into the model by adding more DOF to the flexibility equations. Combining the rigid body motions and the flexible beam motions, the model corresponding to the vehicle body will consider the two rigid body modes (pitch and heave modes) and the first three bending modes. These five mode shapes are shown in Figure 8.3.

By assembling the rigid half-vehicle model with the flexible vehicle body beam model,

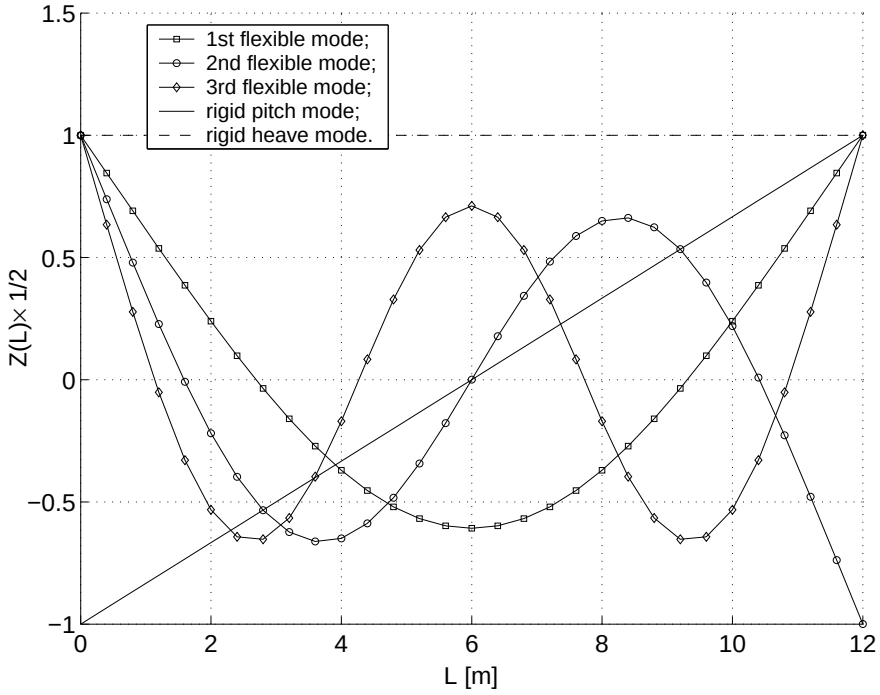

Figure 8.3: The lowest spatial modes of the vehicle body beam, including the two rigid body modes and the three flexible body modes

we obtain the system state equation in matrix form as shown in equation (8.14), where the state variable vector $\mathbf{x}$, actuator force vector $\mathbf{u}$, track displacement excitation vector $\mathbf{w}$, and track velocity excitation vector $\dot{\mathbf{w}}$ are described as follows

$$\begin{cases} \mathbf{x} = \begin{bmatrix} x_2 - x_1 & x_4 - x_3 & \dot{x}_5 & \dot{\varphi} & x_1 & \dot{x}_1 & x_3 & \dot{x}_3 & \Phi_1 & \dot{\Phi}_1 & \Phi_2 & \dot{\Phi}_2 & \Phi_3 & \dot{\Phi}_3 \end{bmatrix}^T \\ \mathbf{u} = \begin{bmatrix} u_1 & u_2 \end{bmatrix}^T \\ \mathbf{w} = \begin{bmatrix} w_1 & w_2 \end{bmatrix}^T \\ \dot{\mathbf{w}} = \begin{bmatrix} \dot{w}_1 & \dot{w}_2 \end{bmatrix}^T \end{cases} \tag{8.27}$$

and matrices $\mathbf{A}$, $\mathbf{B}$, $\mathbf{D}_1$, and $\mathbf{D}_2$ of dimensions 14×14, 14×2, 14×2, and 14×2, respectively, are offered in Appendix B.

Similar to the quarter-vehicle case, if the augmented state vector $\mathbf{x}_a$ is as follows

$$\mathbf{x_a} = \begin{bmatrix} \mathbf{x^T} & \mathbf{w^T} \end{bmatrix}^T \tag{8.28}$$

then we can also obtain the augmented state space equations in matrix form as shown in equation set (8.17). The matrices $\mathbf{A}_a$, $\mathbf{B}_a$, and $\mathbf{D}_a$ are defined as

$$\begin{cases} \mathbf{A}_a = \begin{bmatrix} \mathbf{A} & \mathbf{D}_1 + \mathbf{D}_2\mathbf{F}_w \\ \mathbf{0}_{2\times14} & \mathbf{F}_w \end{bmatrix} \\ \mathbf{B}_a = \begin{bmatrix} \mathbf{B}^T & \mathbf{0}_{2\times2} \end{bmatrix}^T \\ \mathbf{D}_a = \begin{bmatrix} \mathbf{D}_w^T\mathbf{D}_2^T & \mathbf{D}_w^T \end{bmatrix}^T \end{cases} \tag{8.29}$$

where both $\mathbf{F}_w$ and $\mathbf{D}_w$ are of dimension 2×2 and they can be obtained from equation set (8.5).

Since the velocities of the front and rear unsprung masses and two points (the left end and right end) or three points (the left end, right end, and middle point) on the vehicle body are assumed to be measured, the output matrix $\mathbf{C}_a$ has the dimension of 4×16 or 5×16 accordingly. The corresponding output matrix is shown in Appendix B.

8.3 LQG and Kalman Filter Algorithms

In this section, the LQG control algorithm [24, 47, 59, 61, 73, 101, 129] is introduced, then the Kalman filter algorithm [24, 47, 60, 61, 101] is recalled. In this thesis, the "separation principle" [101] is adopted in the development of the LQG controller and Kalman estimator. First, the optimal controller is designed as if full state feedback is available. Second, the optimal estimator is designed to provide the full state estimation.

8.3.1 LQG Control Strategy

The LQG control strategy can be described as an optimization problem: minimize the following objective function or performance index

$$J = \lim_{T\to\infty} \frac{1}{T} E\{\int_0^T \begin{bmatrix} \mathbf{x}_a \\ \mathbf{u} \end{bmatrix}^T \begin{bmatrix} \mathbf{G} & \mathbf{N} \\ \mathbf{N}^T & \mathbf{H} \end{bmatrix} \begin{bmatrix} \mathbf{x}_a \\ \mathbf{u} \end{bmatrix} dt\} \tag{8.30}$$

subject to

$$\dot{\mathbf{x}}_a = \mathbf{A}_a\mathbf{x} + \mathbf{B}_a\mathbf{u} + \mathbf{D}_a\xi \tag{8.31}$$

where $\mathbf{x}_a$ is the state variable vector including system states and input states, $\mathbf{u}$ is the actuator force vector, and ξ is the disturbance vector assumed to be white noise processes. As described previously in the chapter, these white noise processes have zero mean and the covariance matrix, for two input cases, is determined by equation sets (8.8) or (8.9). $\mathbf{G}$, $\mathbf{N}$, and $\mathbf{H}$ are weighting matrices. $\mathbf{A}_a$, $\mathbf{B}_a$, and $\mathbf{D}_a$ are the system, control, and disturbance matrices, respectively. For the linear time invariant system, $\mathbf{A}_a$, $\mathbf{B}_a$, $\mathbf{D}_a$, $\mathbf{G}$, $\mathbf{N}$, and $\mathbf{H}$ are all constant matrices with proper dimensions.

It is assumed that all uncontrollable modes are stable. Thus, the solution of the optimization problem is the control force vector with the following form:

$$\mathbf{u} = -\mathbf{K}\mathbf{x}_a \tag{8.32}$$

where $\mathbf{K}$ is the control gain matrix which is determined by

$$\frac{\partial J}{\partial \mathbf{K}} = \mathbf{0} \tag{8.33}$$

From equation (8.33), the gain matrix $\mathbf{K}$ can be obtained as

$$\mathbf{K} = \mathbf{H}^{-1}(\mathbf{N}^T + \mathbf{B}_a^T\mathbf{S}) \tag{8.34}$$

where the symmetric and positive-definite matrix $\mathbf{S}$ is a solution of the Riccati equation:

$$\mathbf{S}\mathbf{A}_a + \mathbf{A}_a^T\mathbf{S} + \mathbf{G} - (\mathbf{S}\mathbf{B}_a + \mathbf{N})\mathbf{H}^{-1}(\mathbf{S}\mathbf{B}_a + \mathbf{N})^T = \mathbf{0} \tag{8.35}$$

The covariance matrix $\mathbf{X}$ of the state variable vector $\mathbf{x}$ is obtained from:

$$\mathbf{X} = E[\mathbf{x}\mathbf{x}^T] \tag{8.36}$$

where the covariance matrix $\mathbf{X}$ is a function of the autocorrelation of vector ξ. For example, if there are only 2 track inputs, $\mathbf{X}$ is determined by the Lyapunov equation

$$(\mathbf{A}_a - \mathbf{B}_a\mathbf{K})\mathbf{X} + \mathbf{X}(\mathbf{A}_a - \mathbf{B}_a\mathbf{K})^T + \mathbf{Q}_1 = \mathbf{0} \tag{8.37}$$

where the matrix $\mathbf{Q}_1$ is determined by whether there is a time delay between the two inputs or not. The matrix $\mathbf{Q}_1$ can be calculated by

$$\mathbf{Q}_1 = \begin{cases} \mathbf{D}_a\mathbf{Q}\mathbf{D}_a^T & \textit{without time delay} \\ \mathbf{D}_a\mathbf{Q}\mathbf{D}_a^T + Q_0(\mathbf{D}_{a2}\mathbf{D}_{a1}^T\Theta^T(D) + \Theta(D)\mathbf{D}_{a1}\mathbf{D}_{a2}^T) & \textit{with time delay} \end{cases} \tag{8.38}$$

where the matrix $\mathbf{Q}$, the constant Q_0, and the time delay D are given by equation sets (8.9), (8.8), and (8.6), respectively, and $\Theta(D)$ is the system transition matrix that is defined as

$$\Theta(D) \triangleq \exp(\mathbf{A}_a \cdot D) \tag{8.39}$$

$\mathbf{D}_{a1}$ and $\mathbf{D}_{a2}$ are the two columns of $\mathbf{D}_a$, i.e.,

$$\mathbf{D}_a = \begin{bmatrix} \mathbf{D}_{a1} & \mathbf{D}_{a2} \end{bmatrix} \tag{8.40}$$

Finally, we have the resulting performance index as

$$J_{opt} = trace(\mathbf{S}\mathbf{Q}_1) \tag{8.41}$$

It should be noted that if the state vector $\mathbf{x}_a$ includes input states, the system considered is not completely controllable. This is because, as shown in equation (8.16), the track input vector $\mathbf{w}$ can not be changed by applying a control force. In this case, the Riccati equation (8.35) and the Lyapunov equation (8.37) can be solved numerically after dividing the corresponding unknown matrix $\mathbf{S}$ and state covariance matrix $\mathbf{X}$ into four submatrices, respectively. This method has been offered in detail by Hac [59].

8.3.2 Kalman Filter Algorithm

This approach assumes that the measurements are corrupted by noise and the measurement equation can be formulated by modifying the output equation from equation set (8.17) as follows:

$$\mathbf{y}_a = \mathbf{C}_a\mathbf{x}_a + \upsilon \tag{8.42}$$

where, as mentioned previously, $\mathbf{y}_a$ is the output vector, $\mathbf{C}_a$ is the output matrix or the state-to-measurement transformation matrix, and $\mathbf{x}_a$ is the state variable vector including system states and input states. υ is assumed to be Gaussian white noise process vector with zero mean and covariance matrix $\mathbf{R}$ described by

$$\begin{cases} E[\upsilon(t)] = \mathbf{0} \\ E[\upsilon(t)\upsilon(\tau)] = \mathbf{R}\delta(t-\tau) \end{cases} \tag{8.43}$$

where $\mathbf{R}$ is a positive definite matrix with proper dimension.

Thus, the optimal estimator can be formulated as

$$\dot{\hat{\mathbf{x}}}_a = \mathbf{A}_a\hat{\mathbf{x}}_a + \mathbf{B}_a\mathbf{u} + \mathbf{L}(\mathbf{y}_a - \mathbf{C}_a\hat{\mathbf{x}}_a) \tag{8.44}$$

where $\hat{\mathbf{x}}_a$ is the optimal estimate vector of the state variable vector $\mathbf{x}_a$, $\mathbf{u}$ is the actuator force vector, $\mathbf{A}_a$ and $\mathbf{B}_a$ are augmented system and control matrices offered previously, and $\mathbf{L}$ is the Kalman filter gain matrix that is determined by

$$\mathbf{L} = \mathbf{P}\mathbf{C}_a^T\mathbf{R}^{-1} \tag{8.45}$$

where $\mathbf{P}$ is the filter error ($\mathbf{e} = \hat{\mathbf{x}}_a - \mathbf{x}_a$) covariance matrix which can be found from the following steady-state matrix Riccati equation

$$\mathbf{A}_a\mathbf{P} + \mathbf{P}\mathbf{A}_a^T + \mathbf{Q}_1 - \mathbf{P}\mathbf{C}_a^T\mathbf{R}^{-1}\mathbf{C}_a\mathbf{P} = \mathbf{0} \tag{8.46}$$

Notice that for the quarter-vehicle and half-vehicle models described previously, the systems $(\mathbf{A}_a, \mathbf{C}_a)$ are observable. Thus, unlike the cases for solving equations (8.35) and (8.37), the Riccati equation denoted by (8.46) can be solved directly without dividing the unknown matrix $\mathbf{P}$ and relevant matrices into four submatrices and then solving the corresponding equations.

8.3.3 Combination of LQG Controller with Kalman Estimator

Provided that the track excitations and mechanical vehicle system parameters, e.g., inertial property parameters, geometric parameters, and passive suspension parameters, are determined, with the LQG controller and Kalman estimator designed previously based on the separation principle, we can obtain the optimal control structure as shown in Figure 8.4 using cascade arrangement.

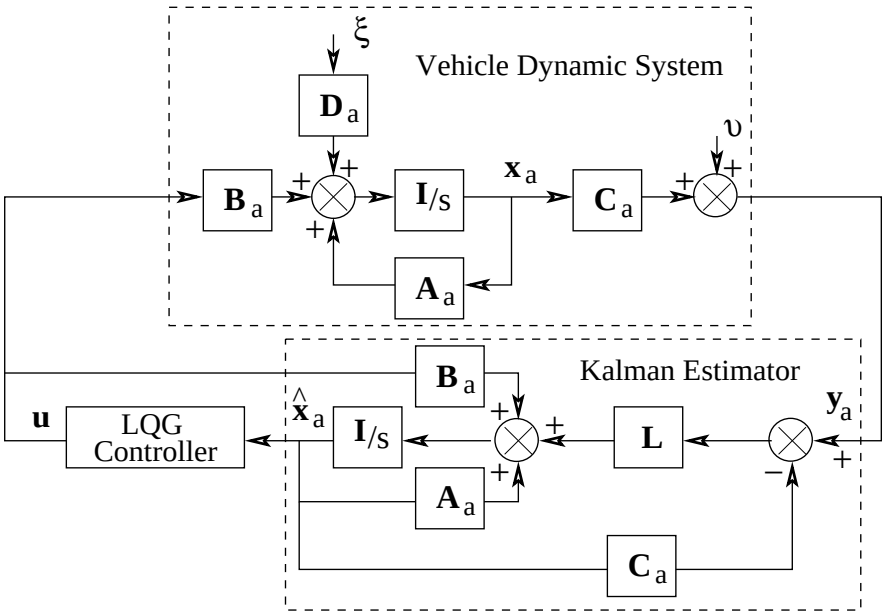

Figure 8.4: Configuration of the cascade arrangement of vehicle dynamic system, Kalman estimator, and LGQ controller

With the assembled control system, the performance index of the optimally controlled system is given by

$$J_{opt} = trace(\mathbf{SQ}_1) + trace(\mathbf{K}^T\mathbf{HKP}) \tag{8.47}$$

The performance index, given by equation (8.47), consists of two parts. The first part denoted by J_Q results from the random track excitation while the second part denoted by J_r is due to the measurement errors. The presence of measurement error increases the performance index since $trace(\mathbf{K}^T\mathbf{HKP})$ is, in general, positive.

8.4 Multidisciplinary Optimization and Implementation

8.4.1 Design Optimization Approach

As shown in Figure 8.5, the All-in-One (A-i-O) multidiscipline optimization (MDO) method is applied to the vehicle system to optimize the mechanical system, controller, and estimator simultaneously.

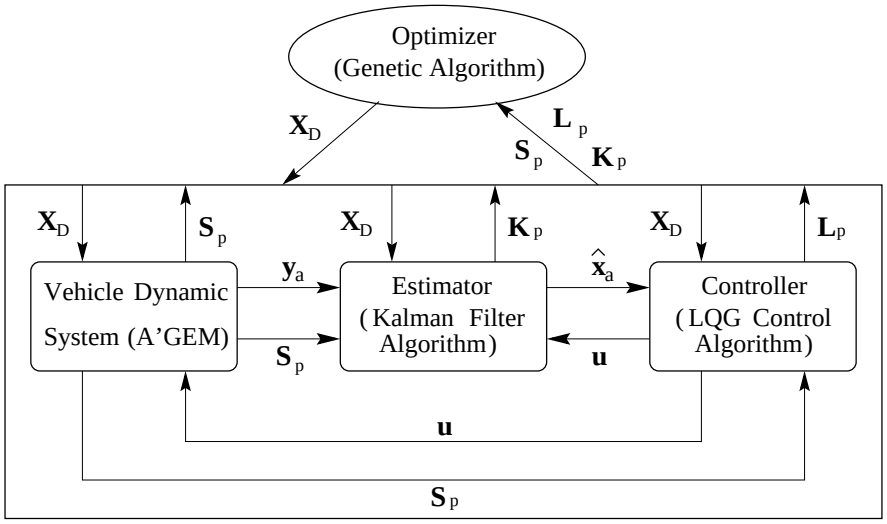

Figure 8.5: Schematic representation of the design optimization approach

The system shown in Figure 8.5 is composed of an optimizer, i.e. a genetic algorithm, which manipulates the relevant objective function and constraints, and three disciplines, i.e. the vehicle dynamic system with A'GEM software, the optimal estimator with Kalman filter algorithm, and the optimal controller with LQG control algorithm. The A-i-O approach to this optimization problem is a two-level optimization method. The optimization problem is solved for each discipline as well as for the system as a whole. The system is nonhierarchical because each discipline is coupled to every other discipline, and no discipline is viewed as being "above" the others.

After a generation evolution of the GA, an individual design variable set $\mathbf{X}_D$ is provided

by the GA to the coupled analysis disciplines. The design variable set $\mathbf{X}_D$ may include the passive design variables for the vehicle system, e.g. inertial property parameters, geometric parameters, and passive suspension parameters, and control parameters such as the weighting factors required in equation (8.30). With this set of design variables, a complete system multidisciplinary analysis (MDA) is performed to obtain vehicle dynamic system output variable vector $\mathbf{y}_a$, optimal estimate vector $\hat{\mathbf{x}}_a$, and actuator force vector $\mathbf{u}$, which are used for evaluating the corresponding objective functions and constraints. In addition to these coupled variables among the three disciplines, the resulting vehicle system parameters $\mathbf{S}_p$, e.g., the system matrix $\mathbf{A}_a$ generated by A'GEM software, are offered to the Kalman filter algorithm and the LQG control algorithm from the vehicle dynamic system for evaluating the above coupled variables. The vehicle system parameters $\mathbf{S}_p$ together with the resulting Kalman estimator parameters $\mathbf{K}_p$ and the resulting LQG controller parameters $\mathbf{L}_p$ are returned to the optimizer for the evaluation of the system objective function and constraints.

8.4.2 Implementation of the Optimization Problem

As shown in Figure 8.6, the A-i-O method is implemented using a two-level optimization approach. At the system or discipline level, the GA is used as the required optimizer to optimize the combined mechanical and control systems, a synergistic whole. At the subsystem or subdiscipline level, the LQG and Kalman filter algorithms are utilized to optimize the controller and estimator, respectively.

For a given vehicle system with a given set of design parameters $\mathbf{X}_D$, A'GEM is used to automatically generate the vehicle system matrix $\mathbf{A}$, such as shown in equation set (8.12), for rigid body vehicle model. The control matrix $\mathbf{B}$, the track excitation matrix $\mathbf{D}$, and flexible modes for the flexible vehicle model case should be assembled with the matrix $\mathbf{A}$ for generating the required equations of motion in state space form as discussed in previous sections.

As illustrated in Figure 8.6, first, a population of n sets of design variables, $\mathbf{X}_{Di}$, $i = 1, 2, ..., n$, are randomly selected in the search space by the GA; the corresponding sets of design variables are sent in parallel to the A'GEM routines which automatically generate equations of motions in a state space form accordingly. With the required vehicle dynamic

system matrices and weighting factors, the LQG algorithm and the Kalman filter algorithm in MATLAB construct and optimize the corresponding controller and estimator resulting in the control gain matrix $\mathbf{K}_i$, covariance matrix $\mathbf{X}_i$ of the state variables, filter error covariance matrix $\mathbf{P}_i$, and performance index $J_{(i)}$. Then these performance indices, i.e. $\{J_{(1)}, J_{(2)}, ..., J_{(n)}\}$, are used as the fitness values. At this point, if the convergence criteria are satisfied, the calculation terminates, otherwise these fitness values are returned to the GA. Based on the returned fitness values corresponding to the given sets of design variables, the GA produces the next generation of design variable sets using genetic operators, such as reproduction, crossover, and mutation. This procedure repeats until the optimized variable set is found.

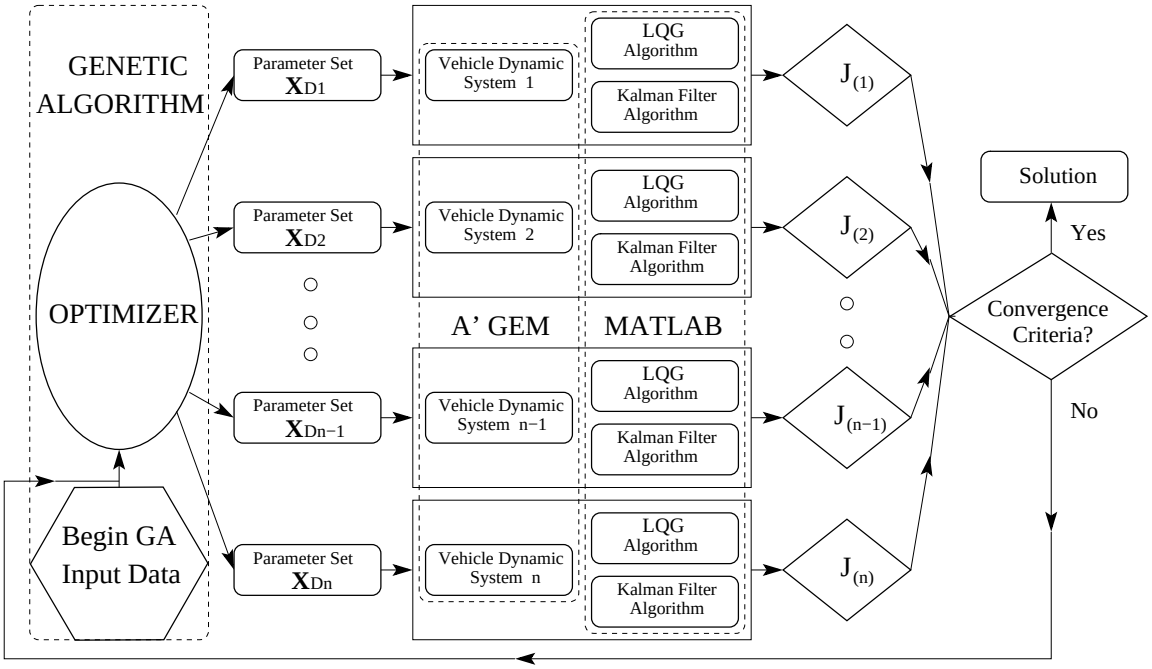

Figure 8.6: Schematic representation of the computer implementation for the A-i-O approach

8.5 Control Power Consumption

In addition to performance measures, two other important aspects that can be used to evaluate active suspensions are the amount of control power and actuator force required. The average power delivered to a hydraulic or other type of actuator can be estimated by considering the forces and motions across that actuator. It is recommended [45, 120] that the approximated average power is

$$P_{av} = u_p V_{av} \tag{8.48}$$

where u_p is the peak force produced by the actuator and V_{av} is the rectified average piston velocity. Suppose the force u_p and velocity V_{av} are individually Gaussian, which are linear combinations of the components of the state vector $\mathbf{x}$. Thus, the force and velocity can be obtained by

$$\begin{cases} u_p = 3\sqrt{E[(u)^2]} \\ V_{av} = \sqrt{2E[(V)^2]/\pi} \end{cases} \tag{8.49}$$

Therefore, the average power can be determined by

$$P_{av} = 3\sqrt{2E[(u)^2] \cdot E[(V)^2]/\pi} \tag{8.50}$$

8.6 Numerical Optimization for 2 DOF Models

In this section, the optimization results for the 2 DOF quarter-vehicle models are presented and discussed. The simulations are carried out for two different cases, i.e. deterministic track inputs and stochastic track inputs. The A-i-O method is used to resolve the conflicting requirements for ride comfort, suspension working spaces, and dynamic wheel loads for ground vehicles based on the quarter-vehicle models.

8.6.1 Deterministic Track Input Case

Vehicle System Optimization

The vehicle model is illustrated in Figure 8.1. It is assumed that the track input w is a unit step. For this vehicle model, the state variable vector $\mathbf{x}$, governing equations, and

dynamic matrices have already been given as described by equation (8.10), equation set (8.11), and equation set (8.12), respectively.

Thus, the optimization problem can be stated as: minimize the following objective function:

$$J = \int_0^\infty [\rho_1(u + \nu f_{pass})^2 + \rho_2 \ddot{x}_2^2 + \rho_3(x_1 - w)^2 + \rho_4(x_2 - x_1)^2]dt \tag{8.51}$$

subject to

$$\dot{\mathbf{x}} = \mathbf{A}\mathbf{x} + \mathbf{B}\mathbf{u} + \mathbf{D}\dot{\mathbf{w}} \tag{8.52}$$

where ν is a constant, ρ_1, ρ_2, ρ_3, and ρ_4 are weighting factors that impose penalties upon the magnitude and durations of the secondary suspension force including actuator force u and passive suspension force f_{pass} , the ride comfort $\ddot{x}_2$, the wheel deflection $x_1 - w$, and the suspension working space $x_2 - x_1$, respectively. The initial state variables $x_1(0)$, $x_2(0)$, $\dot{x}_1(0)$, and $\dot{x}_2(0)$ take the values of zero. The track displacement disturbance w is a unit step input.

For simplicity, the symbols J_1, J_2, J_3 and J_4 are introduced into equation (8.51). The definitions of these symbols are offered in Table 8.1.

Table 8.1: Expressions represented by symbols J_1, J_2, J_3 and J_4.

J_1	J_2	J_3	J_4
$\int_0^\infty (u + \nu f_{pass})^2 dt$	$\int_0^\infty \ddot{x}_2^2 dt$	$\int_0^\infty (x_1 - w)^2 dt$	$\int_0^\infty (x_2 - x_1)^2 dt$

As will be discussed later, to greatly facilitate the optimization and the control law synthesis [2, 24, 28], each term of the right side of equation (8.51) is normalized with the corresponding norm. In the case concerned, the norm of each term is the inverse of the corresponding weighting factor. The weighting factors are assumed to be:

$$\rho_i = 1/J_i^{ref} \tag{8.53}$$

where $i = 1, 2, 3, 4$, and J_i^{ref} is the i^{th} term of the objective function (in the form of equation (8.51)) of a reference quarter-vehicle model with passive or active suspensions. Note that the definition of J_i^{ref} $(i = 1, 2, 3, 4)$ is the same as its counterpart (J_i) shown in Table 8.1.

To find the solution to the optimization problem, equation (8.51) should be rewritten in the standard form as shown in equation (8.30). The resulting weighting matrices **G**, **H**, and **N** are listed in Appendix B. Note that in the deterministic track input case, the track input is not treated as an independent state variable as in the case of random track input.

The problem is actually an optimal tracking problem with the addition of a track disturbance $\dot{\mathbf{w}}$. Then the tracking problem is reduced to an equivalent regulator problem. Moreover, for the deterministic track input case, the Kalman filter algorithm is not introduced. Therefore, the implementation the A-i-O method shown in Figures 8.5 and 8.6 should be modified accordingly.

Results and Discussion

In this subsection, the simulation results from the A-i-O method are discussed and compared with those provided by Thompson [129]. As will be seen, the optimized vehicle model based on the A-i-O method has better performance than the corresponding model with passive suspension and that based on the LQG algorithm (used by Thompson) in all four aspects: ride comfort, suspension working space, dynamic wheel load, and actuator force. Note that the simulation results reported by Thompson [129] have been accurately repeated in this research.

When the quarter-vehicle model with active suspension offered by Thompson [129] is selected as a reference vehicle model, the weighting factors ρ_1, ρ_2, ρ_3, and ρ_4 are calculated to take the values of 0, $6.493 \cdot 10^{-4}$, 74.709, and 13.206, respectively. By including m_1, m_2, k_1, k_2, and c_2 as additional design variables, the control gain matrix **K** obtained using the A-i-O method and that offered by Thompson using the LQG are listed in Table 8.3. These additional passive design variables are permitted to vary by 20% from the nominal values. The optimized passive design variables based on the A-i-O, together with their nominal values (listed in Figure 8.1 as parameter set 1), are provided in Table 8.2.

The resulting unit step responses based on the A-i-O, the LQG (used by Thompson), and the corresponding passive suspension system are shown in Figures 8.7, 8.8, 8.9, and 8.10. Figure 8.7 illustrates the relationship between the sprung mass acceleration and time, Figure 8.8 the secondary suspension forces and time, Figure 8.9 the sprung mass displacement and time, and Figure 8.10 the unsprung mass displacement and time.

Table 8.2: Optimized values for m_1, m_2, k_1, k_2, and c_2.

	$m_1\ [kg]$	$m_2\ [kg]$	$k_1\ [N/m]$	$k_2\ [N/m]$	$c_2\ [N/m/s]$
NV†	28.58	288.9	$1.5590 \cdot 10^5$	$1.9960 \cdot 10^4$	$1.8610 \cdot 10^3$
A-i-O‡ ($\pm 20\%$)	22.864	346.68	$1.2472 \cdot 10^5$	$2.2836 \cdot 10^4$	$1.6698 \cdot 10^3$
A-i-O1* ($\pm 20\%$)	22.864	346.68	$1.2472 \cdot 10^5$	$2.0388 \cdot 10^4$	$1.8821 \cdot 10^3$

† Nominal values; ‡ Optimized values based on A-i-O method with $\rho_1 = 0$;

* Optimized values based on A-i-O method with $\rho_1 = 7.7793 \cdot 10^{-9}$.

Table 8.3: Feedback control gain matrix for optimal suspensions.

	$K_{1,1}$	$K_{1,2}$	$K_{1,3}$	$K_{1,4}$
LQG†	-57240.0	35355.0	-1385.7	4827.0
A-i-O‡	-48683.0	26607.0	240.0	4682.0
A-i-O1*	-15045.0	11265.0	886.0	2873.0

† Thompson's results with passive design variables taking nominal values;

‡ Obtained using the A-i-O method with $\rho_1 = 0$;

* Obtained using the A-i-O method with $\rho_1 = 7.7793 \cdot 10^{-9}$.

It should be noticed that for the LQG case, $k_2 = 0$, $c_2 = 0$, and other passive vehicle system parameters take their nominal values.

Investigation of Figures 8.7, 8.8, 8.9, and 8.10 shows that, compared with the active suspension based on the LQG, the one based on the A-i-O method is better controlled both in sprung mass acceleration and in unsprung mass displacement with less overshoot, the peak actuator force is much less, the peak total secondary suspension force or total sprung mass force is less, and the sprung mass displacement is almost the same. Compared with the passive suspension, the performance improvement based on the A-i-O method is greater than that based on the LQG. Both active suspensions are much better controlled than the passive suspension in sprung mass displacement with lower peak sprung mass forces. The numerical results are listed in Table 8.4. Results demonstrate that the optimized system based on the A-i-O outruns its counterpart based on LQG in the mean-square values of all aspects, i.e. suspension working space $x_2 - x_1$, dynamic wheel load or $x_1 - w$, sprung mass acceleration $\ddot{x}_2$, actuator force u, and total sprung mass force $u + f_{pass}$. Based on the

quadratic performance indices shown in Table 8.4, the active suspensions based on both the LQG and A-i-O are superior to the passive suspension.

To further investigate the actuator forces based on the A-i-O and LQG, part of Figure 8.8 is plotted in Figure 8.11. A close observation of Figure 8.11 reveals that, at a point when the track unit input imposes on the unsprung mass, the corresponding active suspension force actively resists the disturbance immediately, but the corresponding passive suspension force just follows the disturbance. The resistance to the track disturbance contributes to the performance improvement of the corresponding suspension. Compared with the case of LQG, in the case of A-i-O, the active force resistance to the track disturbance lasts longer and the active force and the corresponding passive force are almost out of phase. This outphase between the active and passive forces in the case of A-i-O makes the corresponding total force smaller than the active force based on the LQG and leads to the performance improvement over the active suspension based on the LQG algorithm. In the case of LQG, although the active force resists the track disturbance, this resistance lasts a very short period of time. Then the active force follows the trends of the passive suspension force based on the A-i-O. Thus, the actuator force based on the A-i-O and that based on the LQG are also almost out of phase. This outphase of the actuator force between the two cases can be explained by the opposite sign of $K_{1,3}$ in the control gain matrices for the two cases as shown in Table 8.3

Notice that the optimized vehicle system based on the A-i-O achieves the above superior performance though the sprung mass is 20% larger than the mass used in the corresponding vehicle model with the active suspension based on the LQG and the passive suspension.

To examine the effect of the weighting factor or components of objective function shown in equation (8.51) on the performance of the vehicle system, the weighting factor ρ_1 takes the value of $7.779 \cdot 10^{-9}$ instead of 0.0, the constant ν is set to the value of 1.0, and the other weighting factors take the values as those in the case of A-i-O. To distinguish this case from the previous cases, this case is denoted as A-i-O1. In the case of A-i-O1, the passive vehicle system design variables m_1, m_2, k_1, k_2, and c_2 are also permitted to vary by 20% from the nominal values. We can obtain the optimized passive design variables for this case as listed in the Table 8.2 using the A-i-O method. It can be found that the

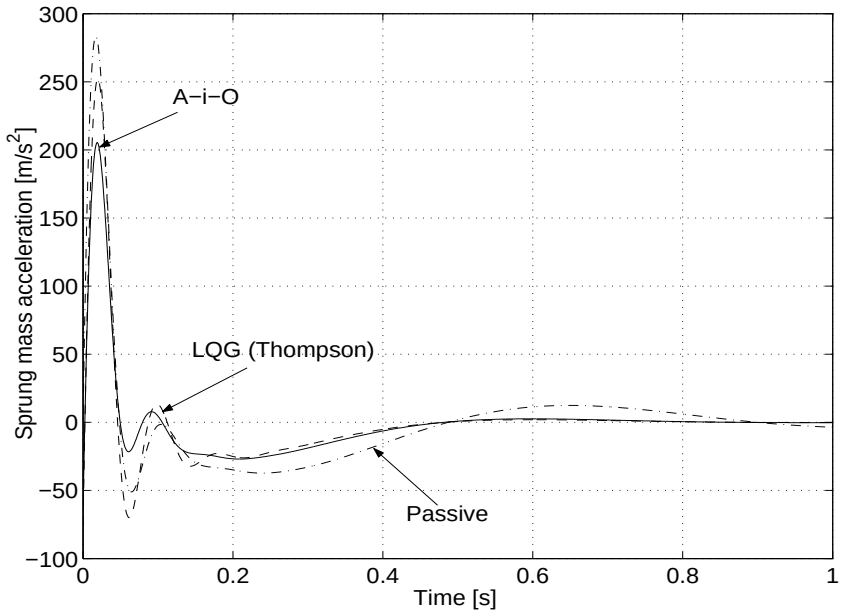

Figure 8.7: Sprung mass acceleration versus time

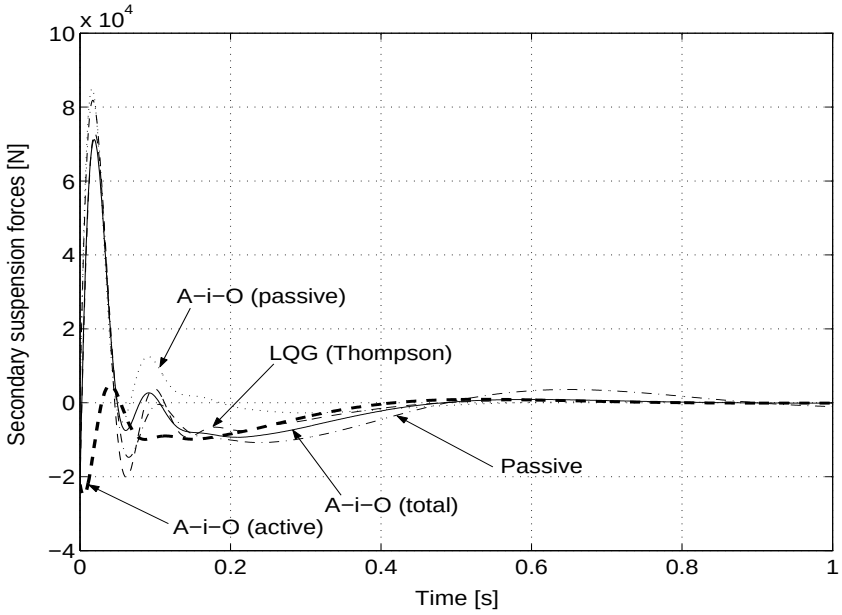

Figure 8.8: Secondary suspension forces versus time

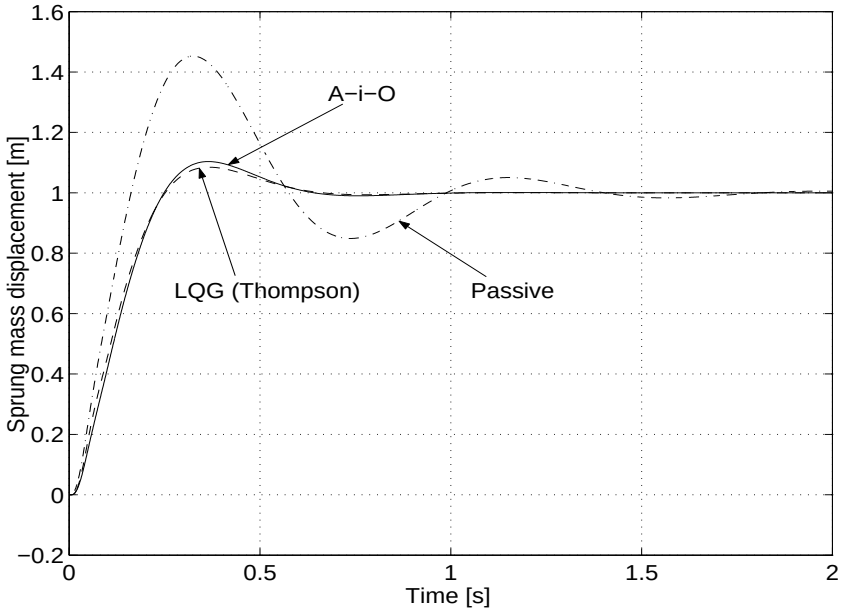

Figure 8.9: Sprung mass displacement versus time

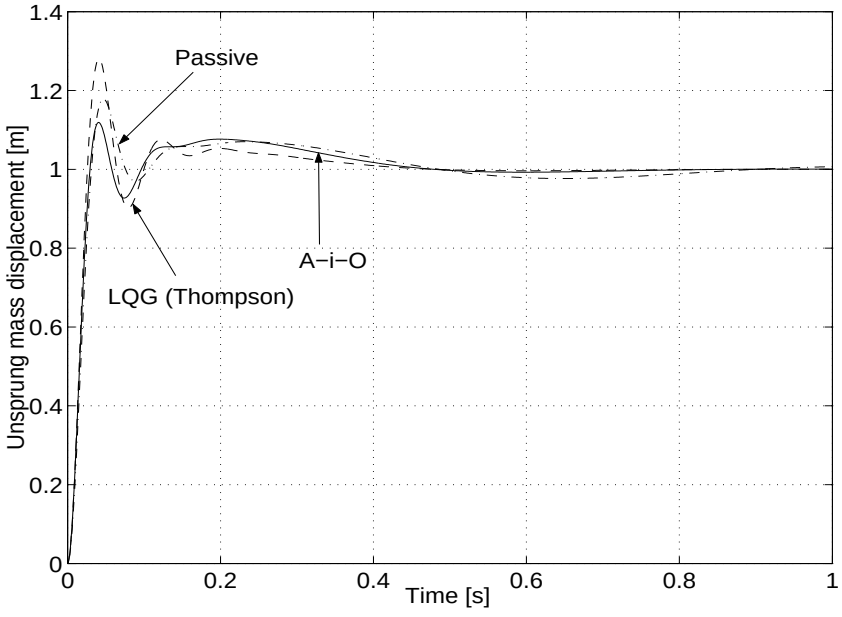

Figure 8.10: Unsprung mass displacement versus time

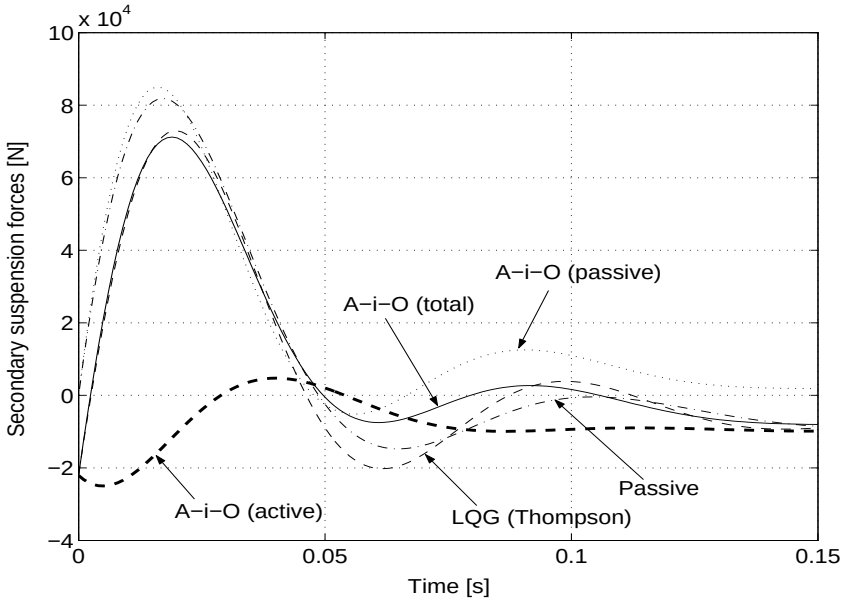

Figure 8.11: Secondary suspension forces versus time

Table 8.4: Comparison of the response characteristics for passive and active suspensions.

	LQG	Passive	A-i-O	A-i-O1
m_2 displacement overshoot %	8.5	45.3	10.4	8.5
m_1 displacement overshoot %	28.0	18.0	11.9	25.9
Peak total m_2 force $[N]$	$7.3 \cdot 10^4$	$8.2 \cdot 10^4$	$7.12 \cdot 10^4$	$5.75 \cdot 10^4$
Peak actuator force $[N]$	$7.3 \cdot 10^4$	0.0	$-2.50 \cdot 10^4$	$-4.35 \cdot 10^4$
Peak m_2 acceleration $[m/s^2]$	252.5	283.3	205.4	165.8
$\int_0^\infty (x_2 - x_1)^2 dt$	0.076	0.085	0.073	0.089
$\int_0^\infty 10(x_1 - w)^2 dt$	0.134	0.144	0.129	0.141
$\int_0^\infty \ddot{x}_2^2 dt$	1540.1	2145.2	1016.9	721.8
$\int_0^\infty \rho u^2 dt$ †	0.103	0.0	0.021	0.041
$\int_0^\infty \rho(u + f_{pass})^2 dt$	0.103	0.143	0.098	0.069

† $\rho = 8.0 \cdot 10^{-10}$ [129].

obtained passive system design variables are the same as those obtained in the A-i-O case except for the minor difference of the variables k_2 and c_2. As a matter of fact, during the numerical experiments using the A-i-O method, the GA does not converge at certain values for the design variables k_2 and c_2 over a narrow value range for both k_2 and c_2 where the performance index J reaches its minimum value. This can be interpreted that, within certain value ranges of k_2 and c_2, since the introduction of the actuator, the vehicle system performance is not sensitive to the passive suspension design variables k_2 and c_2.

In the case of A-i-O1, the obtained control gain matrix $\mathbf{K}$ and the numerical simulation results are also offered in Tables 8.3 and 8.4, respectively. By including the total secondary suspension force as an additional performance index term, from the optimization point of view, we lay more emphasis on reducing the total sprung mass force and sprung mass acceleration. Simulation results match this expectation. As shown in Table 8.4, compared with the case of A-i-O, the active suspension denoted as A-i-O1 is much better controlled in total sprung mass force, sprung mass acceleration, and sprung mass displacement overshoot. However, the vehicle performance in suspension working space, dynamic wheel load, and actuator force suffers.

The objective function, as provided by equation (8.51), penalizes, quadratically, large deviations of the state and control vectors from their desired set point values. Numerical experiments show that the selection of the weighting factors for the objective function is important and greatly affects the implementation of the A-i-O method. With each penalized variable normalized by the mean-square value of the corresponding variable of a reference vehicle model (see equation (8.53)), each term of the objective function can be guaranteed to be at the same order of digital value during the optimization and the GA can effectively coordinate the design criteria of ride comfort, suspension working space, wheel dynamic load, and actuator force. From the designer's point of view, this is a meaningful form of objective function because it requires that only an appropriate reference vehicle model be selected.

8.6.2 Random Track Input Case

Vehicle System Optimization

The vehicle model for this case is also presented in Figure 8.1. The track input w is the filtered white noise process described previously. In this case, the state variable vector $\mathbf{x}_a$, governing equations, and system dynamic matrices are provided by equation (8.16), equation set (8.17), and equation set (8.18), respectively.

The vehicle model was optimized with respect to ride comfort, suspension working space, and dynamic wheel load. Hence the performance index J has the following simple format

$$J = \rho_1 J_1 + \rho_2 J_2 + \rho_3 J_3 + \rho_4 J_4 \tag{8.54}$$

where ρ_1, ρ_2, ρ_3, and ρ_4 are weighting factors, J_1, J_2, J_3 and J_4 are defined in Table 8.5. The products $\rho_1 J_1$, $\rho_2 J_2$, $\rho_3 J_3$, and $\rho_4 J_4$ mean the measures of actuator force, ride comfort, wheel dynamic load, and suspension working space, respectively.

Table 8.5: The definition of the symbols J_1, J_2, J_3 and J_4.

J_1	J_2	J_3	J_4
$E[u^2]$	$E[\ddot{x}_2^2]$	$E[(x_1 - w)^2]$	$E[(x_2 - x_1)^2]$

The performance index formulation (8.54) should be expressed in the standard format as shown in equation (8.30) for the purpose of finding the solution to the optimization problem. With the performance index (8.54) and governing equation set (8.17), based on the methods described in Section 8.3, the solution to the optimization problem can be obtained.

Results and Discussion

In this subsection, the simulation results from the A-i-O method are discussed and compared with those reported by Hac [59]. As will be seen, the optimal vehicle model derived from the A-i-O method has better performance than the corresponding model based on the LQG algorithm (used by Hac) in the mean-square values of actuator force, vertical

sprung mass acceleration, suspension working space, and dynamics wheel load. Note that the simulation results reported by Hac [59] have been accurately repeated in this research.

The vehicle system parameters are listed in Figure 8.1 as parameter set 2 together with the random track characteristics. When the vehicle is moving at the speed $V = 30\ [m/s]$ and the weighting factors $\rho_2 = 1.0$, $\rho_3 = 10^5$ and $\rho_4 = 10^4$, Hac [59] offered the simulation results as shown in Figure 8.12 in dashed lines. Figure 8.12 illustrates the dependence of the performance index (J) and its parts (J_1, J_2, J_3, J_4) upon the weighting factor ρ_1.

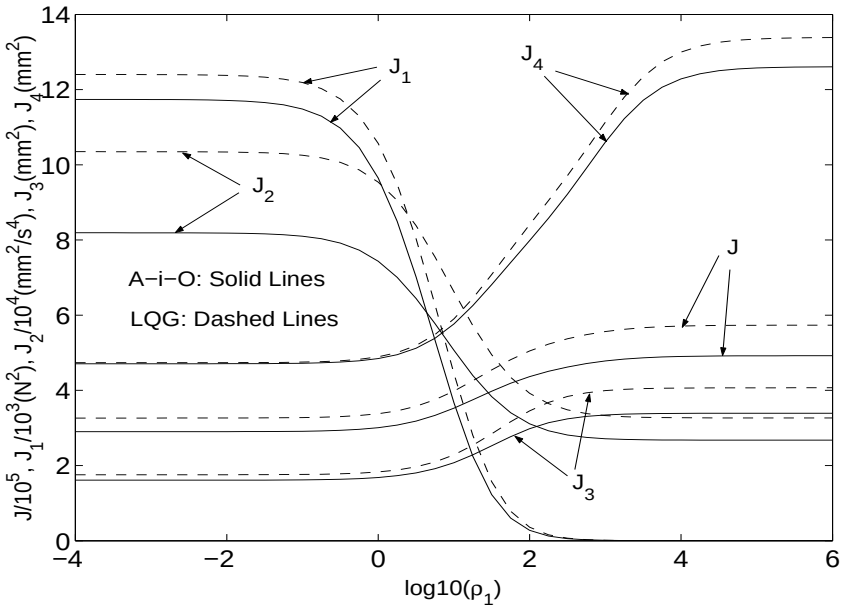

Figure 8.12: Performance index J and its parts J_1, J_2, J_3, and J_4 versus ρ_1

The A-i-O method is also used to optimize the vehicle model with passive and active suspensions. The same values used by Hac [59] are assigned to the weighting factors ρ_2, ρ_3, and ρ_4, respectively. However, the vehicle system parameters, i.e. m_1, m_2, k_1, k_2 and c_2 are introduced as additional design variables and these variables are permitted to vary by 10% from the nominal values. Numerical experiments show that the optimized values (denoted as A-i-O) for these design variables are independent of weighting factor ρ_1. The optimal values for these variables are listed in Table 8.6.

In Figure 8.12, the solid curves indicate the relationships J, J_1, J_2, J_3, J_4 versus ρ_1

obtained using the A-i-O method. Compared with the optimal suspension based on the LQG, the counterpart based on the A-i-O improves the performance index J and its parts J_1, J_2, J_3, and J_4 over a wide range of weighting factor ρ_1. A close observation shows that, when $\rho_1 < 1$, the latter can achieve much better ride comfort, better track holding capability, and almost the same suspension work space with less actuator force. When $\rho_1 > 10^3$, both suspensions behave like passive suspensions because the actuator force is very small and the latter is superior to the former in ride comfort, suspension work space, and track holding capability.

Table 8.6: Optimized values for m_1, m_2, k_1, k_2, and c_2.

	$m_1\ [kg]$	$m_2\ [kg]$	$k_1\ [N/m]$	$k_2\ [N/m]$	$c_2\ [N/m/s]$
NV†	100.0	500.0	$2.0 \cdot 10^5$	$5.0 \cdot 10^3$	$1.0 \cdot 10^3$
A-i-O‡ ($\pm 10\%$)	90.0	550.0	$1.8 \cdot 10^5$	$5.5 \cdot 10^3$	$1.1 \cdot 10^3$
Pass* ($\pm 10\%$)	90.0	450.0	$1.8 \cdot 10^5$	$4.5 \cdot 10^3$	$1.1 \cdot 10^3$

† Nominal values; ‡ Optimized values based on A-i-O method;

* Optimized values for the passive vehicle suspension system using the GA.

To investigate whether a sequential optimization process (SOP), i.e. optimizing the passive vehicle suspension system first, then designing a controller for the system based on the optimized passive vehicle system parameters using the LQG algorithm, can achieve the same results as the A-i-O method does, the GA is used to optimize the passive vehicle suspension system first, then the LQG is applied to the design of the optimal controller for the optimized vehicle system. In these simulations, the weighting factors ρ_2, ρ_3, and ρ_4 are the same as those used with the A-i-O method. The optimized passive vehicle parameters (denoted as Pass) are also listed in Table 8.6.

Figures 8.13 and 8.14 show the corresponding R.M.S. (root mean square) trade-off solutions of vertical sprung mass acceleration versus suspension working space and R.M.S. trade-off solutions of vertical sprung mass acceleration versus wheel dynamic load for the optimal suspension systems based on the A-i-O (denoted as A-i-O), the LQG (based on nominal passive vehicle parameter, denoted as LQG), and the SOP. It is clear that the suspension based on the A-i-O method has the best overall performance among the three optimal suspensions. From Figure 8.13, we can see that, within a certain acceleration

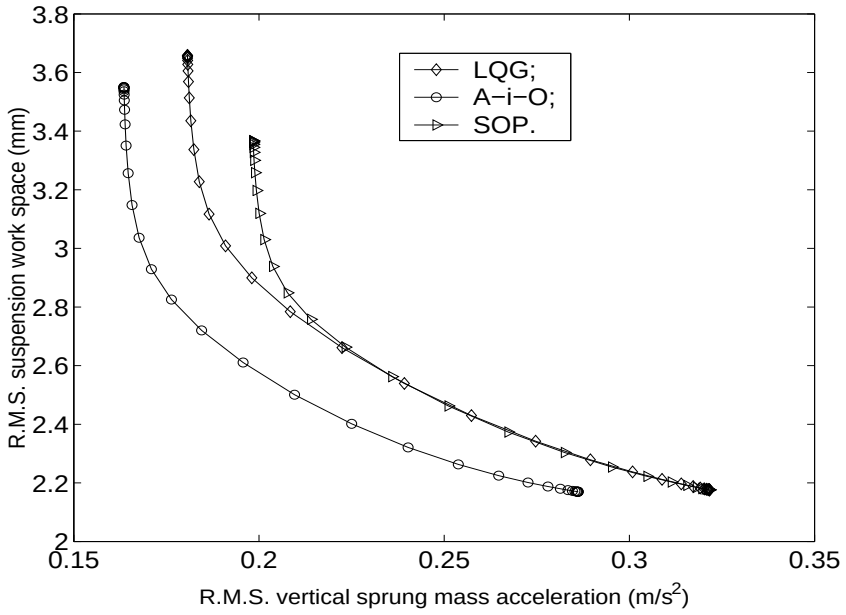

Figure 8.13: R.M.S. trade-off solutions of vertical sprung mass acceleration versus suspension working space

range, the suspension based on the SOP method requires the largest suspension working space among the three suspensions.

In the simulations, the availability of a limited number of the state variables is considered. As mentioned previously, it is assumed that the absolute vertical velocities of both the sprung mass and unsprung mass (wheel) are available. The simulation results are offered here. In the simulations the measurement noises are set to 5% of the R.M.S. value of vertical wheel velocity. The simulation results are shown in Figure 8.15 which illustrates the dependence of performance indices and measurement errors upon the weighting factor ρ_1. For these simulations, ρ_2, ρ_3, ρ_4, and V still take the values offered previously. In the LQG case (denoted as J_{LQG}), the vehicle system parameters take their nominal values, while in cases of the A-i-O without the Kalman filter (denoted as J_{A1}) and the A-i-O with the Kalman filter (denoted as J_{A2}), the vehicle system parameters are treated as design variables and are permitted to vary by 10% from their nominal values.

As expected, by comparing the results from J_{A1} and J_{A2}, we can see that the perfor-

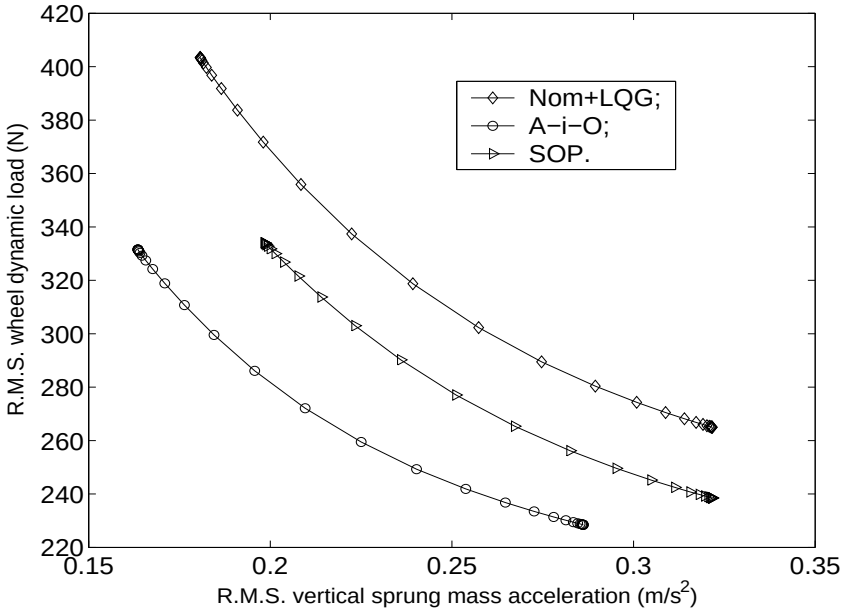

Figure 8.14: R.M.S. trade-off solutions of vertical sprung mass acceleration versus dynamic wheel load

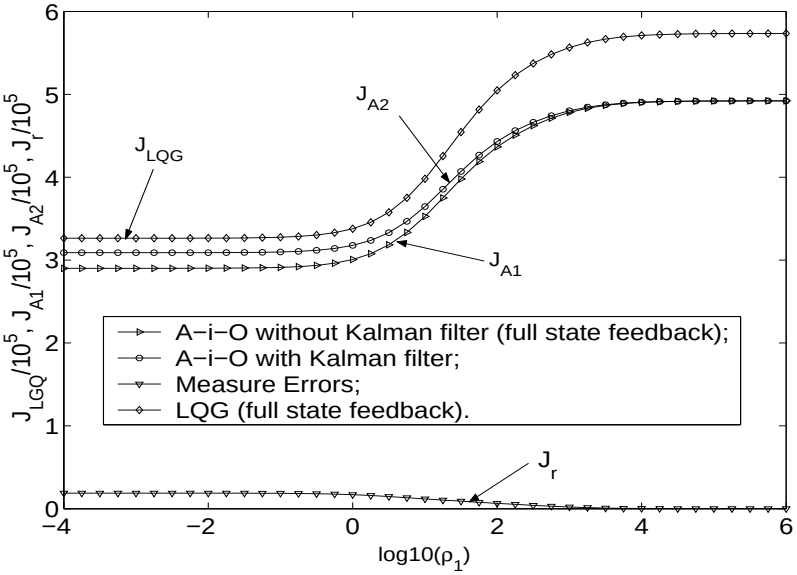

Figure 8.15: Performance indices and measurement error Jr versus weighting factor ρ_1

mance of the active suspension based on J_{A2} suffers from the measurement corruption. As mentioned previously, when $\rho_1 > 10^3$, the active suspensions behave like passive suspensions. This point can be further demonstrated by the fact that the measurement error J_r becomes very small and the performance indices from J_{A1} and J_{A2} are very close when $\rho_1 > 10^3$. By comparing the results based on J_{LQG} and J_{A2}, we can observe that even though the suspension system based on J_{A2} suffers from the measurement errors, its performance is still better than that of the suspension system based on J_{LQG}.

8.7 Numerical Optimization for Half-Vehicle Models

In this section, the optimization results for the half-vehicle models with rigid vehicle body and flexible vehicle body are provided and analyzed. For the rigid body vehicle model, the numerical optimization is carried out with the track inputs selected as unit step inputs corresponding to the integrated white noise track input case. For the flexible body vehicle model, the numerical optimization is performed under the condition that the track inputs are the filtered white noise processes. For both vehicle models, it is assumed that the track disturbance inputs at the front unsprung mass and at the rear unsprung mass are identical except that the latter is delayed by the time interval D (see equation set (8.6)) with respect to the former. Once again the numerical results based on the A-i-O method are compared with those based on the LQG algorithm and the corresponding passive suspensions.

8.7.1 Deterministic Track Input Case

Vehicle System Optimization

For the vehicle model as shown in Figure 8.2, the state variable vector $\mathbf{x}$, actuator force vector $\mathbf{u}$, and track excitation vector $\dot{\mathbf{w}}$ are descirbed by equation set (8.20), the governing equations are given by equation set (8.11), and the corresponding system, control, output, and disturbance matrices $\mathbf{A}$, $\mathbf{B}$, $\mathbf{C}$, and $\mathbf{D}$ are provided in Appendix B, respectively.

Hence, the vehicle system optimization problem can be described as: minimize the

following objective function,

$$J = \sum_{i=1}^{6} \rho_i J_i \tag{8.55}$$

subject to

$$\begin{cases} \dot{\mathbf{x}} = \mathbf{A}\mathbf{x} + \mathbf{B}\mathbf{u} + \mathbf{D}\dot{\mathbf{w}} \\ \mathbf{y} = \mathbf{C}\mathbf{x} \end{cases} \tag{8.56}$$

where ρ_1 to ρ_6 are the weighting factors, J_1 to J_6 are defined in Table 8.7, and $\rho_1 J_1$ to $\rho_6 J_6$ imply the measurements of the accelerations of the vehicle body at points A and B (see Figure 8.2), the dynamic loads of unsprung masses m_1 and m_2, front and rear secondary suspension working spaces, respectively. Due to the fact that, for the quarter-vehicle model

Table 8.7: Expressions represented by symbols J_1 to J_6.

J_1	J_2	J_3	J_4	J_5	J_6
$\int_0^\infty \ddot{x}_2^2 dt$	$\int_0^\infty \ddot{x}_4^2 dt$	$\int_0^\infty (x_1 - w_1)^2 dt$	$\int_0^\infty (x_3 - w_2)^2 dt$	$\int_0^\infty (x_2 - x_1)^2 dt$	$\int_0^\infty (x_4 - x_3)^2 dt$

case discussed previously, the introduction of the secondary suspension force term into the objection function (8.51) does not improve the overall performance of the vehicle system, the secondary suspension force term is not included in the objective function (8.55). The governing equations of the vehicle system show that $\ddot{x}_2$ and $\ddot{x}_4$ are dependent on the front and rear secondary suspension force, respectively. Hence, constraining the accelerations at points A and B of the vehicle body also constrains the actuator forces u_1 and u_2 and front and rear passive secondary suspension forces.

As discussed previously, each term on the right hand side of objective function (8.55) is also normalized with the corresponding norm or the corresponding inverse of the weighting factor. Once again, these weighting factors can be obtained based on the corresponding objective function terms of J_1 to J_6 calculated from the dynamic responses of a selected reference half-vehicle model with passive or active suspensions.

Once more, to find the solution to the optimization problem, equation (8.55) should also be formulated in the standard matrix form as shown in equation (8.30). The resulting weighting matrices $\mathbf{G}$, $\mathbf{H}$ and $\mathbf{N}$ are provided in Appendix B.

Results and Discussion

In this subsection, the simulation results from the A-i-O method are discussed and compared with those reported by Thompson [131]. As will be seen, the optimized vehicle model based on the A-i-O method has better performance than the corresponding model with passive suspension and that based on the LQG algorithm (used by Thompson) in all the four aspects, ride comfort, suspension working spaces, dynamic wheel loads, and actuator forces. Note that the simulation results reported by Thompson [131] have been accurately repeated in this research.

Based on the half-vehicle model with active suspension designed by Thompson [131], the weighting factors ρ_1, ρ_2, ρ_3, ρ_4, ρ_5, and ρ_6 are assigned the values of $5.4190 \cdot 10^{-4}$, $2.2261 \cdot 10^{-4}$, 78.8781, 50.7307, 13.7052, and 14.6588, respectively. Using the A-i-O method, we can find the control gain matrix $\mathbf{K}$ listed in Table 8.8 together with that based on Thompson's method (LQG algorithm). In the A-i-O case, the additional design variables are selected as m_1, m_2, M, I_c, a, b, k_1, c_1, k_2, c_2, k_3, and k_4. The design variables k_1, c_1, k_2, and c_2 are permitted to vary by 50% from their nominal values and the rest to vary by 10% from the nominal values. The corresponding optimal values for these design variables are provided in Table 8.9.

Table 8.8: Feedback control gain matrix for optimal suspensions.

	$K_{1,1}$	$K_{1,2}$	$K_{1,3}$	$K_{1,4}$	$K_{1,5}$	$K_{1,6}$	$K_{1,7}$	$K_{1,8}$
A-i-O	−51636.0	30492.0	−315.0	352.0	61.0	4506.0	−8.0	38.0
LQG	−58092.0	35355.0	1392.0	−75.0	−1379.0	4620.0	−18.0	215.0
	$K_{2,1}$	$K_{2,2}$	$K_{2,3}$	$K_{2,4}$	$K_{2,5}$	$K_{2,6}$	$K_{2,7}$	$K_{2,8}$
A-i-O	−1111.0	381.0	−61896.0	48182.0	−12.0	52.0	553.0	3239.0
LQG	1058.0	75.0	−68826.0	35355.0	−8.0	233.0	−1774.0	4047.0

In the A-i-O, LQG, and passive suspension cases, the resulting vehicle dynamic responses in time domain for the unsprung mass displacements of both m_1 and m_2, and the working spaces of both front and rear secondary suspensions are illustrated in Figures 8.16, 8.17, 8.18, and 8.19, respectively. Once again, in both the LQG and passive suspension cases, the parameters listed in Table 8.9 take the nominal values. Figures 8.16 and 8.17 show that, among the three cases, the active suspension based on the A-i-O method is

best controlled with the smallest overshoot in both m_1 and m_2 displacements but the one based on the LQG has the largest overshoot. Observation of Figures 8.18 and 8.19 reveals that, compared with the active suspension based on the LQG, the one based on the A-i-O behaves better with less overshoot in both front and rear secondary suspension working spaces. Although the passive suspension has less front and rear secondary suspension working space overshoot than the active suspensions, the oscillation is damped out much slower than those in the active suspensions.

Table 8.9: Optimized values for passive vehicle system design variables.

	$m_1\ [kg]$	$m_2\ [kg]$	$M\ [kg]$	$I_c\ [kg \cdot m^2]$	$a_1\ [m]$	$a_2\ [m]$
NV†	28.58	54.43	505.1	651.0	1.0978	1.4676
A-i-O	25.72	48.99	555.5	715.9	0.9880	1.3215
	$k_1\ [N/m]$	$c_1\ [N/m/s]$	$k_2\ [N/m]$	$c_2\ [N/m/s]$	$k_3\ [N/m]$	$k_4\ [N/m]$
NV	19960.0	2014.0	22590.0	2082.0	155900.0	155900.0
A-i-O	19777.2	1540.1	12365.2	2316.6	140802.9	170755.4

† Nominal values.

Notice that the negative front and rear secondary suspension working spaces mean that these suspensions are in the strokes of compression. In the above analysis, it is assumed there are no limitations for the suspension working spaces. Practically, the suspension working spaces can not take such large values because of the existence of bump stops in both the front and rear secondary suspensions.

Figures 8.20, 8.21, and 8.22 demonstrate the relationships of vertical accelerations of the vehicle body at points A and B versus time and the pitch angular acceleration of the vehicle body versus time. Based on Figures 8.20 and 8.21, we find that, among the three cases, the active suspension based on the A-i-O is best controlled with the smallest overshoots in accelerations of the vehicle body at both points A and B and the passive suspension behaves the worst with the largest overshoots. A close observation of Figure 8.20 discloses that at the time the unit step input imposes on the unsprung mass m_2, this track disturbance affects the acceleration of the vehicle body at point A for all of the three cases. The disturbance is reflected by the arising of the second peak around the time on the

corresponding acceleration curve for each case. In both the LQG and passive suspension cases, the time delay between the front and rear inputs is about $0.086[s]$. In the A-i-O case, the time delay is about $0.077[s]$. Compared with the acceleration of the vehicle body at point A, the track input at m_2 has a much more significant effect on the acceleration at point B. This difference can be found by the comparison of the second peak on each acceleration curve in Figure 8.20 with the corresponding first peak in Figure 8.21 for all of the three cases. Moreover, as we can see from Figure 8.21, in the case of LQG, the acceleration of the vehicle body at point B trembles immediately after the unit step input imposes on the unsprung mass m_2. In the aspect of the angular acceleration of the vehicle body, as shown in Figure 8.22, the active suspension based on the A-i-O method outruns that based on the LQG algorithm and the passive suspension with less magnitude.

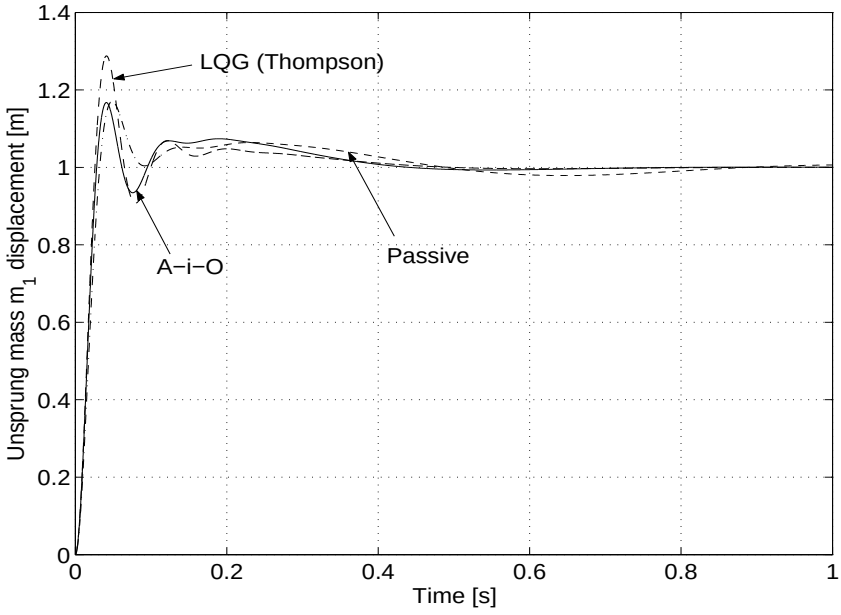

Figure 8.16: Unsprung mass m_1 displacement versus time

Figures 8.23 and 8.24 illustrate the relationship between the corresponding secondary suspension force and time for both the front and rear secondary suspensions. For the purpose of visibility, parts of Figures 8.23 and 8.24 are repeated in Figures 8.25 and 8.26, respectively. A close comparison of the Figure 8.25 with Figure 8.11 demonstrates that

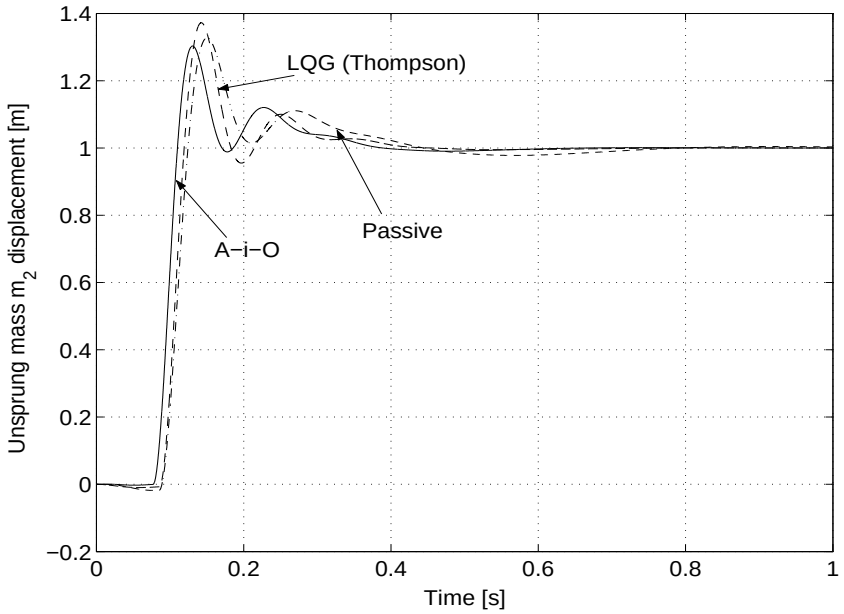

Figure 8.17: Unsprung mass m_2 displacement versus time

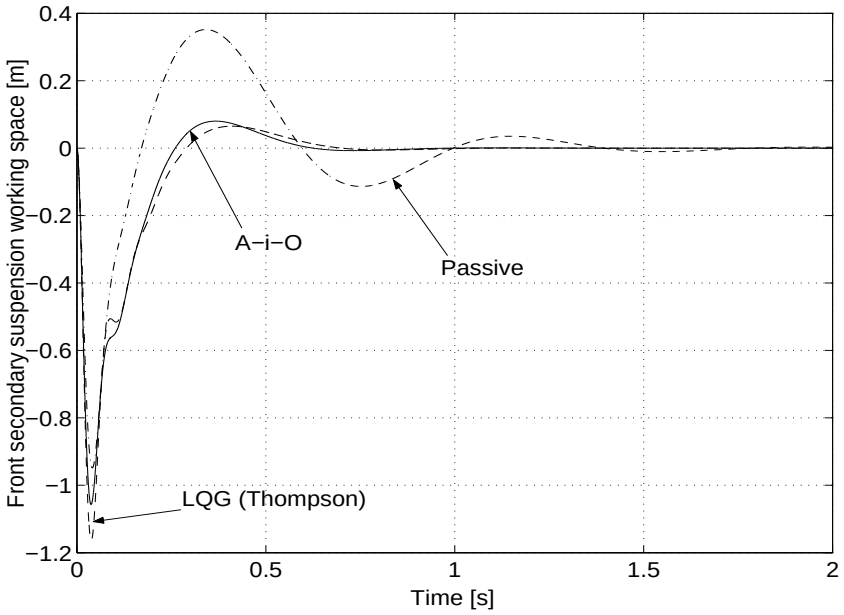

Figure 8.18: Front secondary suspension working space versus time

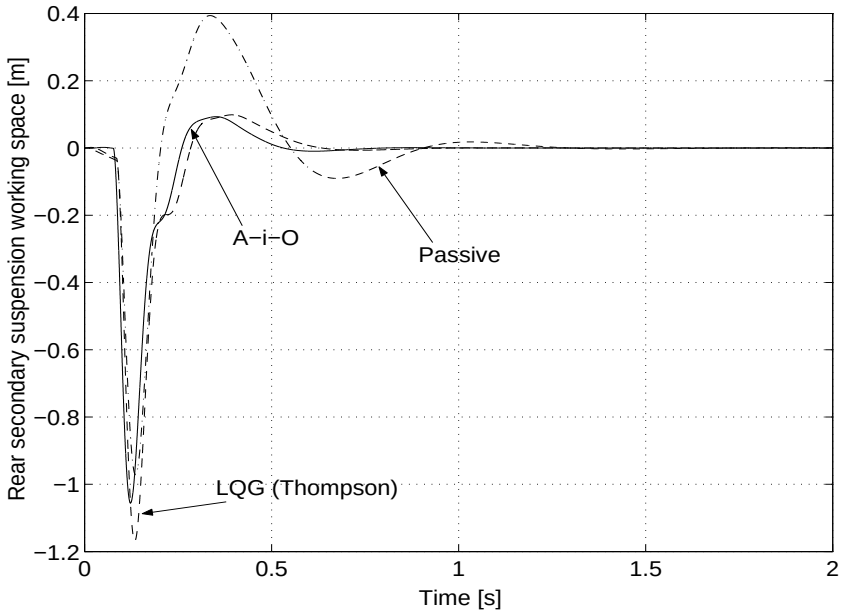

Figure 8.19: Rear secondary suspension working space versus time

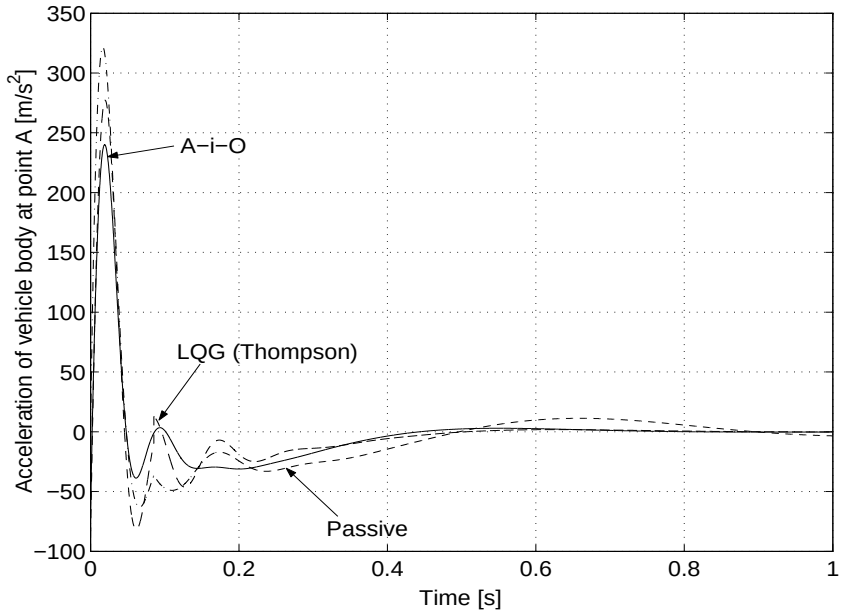

Figure 8.20: Acceleration of vehicle body at point A versus time

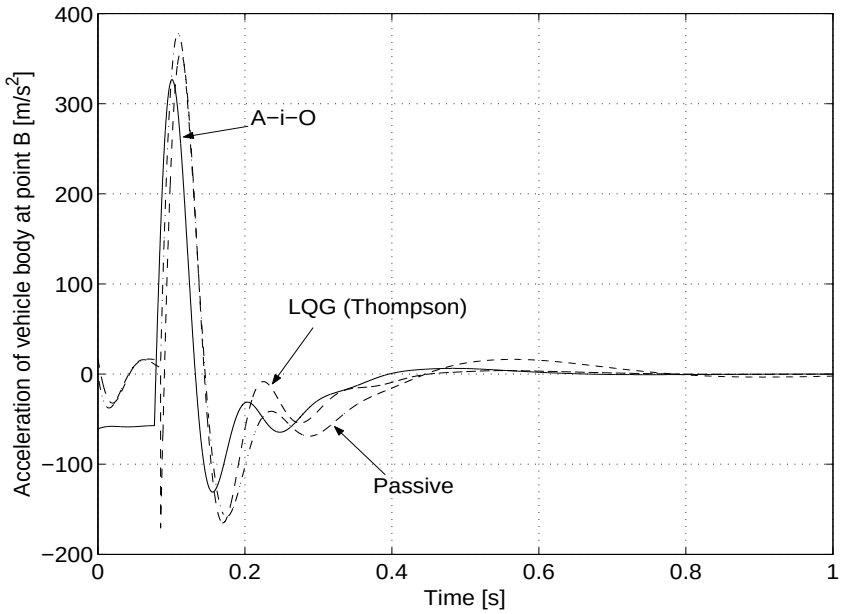

Figure 8.21: Acceleration of vehicle body at point B versus time

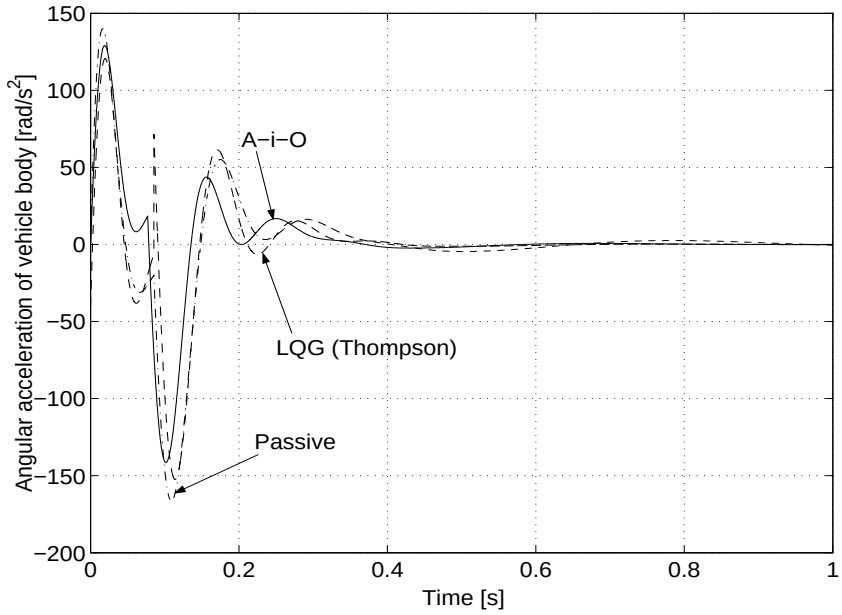

Figure 8.22: Pitch angular acceleration of vehicle body versus time

the corresponding curves in the two figures are very similar. This similarity is due to the fact that the relevant vehicle system parameters for the previous quarter-vehicle model are the same as those in the front part of the half-vehicle model, e.g. the unsprung mass and the primary suspension spring stiffness coefficient. This similarity also verifies the correctness of the calculation for the half-vehicle model. Moreover, this similarity implies that the secondary suspension force analysis for the previous quarter-vehicle model with deterministic track input also holds for the front secondary suspension force analysis for the half-vehicle model with deterministic track inputs. A detailed comparison of Figures 8.23 with 8.24 also reveals that, after the point where the unit step input imposes on the unsprung mass m_2, the trend of each curve in Figure 8.24 is very similar to that of its counterpart in Figure 8.23. Therefore, the previous force analysis for the quarter-vehicle model is also true for the rear secondary suspension of the half-vehicle model.

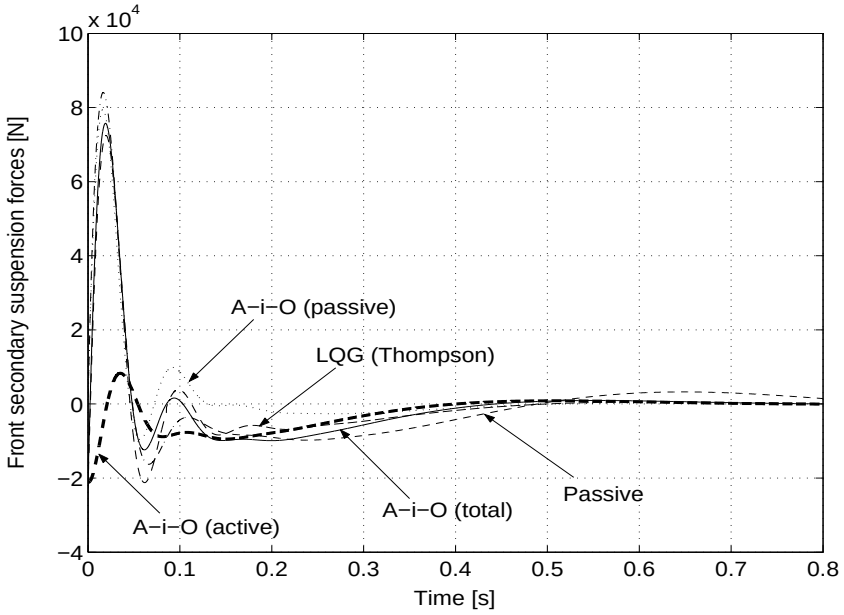

Figure 8.23: Front secondary suspension forces versus time

To quantitatively analyze the vehicle performance based on the A-i-O, LQG, and passive suspension, the numerical results are provided in Table 8.10. The numerical results reveal that the active suspension based on the A-i-O method exhibits superior performance than

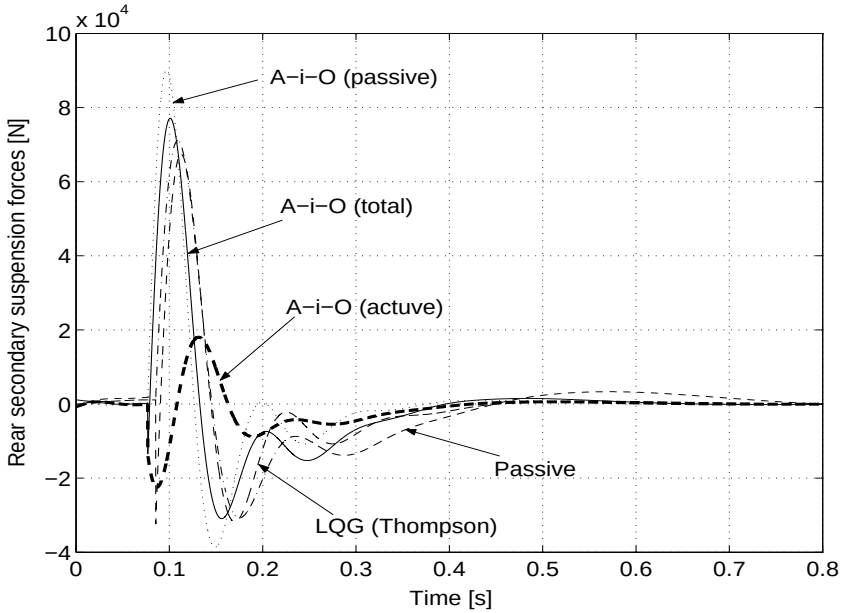

Figure 8.24: Rear secondary suspension forces versus time

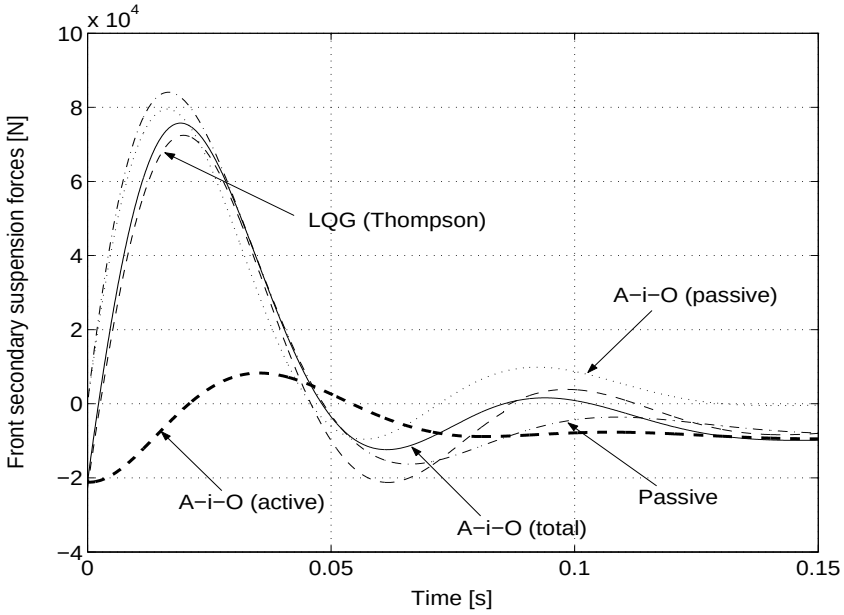

Figure 8.25: Front secondary suspension forces versus time

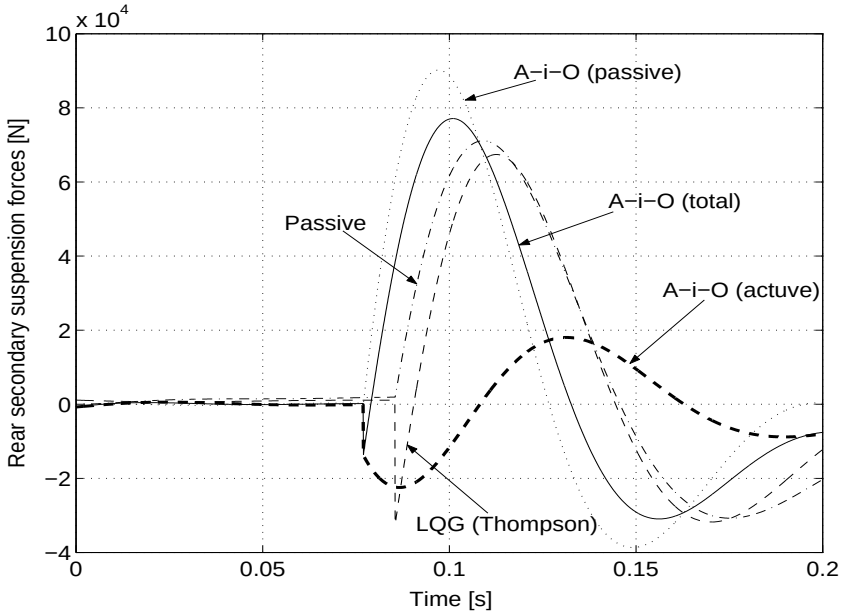

Figure 8.26: Rear secondary suspension forces versus time

its counterpart based on the LQG algorithm and the passive suspension in the mean-square values of front and rear actuator forces, front and rear unsprung mass deflections, front and rear secondary suspension working spaces, accelerations of the vehicle body at points A and B, and pitch angular acceleration of the vehicle body. In short, the active suspension based on the A-i-O method has the best overall performance among the three cases.

8.7.2 Random Track Input Case

Vehicle System Optimization

The vehicle model with flexible vehicle body is illustrated in Figure 8.2. The system governing equations are described in equation set (8.17), the state variable vector $\mathbf{x}_a$ in equation (8.28), actuator force vector $\mathbf{u}$, track excitation vectors $\mathbf{w}$, $\dot{\mathbf{w}}$, and ξ in equation sets (8.27) and (8.5). The relevant system dynamic matrices are determined in equation set (8.29) and the detailed information is listed in Appendix B.

The vehicle system optimization, therefore, can be stated as: minimize the objective

Table 8.10: Comparison of the response characteristics for passive and active suspensions.

	LQG	Passive	A-i-O
m_1 displacement overshoot [%]	28.80	17.05	16.57
m_2 displacement overshoot [%]	37.26	32.79	30.34
Peak front suspension working space $[m]$	-1.1632	-0.9484	-1.0572
Peak rear suspension working space $[m]$	-1.1683	-0.9715	-1.0558
Peak acceleration at point A $[m/s^2]$	277.2731	321.7271	240.1095
Peak acceleration at point B $[m/s^2]$	356.5036	377.8960	326.8214
Peak pitch acceleration $[rad/s^2]$	-152.4799	-166.4148	-141.5128
Peak front actuator force $[N]$	$7.2464 \cdot 10^4$	0.0	$-2.1161 \cdot 10^4$
Peak rear actuator force $[N]$	$6.7411 \cdot 10^4$	0.0	$-2.2465 \cdot 10^4$
Peak passive front suspension force $[N]$	0.0	$8.4080 \cdot 10^4$	$7.9535 \cdot 10^4$
Peak passive rear suspension force $[N]$	0.0	$7.1121 \cdot 10^4$	$9.0198 \cdot 10^4$
Peak total front suspension force $[N]$	$7.2464 \cdot 10^4$	$8.4080 \cdot 10^4$	$7.5759 \cdot 10^4$
Peak total rear suspension force $[N]$	$6.7411 \cdot 10^4$	$7.1121 \cdot 10^4$	$7.7115 \cdot 10^4$
$\int_0^\infty (x_1 - w_1)^2 dt$	0.0134	0.0144	0.0129
$\int_0^\infty (x_3 - w_2)^2 dt$	0.0197	0.0221	0.0176
$\int_0^\infty (x_2 - x_1)^2 dt$	0.0730	0.0728	0.0679
$\int_0^\infty (x_4 - x_3)^2 dt$	0.0682	0.0695	0.0534
$\int_0^\infty \ddot{x}_2^2 dt$	$1.8454 \cdot 10^3$	$2.6789 \cdot 10^3$	$1.3900 \cdot 10^3$
$\int_0^\infty \ddot{x}_4^2 dt$	$4.4921 \cdot 10^3$	$5.7069 \cdot 10^3$	$3.8483 \cdot 10^3$
$\int_0^\infty \ddot{\varphi}^2 dt$	$1.0937 \cdot 10^3$	$1.4312 \cdot 10^3$	$1.0132 \cdot 10^3$
$\int_0^\infty u_1^2 dt$	$1.2595 \cdot 10^8$	0.0	$1.9019 \cdot 10^7$
$\int_0^\infty u_2^2 dt$	$1.6164 \cdot 10^8$	0.0	$2.2853 \cdot 10^7$
$\int_0^\infty f_{1pass}^2 dt$ †	0.0	$1.8376 \cdot 10^8$	$1.3538 \cdot 10^8$
$\int_0^\infty f_{2pass}^2 dt$ ‡	0.0	$2.0584 \cdot 10^8$	$2.4395 \cdot 10^8$
$\int_0^\infty (u_1 + f_{1pass})^2 dt$	$1.2595 \cdot 10^8$	$1.8376 \cdot 10^8$	$1.3867 \cdot 10^8$
$\int_0^\infty (u_2 + f_{2pass})^2 dt$	$1.6164 \cdot 10^8$	$2.0584 \cdot 10^8$	$1.9992 \cdot 10^8$

† f_{1pass} means passive front secondary suspension force;

‡ f_{2pass} means passive rear secondary suspension force.

function:

$$J = \sum_{i=1}^{4} \rho_i J_i \tag{8.57}$$

subject to

$$\begin{cases} \dot{\mathbf{x}}_a = \mathbf{A}_a \mathbf{x}_a + \mathbf{B}_a \mathbf{u} + \mathbf{D}_a \xi \\ \mathbf{y}_a = \mathbf{C}_a \mathbf{x}_a \end{cases} \tag{8.58}$$

where ρ_1 to ρ_4 are weighting factors, J_1 to J_4 are defined in Table 8.11. J_2 stands for mean-square acceleration at three or two body points denoted by L_1, L_2, and L_3 or by L_1 and L_2, which correspond to the left end, right end, and middle point of the vehicle body or the left end and right end of the vehicle body, respectively. Due to the fact that the pitch mode and the first three bending modes of the elastic vehicle body are taken into account, the consideration of the acceleration at just one point is not justified. J_1, J_3, and J_4 are mean-square values of actuator forces, primary and secondary suspension deflections, respectively. To utilize the weighting constants used in the previous quarter-vehicle model with random track input and compare the results from the research with those offered by Hac [60], factors of 1/2 and 1/3 are introduced for the definitions described in Table 8.11. The vehicle system, therefore, is optimized with respect to ride quality, unsprung

Table 8.11: Expressions represented by symbols J_1 to J_4.

J_1	J_2
$E[u_1^2 + u_2^2]/2$	$E\{\sum_{i=1}^{3or2}[\ddot{x}_5 + (L_i - a_2 - b_2)\ddot{\varphi} + \sum_{j=1}^{3}\ddot{\Phi}_j(t)Z_j(L_i)]^2\}/3$
J_3	J_4
$E\{[x_1 - w(t-D)]^2 + [x_3 - w(t)]^2\}/2$ †	$E[(x_2 - x_1)^2 + (x_4 - x_3)^2]/2$

† $w(t-D) = w_1$; $w(t) = w_2$.

mass dynamic loads, and secondary suspension working spaces while the expenditure of actuator forces is limited.

As mentioned previously, to find the solution to the optimization problem, equation (8.57) should be rewritten in the standard matrix format as shown in equation (8.30).

Validation of the Simulation Results

In the research, using the LQG algorithm, the vehicle model (half-vehicle model with flexible vehicle body), and the system parameters provided by Hac [60], numerical simulations were performed. Unfortunately, the simulation results reported by Hac could not be repeated. Expressed in terms of state and control variables and expanded in Maple [70] symbolic form, the objective function for the flexible vehicle model in equation (8.57) covers 372 pages ($A4$ paper). The complex and lengthy objective function seems to be the reason why Hac's numerical results do not agree with those from the research. Thus, the validation of the simulation results from the research becomes necessary.

To validate the simulation results from the research, the numerical results based on a modified half-vehicle model are verified by those based on a simple quarter-vehicle model. As mentioned previously, based on the LQG algorithm, the quarter-vehicle model, and the system parameters used by Hac [59], Hac's results were accurately repeated in the research.

To facilitate the validation, the vehicle body is assumed to be a rigid body and the geometric parameter (b_2) and the pitch moment of inertia (I_c) of the vehicle body are set to $0.0[m]$ and $1.6 \cdot 10^5[kg \cdot m^2]$ instead of the nominal values of $2.0[m]$ and $1.2 \cdot 10^5[kg \cdot m^2]$ respectively so that the front and rear suspensions of the modified vehicle model are inertially de-coupled. The rest of the vehicle system parameters take their nominal values. Furthermore, it is assumed that, during the simulation, the time delay between the track input imposed on the front unsprung mass and that on the rear unsprung mass should be neglected. Thus, using the lumped mass method, we obtain the modified half-vehicle model which is equivalent to two independent identical quarter-vehicle models. For the equivalent quarter-vehicle models, the sprung mass takes the value of $5000.0[kg]$ and the rest system parameters take the values of those of the modified half-vehicle model.

The objective function for the modified half-vehicle model is the same as that described in equation (8.57) except that the terms relevant to the bending modes of the flexible vehicle body are set to zeros and J_2 is defined as $E[\ddot{x}_2^2 + \ddot{x}_4^2]/2$. The objective function of the corresponding quarter-vehicle model is the same as that described in equation (8.54).

Assume the velocity of both the modified half-vehicle model and the corresponding quarter-vehicle model $V = 20.0[m/s]$ and the coefficients in formula (8.3) describing track irregularities $a_t = 0.45[m^{-1}]$ and $\sigma_t = 3.0 \cdot 10^{-4}[m^2]$. For both the modified half-vehicle

model and the equivalent quarter-vehicle model, with the weighting factors $\rho_2 = 1$, $\rho_3 = 10^5$, and $\rho_4 = 10^4$, based on the LQG algorithm, we can obtain the results illustrated in Table 8.12.

Table 8.12: Comparison of the simulation results for the modified half-vehicle model and the equivalent quarter-vehicle model.

Equivalent Quarter–Vehicle Model					
ρ_1	$J/10^6$	J_1 $[N^2]$	$J_2/10^6$ $[mm^2/s^4]$	$J_3/10$ $[mm^2]$	$J_4/10^2$ $[mm^2]$
10^6	22.67194237	$6.11420577 \cdot 10^{-7}$	4.44329323	14.1729511	4.05569743
10^2	22.66585547	60.60964055	4.44333608	14.1701350	4.04632342
10^0	22.23322899	$3.25419349 \cdot 10^5$	4.49419024	13.9139521	3.49966726
10^{-2}	20.16447360	$2.03248582 \cdot 10^7$	6.11463790	11.4086591	2.43792797
10^{-4}	19.93633651	$2.62068886 \cdot 10^7$	6.44708294	11.0998273	2.38680554
Modified Half-Vehicle Model					
ρ_1	$J/10^6$	J_1 $[N^2]$	$J_2/10^6$ $[mm^2/s^4]$	$J_3/10$ $[mm^2]$	$J_4/10^2$ $[mm^2]$
10^6	22.67194237	$6.11420576 \cdot 10^{-7}$	4.44329323	14.1729511	4.05569743
10^2	22.66585547	60.60964053	4.44333608	14.1701350	4.04632342
10^0	22.23322899	$3.25419349 \cdot 10^5$	4.49419024	13.9139521	3.49966726
10^{-2}	20.16447360	$2.03248583 \cdot 10^7$	6.11463791	11.4086591	2.43792797
10^{-4}	19.93633651	$2.62068886 \cdot 10^7$	6.44708294	11.0998273	2.38680554

The comparison of the simulation results shown in Table 8.12 demonstrates that the simulation results for the modified half-vehicle model accurately matches those for the equivalent quarter-vehicle model. Therefore, at least the rigid body half-vehicle model and the corresponding objective function are validated. This validated rigid body half-vehicle model and objective function can be used to serve as a reference to check the simulation results of the corresponding half-vehicle model with the flexible vehicle body.

To check the simulation results of the half-vehicle model with the flexible vehicle body with those based on the validated rigid body half-vehicle model, assume that for both vehicle models, the vehicle system parameters are set to their nominal values as listed in Table B.2 in Appendix B; the objective function takes the form described in equation (8.57); the random track characteristic parameters, vehicle speed, and the weighting factors ρ_2, ρ_3, ρ_4 take the values offered previously in the subsection; the time delay between the

Table 8.13: Comparison of the simulation results for the rigid half-vehicle model and the flexible half-vehicle model.

Flexible Half-Vehicle Model					
ρ_1	$J/10^6$	J_1 $[N^2]$	$J_2/10^6$ $[mm^2/s^4]$	$J_3/10$ $[mm^2]$	$J_4/10^2$ $[mm^2]$
10^6	27.0252	$5.3235 \cdot 10^{-7}$	8.8036	14.3577	3.8638
10^2	27.0199	52.7369	8.8018	14.3570	3.8558
10^0	26.6553	$2.6311 \cdot 10^5$	8.7125	14.2882	3.3915
10^{-2}	25.4346	$7.9631 \cdot 10^6$	9.2387	13.4871	2.6290
10^{-4}	25.3494	$9.2990 \cdot 10^6$	9.3393	13.4105	2.5987
Rigid Half-Vehicle Model					
ρ_1	$J/10^6$	J_1 $[N^2]$	$J_2/10^6$ $[mm^2/s^4]$	$J_3/10$ $[mm^2]$	$J_4/10^2$ $[mm^2]$
10^6	26.3059	$5.5123 \cdot 10^{-7}$	8.1317	14.2957	3.8785
10^2	26.3004	54.6229	8.1298	14.2947	3.8704
10^0	25.9181	$2.8002 \cdot 10^5$	8.0441	14.1904	3.4036
10^{-2}	24.4349	$1.2310 \cdot 10^7$	8.7743	12.9029	2.6347
10^{-4}	24.2985	$1.5485 \cdot 10^7$	8.9541	12.7367	2.6062
Rigid Half-Vehicle Model with Time Delay					
ρ_1	$J/10^6$	J_1 $[N^2]$	$J_2/10^6$ $[mm^2/s^4]$	$J_3/10$ $[mm^2]$	$J_4/10^2$ $[mm^2]$
10^6	26.2340	$5.3767 \cdot 10^{-7}$	8.3051	14.2878	3.7129
10^2	26.2277	53.2799	8.3031	14.2865	3.7055
10^0	25.7958	$2.7273 \cdot 10^5$	8.2043	14.1648	3.2763
10^{-2}	24.2993	$1.2204 \cdot 10^7$	8.8644	12.8224	2.6261
10^{-4}	24.1704	$1.5376 \cdot 10^7$	9.0365	12.6568	2.6036

random track input imposed on the front unsprung mass and that on the rear unsprung mass is neglected. Based on the LQG algorithm, we can obtain the simulation results offered in Table 8.13.

The comparison of the results offered in Table 8.13 shows that the simulation results based on the flexible vehicle model are consistent with those based on the rigid vehicle model. The average performance index J of the flexible vehicle model is about 3.4% higher than that of the rigid vehicle model. This difference results from the fact that the first three bending modes of the flexible vehicle body degrade the overall performance of the flexible vehicle model. This overall performance degradation of the flexible vehicle model

also reflects on the higher partial performance indices of the acceleration and unsprung mass displacement of the model than those of the rigid vehicle model.

To investigate the effect of the time delay on the performance of the vehicle models, the simulation results with time delay for the rigid half-vehicle model are also provided in Table 8.13. The simulation results show that, with the time delay considered, the overall performance improves and demonstrates that "the time delay available between the front and rear inputs appears to provide, in principle, an excellent opportunity to improve the rear axle actuator control" [61]. However, under the given simulation conditions, the degree of performance improvement is not high. However, numerical experiments show that if the weighting factors $\rho_1 = 10^{-8}$, $\rho_2 = 1.0$, $\rho_3 = 10^4$, and $\rho_1 = 10^3$, the performance index J with time delay is 6.222% lower than that without time delay.

It should be mentioned that with the time delay considered, by using the LQG algorithm, we should calculate the required transition matrix. In the case of the rigid half-vehicle model, the calculation of the transition matrix in Matlab does not converge until the 60^{th} term of the series is reached. However, in the case of the flexible half-vehicle model, the calculation of the corresponding transition matrix does not converge even when the 80^{th} term of the series is reached. When the calculation is carried out until the 100^{th} term of the series, the result overflows.

Therefore, it seems that it is not practical to calculate the transition matrix for complicated vehicle dynamic models when the time delay is considered. To circumvent the calculation of transition matrix, the Pade approximation method is recommended [61], but additional state variables should be introduced. In the next subsection, the numerical simulations for the half-vehicle model with flexible vehicle body are restricted to the case where the time delay is not taken into account.

Results and Discussion

In this subsection, for the half-vehicle model with flexible vehicle body and without the time delay between front input and rear input, the numerical simulation results based on the A-i-O method are compared with those based on the LQG algorithm. As will be seen, the optimized vehicle system derived from the A-i-O method is superior to that based on the LQG algorithm in the aspects of ride comfort, suspension working spaces, and dynamic

wheel loads with almost the same power consumption.

In the A-i-O method case, the vehicle system parameters EI, ρA, c_3, and c_4 take their nominal values, M, m_1, m_2, I_c, k_3, k_4, a_1 ($a_1 = a_2$), and b_2 ($b_2 = l - b_1$) are permitted to vary by 10% from their nominal values, k_1, k_2, c_1, and c_2 are allowed to change by 50% from their nominal values, the standard deviations of the sensors' random errors are taken as $0.06[m/s]$. Note that the nominal system parameters are listed in Table B.2 in Appendix B. The vehicle speed and the random track characteristic parameters are assigned the values offered in the last subsection. The weighting factors are: $\rho_1 = 10^{-8}$, $\rho_2 = 1$, $\rho_3 = 10^5$, and $\rho_4 = 10^4$. By using the A-i-O method, we can obtain the optimal design variables for the half-vehicle model with a flexible vehicle body as listed in Table 8.14. For the purpose of comparison, the corresponding nominal values for these design variables are also provided in the table. The obtained optimal feedback control gain matrix based on the A-i-O together with that based on the LQG are also offered in Table 8.15. Note that in the LQG case, the simulation condition is the same as that of the A-i-O case except that the vehicle system parameters take their nominal values.

Table 8.14: Optimized values for vehicle system design variables.

	$m_1\ [kg]$	$m_2\ [kg]$	$M\ [kg]$	$I_c\ [kg \cdot m^2]$	$a_1\ [m]$	$b_2\ [m]$
NV†	$1.0 \cdot 10^3$	$1.0 \cdot 10^3$	$1.0 \cdot 10^4$	$1.2 \cdot 10^5$	4.0	2.0
A-i-O	900.0	900.0	$1.1 \cdot 10^4$	$1.32 \cdot 10^5$	3.60	1.92
	$k_1\ [N/m]$	$c_1\ [N/m/s]$	$k_2\ [N/m]$	$c_2\ [N/m/s]$	$k_3\ [N/m]$	$k_4\ [N/m]$
NV	$2.0 \cdot 10^5$	$2.0 \cdot 10^4$	$2.0 \cdot 10^5$	$2.0 \cdot 10^4$	$2.0 \cdot 10^6$	$2.0 \cdot 10^6$
A-i-O	$1.258 \cdot 10^5$	$2.035 \cdot 10^4$	$2.134 \cdot 10^5$	$2.767 \cdot 10^4$	$1.8 \cdot 10^6$	$1.8 \cdot 10^6$

† Nominal values.

As mentioned in the quarter-vehicle model case (random track input), the optimized values of the design variables shown in Table 8.14 are almost independent of the weighting factor ρ_1 by using the A-i-O method. Figure 8.27 shows the dependence of the performance index (J) and its parts (J_1, J_2, J_3, J_4) upon the weighting factor ρ_1; Figure 8.28 illustrates the trade-off solutions of weighted R.M.S. vertical body acceleration and weighted R.M.S. wheel dynamic load; Figure 8.29 offers the the trade-off solutions of weighted R.M.S.

Table 8.15: Feedback control gain matrix for optimal suspensions.

	$K_{1,1}/10^5$	$K_{1,2}/10^5$	$K_{1,3}/10^4$	$K_{1,4}/10^5$	$K_{1,5}/10^5$	$K_{1,6}/10^4$	$K_{1,7}/10^5$
A-i-O	9.6089	−5.6295	6.6631	9.4087	−7.9097	−4.8001	6.7035
LQG	4.5908	1.1374	10.3630	2.7474	−2.0241	−2.4724	1.3482
	$K_{1,8}/10^4$	$K_{1,9}/10^7$	$K_{1,10}/10^5$	$K_{1,11}/10^8$	$K_{1,12}/10^7$	$K_{1,13}/10^8$	$K_{1,14}/10^7$
A-i-O	3.2283	−1.0010	−0.9183	5.6463	1.0728	−1.9243	−0.3944
LQG	−0.9422	−1.6119	−1.5065	1.8915	0.3613	−5.8641	−1.1726
	$K_{2,1}/10^5$	$K_{2,2}/10^5$	$K_{2,3}/10^5$	$K_{2,4}/10^5$	$K_{2,5}/10^5$	$K_{2,6}/10^4$	$K_{2,7}/10^5$
A-i-O	−5.6309	8.7313	0.5922	−9.1449	6.7078	3.2284	−7.9004
LQG	1.1373	4.5908	1.0363	−2.7474	1.3482	−0.9422	−2.0241
	$K_{2,8}/10^4$	$K_{2,9}/10^7$	$K_{2,10}/10^5$	$K_{2,11}/10^8$	$K_{2,12}/10^7$	$K_{2,13}/10^8$	$K_{2,14}/10^7$
A-i-O	−4.0671	−1.0019	−0.9506	−5.6463	−1.0724	−1.9240	−0.3936
LQG	−2.4724	−1.6119	−1.5065	−1.8915	−0.3613	−5.8641	−1.1726

vertical body acceleration and weighted R.M.S. suspension working space. Note that the weighted R.M.S. vertical body acceleration, wheel dynamic load, and suspension working space are based on the performance terms J_2, J_3, and J_4, respectively.

Investigation of Figures 8.27, 8.28, and 8.29 demonstrates that as in the case of the quarter-vehicle model, the overall performance of the active suspensions based on the A-i-O method is superior to that based on the LQG. The active suspensions based on the A-i-O method achieves the overall performance improvement at the expense of using larger control forces than those based on the LQG. However, under the above simulation conditions, the total average control power consumption for the A-i-O based active suspensions is just 1.4% higher than that (3.1896$[kw]$) required for the LQG based active suspensions. The reason for this phenomenon is that although the actuators for the A-i-O based suspensions use larger control forces, the relative motions between the sprung mass and the unsprung masses are better controlled than those of the LQG based suspensions. Thus, the rectified average piston velocities of the actuators for the the A-i-O based suspensions are lower than those of the actuators for the LQG based suspensions and the amounts of total average control power consumption for both cases are almost the same. Figure 8.30 provides the relationship between vehicle speed and control power consumption.

Based on equation (8.46), the filtering error covariance matrix $\mathbf{P}$ depends on the sensor

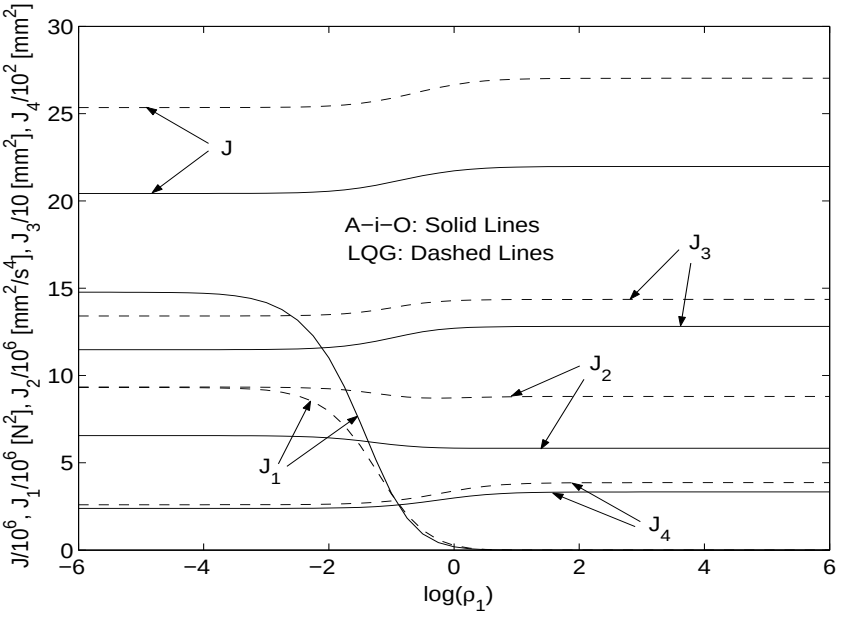

Figure 8.27: Performance index J and its parts J_1, J_2, J_3, and J_4 versus ρ_1

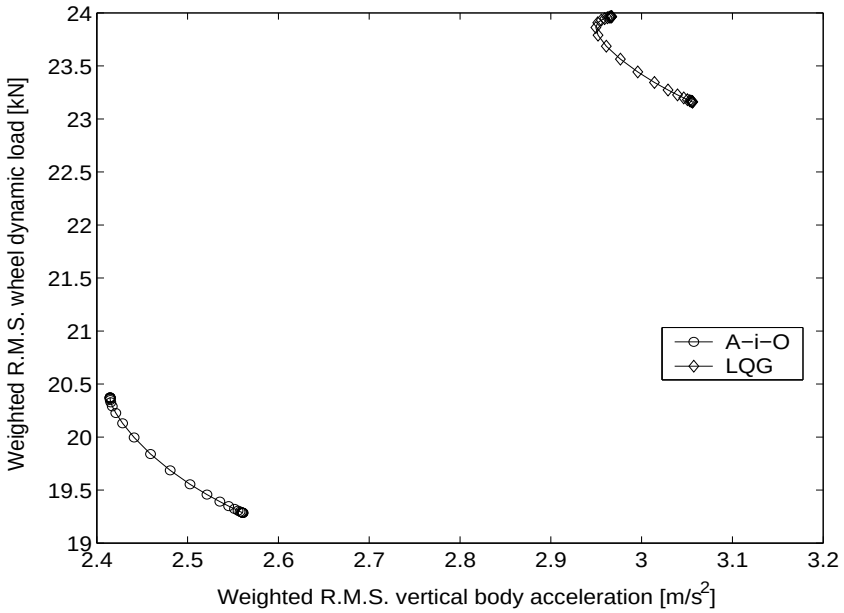

Figure 8.28: R.M.S. trade-off solutions of vertical body acceleration versus dynamic wheel load

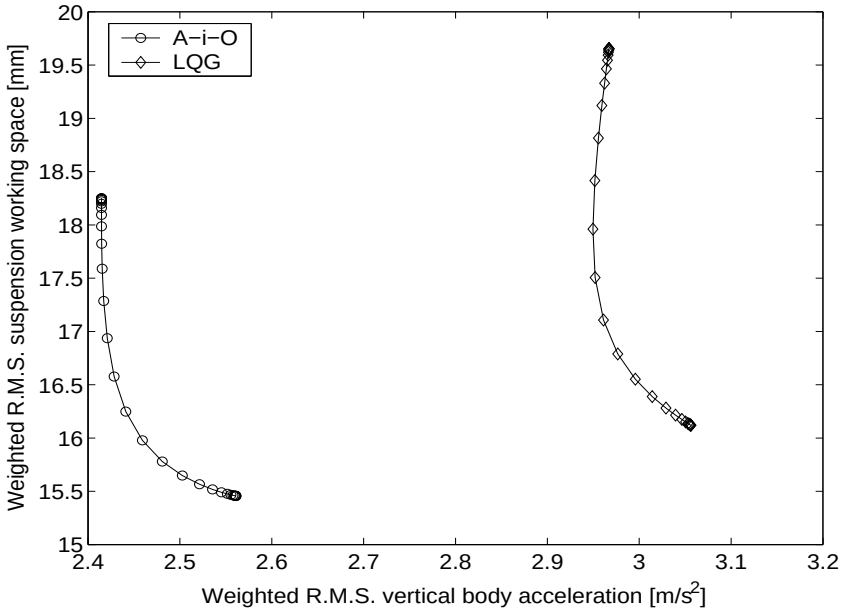

Figure 8.29: R.M.S. trade-off solutions of vertical body acceleration versus suspension working space

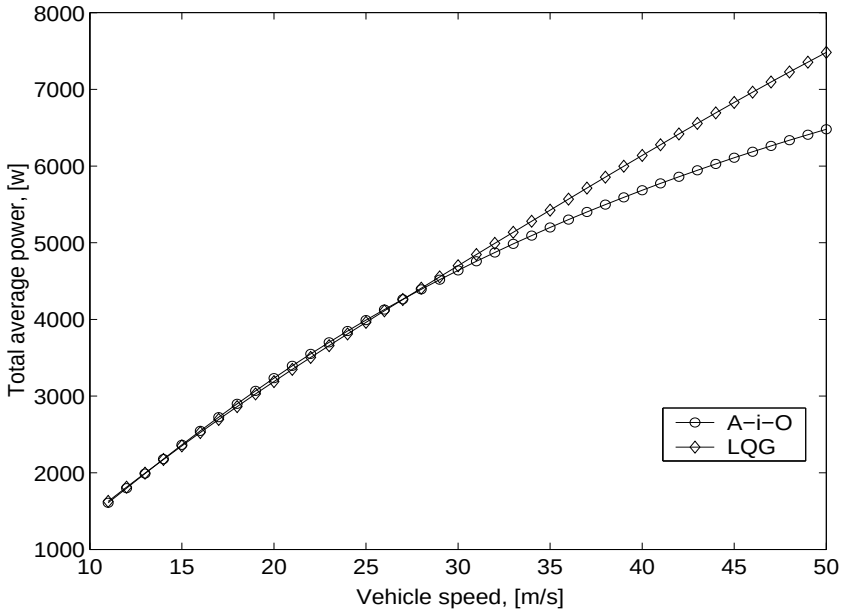

Figure 8.30: Total average control power consumption versus vehicle speed

accuracy due to $\mathbf{R}$ in equation set (8.43) and the sensor arrangement due to $\mathbf{C}_a$ in equation (8.42). According to equation (8.47), as mentioned previously, the performance index J_{opt} contains two parts. The first part, J_Q, arises because of the random track excitations; the second part, J_r, results from inexact state estimation due to the existence of the matrix $\mathbf{P}$. J_r vanishes when $\mathbf{P}$ vanishes. Thus, the two factors, the sensor accuracy and the sensor arrangement, influence J, J_r, and $\mathbf{P}$. Figure 8.31 shows the effect of sensor errors on J, J_r and $\mathbf{P}$ of both the A-i-O based active suspensions and the LQG based active suspensions. Note that the results in Figure 8.31 are based on the sensor arrangement with five sensors measuring the vertical velocities of the front and rear unsprung masses and the vertical velocities at the three vehicle body points, i.e., the left end, the right end, and the middle point.

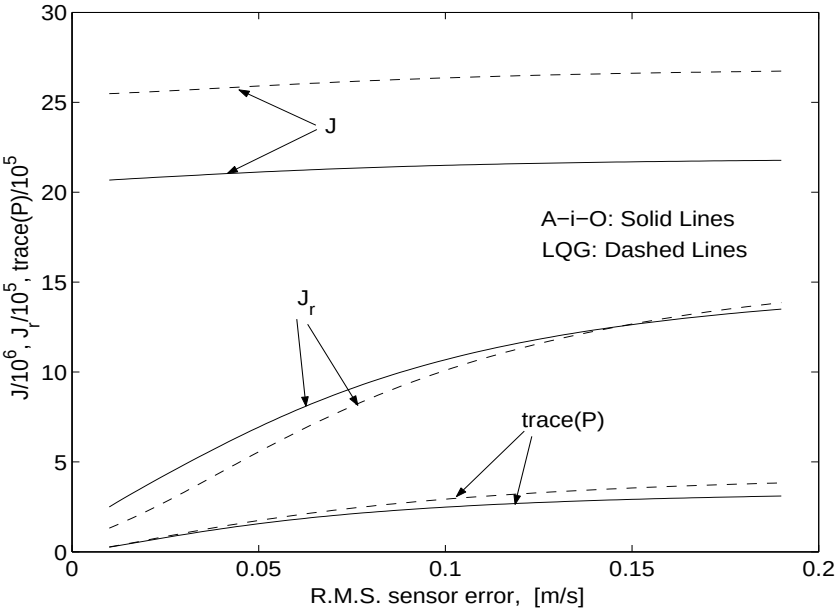

Figure 8.31: Effect of R.M.S. sensor errors on performance indices J, J_r, and $trace(\mathbf{P})$

It is obvious that in both the A-i-O and the LQG cases, as sensor errors increase, J, J_r and $trace(\mathbf{P})$ increase. Over the sensor error range offered, the J and $trace(\mathbf{P})$ based on the A-i-O method are smaller than those based on the LQG algorithm, respectively. However, over the lower sensor error value range, the J_r based on the LQG algorithm is

smaller than that based on the A-i-O method. The reason for the phenomenon is that J_r depends not only on the filtering error covariance matrix $\mathbf{P}$ but also on the control feedback gain matrix $\mathbf{K}$ and weighting matrix $\mathbf{H}$ (see equation (8.47)).

To investigate the influence of sensor arrangement on the state estimation, in this research different sensor arrangements are used. For all the sensor arrangements, two sensors are used to measure the vertical velocities of the front and rear unsprung masses. Numerical experiments show that among all possible combinations of locations for two sensors for measuring the vehicle body vertical velocities, the optimal plan with minimal J_r is the one that the two sensors are located at the right end and the left end of the vehicle body respectively. With the third sensor introduced, the best location is the middle of the vehicle body. This sensor arrangement is consistent with what Hac [60] found:"the body motion consists mainly of vibration connected with the lowest mode and to minimize measurement errors the sensors should be located at extreme points of the functions of these mode shapes". Figure 8.32 offers the relationship between J_r and weighting factor ρ_1 in the A-i-O case when 4 and 5 sensors are used with the above optimal arrangements. With the additional sensor located at the middle of the vehicle body, the value of J_r is lower than that for the 4 sensor arrangement over the lower ρ_1 value range within which the active suspensions take effect.

To examine the behavior of the A-i-O based active suspensions (optimized without Kalman filter at $20.0[m/s]$) at other speeds, the performance indices of acceleration, wheel dynamic deflection, and suspension working space based on the A-i-O are compared with those based on the LQG. Figure 8.33 illustrates the dependence of these performance indices on vehicle speed. Results shown in Figure 8.33 together with those offered in Figure 8.30 demonstrate that the optimized vehicle system based on the A-i-O method is better controlled than that based on the LGQ algorithm in vertical acceleration, wheel dynamic load, and suspension working space with almost the same control power consumption over the lower speed range and with less control power consumption within the higher speed range. It should be noted that the optimized vehicle system based on the A-i-O method achieves the above improvements even though its vehicle body mass (M) is 10% larger than its nominal value.

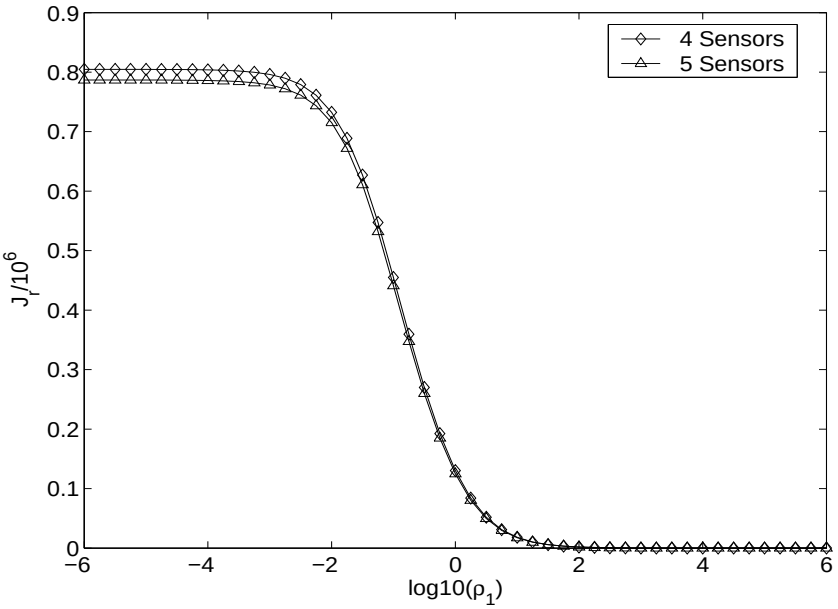

Figure 8.32: Effect of sensor arrangement on J_r

8.8 Summary

This chapter has demonstrated the feasibility and efficacy of applying the A-i-O multidisciplinary optimization method integrating GAs, multibody dynamics, the LQG control strategy, and the Kalman filter algorithm to the design optimization of ground vehicles with active suspensions. The A-i-O method is implemented in a sophisticated simulation environment in such a way that the linear mechanical vehicle model is designed in the A'GEM program, the optimal controller and Kalman estimator are constructed in MATLAB, then the combined system including the mechanical vehicle model, optimal controller, and Kalman estimator is optimized simultaneously by using genetic algorithms.

The A-i-O method is used to resolve the conflicting requirements for ride comfort, suspension working spaces, and dynamic wheel loads in the optimization of quarter-vehicle models and half-vehicle models (with or without vehicle body flexibility) with passive and active suspensions. In the simulations, both random and deterministic track inputs and both perfect measurement of full state variables and limited state variables with Kalman filter cases are considered. The time domain analysis and a systematic covariance analysis

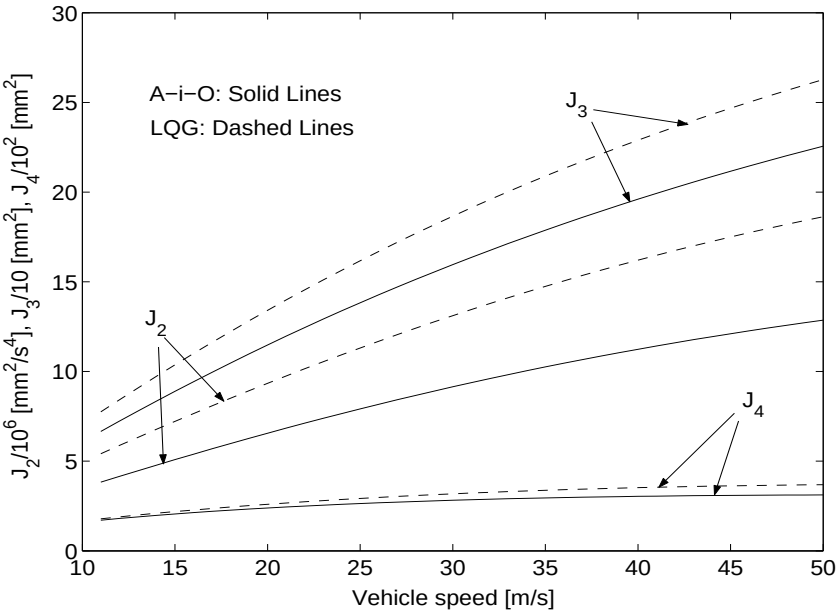

Figure 8.33: Performance indices of acceleration, wheel dynamic deflection, and suspension working space as a function of vehicle velocity

are carried out.

Numerical results show that the optimized vehicle system based on the A-i-O method has better overall performance than that derived using the LQG algorithm not only in ride comfort and suspension working spaces, but also in wheel dynamic loads with almost the same control power consumption over lower speed range and less control power consumption within higher speed range. However, compared with passive suspensions, traditional active vehicle suspension systems often achieve better performance which is a compromise among ride comfort, suspension working space, and wheel dynamic load. These traditional active vehicle suspension systems can rarely improve the vehicle performance in all of these three aspects simultaneously [60]. Furthermore, the numerical results obtained in this research demonstrate that the sequential optimization method, i.e. optimizing the passive vehicle system parameters first then designing controllers for the vehicle active suspensions based on these optimized passive system parameters using the LQG algorithm, can not achieve the results obtained by the A-i-O method. Based on an appropriately selected reference vehicle

dynamic model, by means of normalizing each term of the required objective function, the design optimization using the A-i-O method is greatly facilitated. The simulation results based on the simple quarter-vehicle model can be used not only to analyze the vehicle dynamic behavior qualitatively but also to validate the simulation results based on complex vehicle models. With the co-existence of passive and active components in vehicle suspensions and the design variables determined by using the A-i-O method, the corresponding actuator forces can actively resist track disturbances much longer than the actuator forces based on the case where the corresponding suspensions have no passive elements and the design variables are determined by using the LQG algorithm. Although a vehicle system is optimized at a specified vehicle speed based on the A-i-O method, the resulting overall vehicle performance is still superior to that based on the LQG algorithm.

The above A-i-O method can be applied to the design optimization of complex ground vehicle models with active suspensions. As a continuation of this research, the application of the A-i-O method to the design optimization of a 9 DOF three-dimension rail vehicle model with additional first bending mode and first torsional mode with active suspensions is under way.

Chapter 9

Conclusions

9.1 Introduction

As discussed and identified in Chapter 1, the ultimate objective of the research is to develop a novel methodology for the design optimization of rail vehicles with passive and active suspensions. This goal has been successfully achieved. The feasibility and efficacy of the methodology has been demonstrated by the optimization of the lateral stability, vertical ride quality, curving performance, compatibility of lateral stability and curving performance, and combined mechanical and control system of vehicles with passive and active suspensions. This design methodology and the numerous conclusions drawn from the above numerical experimental practices are believed to be significant contributions to the design optimization of rail vehicles, rail vehicle dynamics, mechatronic systems, and numerical optimization.

In this chapter, the achievements of the research are addressed and the related areas for future research are proposed.

9.2 Proposed Design Optimization Methodology

The methodology for the design optimization of rail vehicles with passive and active suspensions was proposed and developed in the research program. The essence of this methodology

is that:

- The effective dynamic system modelling technique (multibody dynamics) is utilized for the generation of complex realistic objective-oriented models (e.g. lateral stability models, curving performance models, etc.).
- By means of multidisciplinary optimization methods, these coupled objective-oriented models and/or additional control systems are integrated as a synergistic whole.
- With the scalarization technique, a vector optimization problem is converted into a scalar optimization problem.
- With a genetic algorithm used at system level and the appropriately selected search algorithms used at subsystem level, the passive and/or active design variables are optimized simultaneously.

Numerical experiments demonstrated the feasibility and efficacy of the proposed design optimization methodology for resolving conflicting design requirements. This methodology is suitable for complex design optimization problems where:

1. There is interaction between different systems or analysis disciplines.
2. There are multiple design criteria.
3. There are multiple local optima.
4. No matter whether the scalar objective function is continuous or discontinuous, there is no need for sensitivity analysis for the system solver or the GA.
5. There are multiple design variables.

The limitation of the application of the methodology is that the associated computational burden is heavy. However, parallel processing, for which the methodology is ideally suited, could be used for reducing the computer time required for the optimization.

Although the methodology was originally intended for the design optimization of rail vehicles with passive and active suspensions, this general design methodology is also applicable to the design of other complex dynamic systems, e.g. automobile systems, robots, and other mechatronic systems, with little modification.

9.3 Optimization Methods and Algorithms

The proposed hybrid method, i.e. the combination of the All-in-One and Individual Discipline Feasible methods, extends the spectrum of existing multidisciplinary optimization formulation methods. The hybrid method is especially suitable for the design problem where, in addition to the interaction between systems or analysis disciplines, there is also strong interaction between subsystems or subdisciplines within a system or discipline. This hybrid method illustrated its effectiveness in resolving the conflicting requirements from the lateral stability, vertical ride quality, and curving performance in the design optimization of a rail vehicle with passive and active suspension.

Based on the results from the comparative study of optimization algorithms used in rail vehicle suspension design, the GA is an effective optimization algorithm when numerical multibody dynamics programs, such as A'GEM, are introduced into the design optimization. In addition to its high reliability for finding the global optimum, the other advantage of using GAs is that the algorithms can be directly combined with the included multibody dynamics program, without the need for additional sensitivity analyses. In contrast, for traditional gradient-guided algorithms, such as SQP, whether or not the multibody dynamics program can be successfully included into the design optimization depends on finding an effective link between the algorithm and the multibody dynamics program for sensitivity analyses. An efficient and reliable procedure for computing gradients is vital to these algorithms. Numerical experiments showed that in order to ensure the effectiveness of SQP, even for local optimum searching, sensitivity analysis and scaling the optimization problems concerned are necessary and important steps. When the SQP works with a numerical multibody dynamics program, if the dynamic system model is a linear model and the objective and constraint functions are algebraic functions in terms of design variables, the numerical differentiation technique can be used to offer reliable gradients for SQP. Choosing an appropriate difference interval for specific design variables and using suitable scaling schemes for the optimization problem are important for the numerical differentiation technique.

When both SQP and Simplex are used for optimizing complicated numerical multibody models, the corresponding problems are usually highly nonlinear problems with multiple local optima. With the increase of the number of design variables, the reliability of these

algorithms to find the global optimum decreases. For a simple analytical model, where the objective function and constraint functions can be explicitly expressed in terms of design variables and these functions are smooth, SQP outperforms Simplex and GA. In both computation efficiency and reliability for global search, Simplex is generally a compromise option between SQP and GA.

9.4 Rail Vehicle Dynamics

The approach (using the SQP algorithm) proposed by Baumal, McPhee and Calamai [12] for automatically identifying the critical speed of rail vehicles was investigated by optimizing the lateral stability of a rail vehicle model with 17 DOF. The author developed a novel approach by extending the existing SQP approach to include the dynamic mode tracking (DMT) technique proposed by Anderson [7]. This novel approach is more reliable than the SQP approach for identifying the critical speed. This new method converts a stability problem into a dynamic mode tracking and a nonlinear programming problem by using SQP and DMT instead of the Routh-Hurwitz criteria for this purpose for almost a century. Since the governing equations similar to those of rail vehicles are found in rotor dynamics, wind turbine dynamics, aeronautics, and road vehicle dynamics [82], the integrated approach using multibody dynamics, SQP and DMT can also be applied to these problems in identifying the corresponding stability limit automatically.

The existence of sharply-discontinuous "cliffs" in the plots of critical speed versus suspension stiffness was identified and originally interpreted using a modal analysis technique. This sharp discontinuity in the critical speed occurs when the least-damped mode (eigenvector) determining the critical speed switches. In recognition of the cliff phenomenon, the definition of critical speed is generalized in this thesis to make it a more practical measure of lateral stability.

In the design optimization of a rail vehicle with respect to the lateral stability, curving performance, and vertical ride quality, the resulting EP-optimal sets clearly demonstrated that the vertical ride quality is almost independent of both lateral stability and curving performance. This interesting numerical result coincides with the statement [54]: "It has been observed that a relatively weak coupling exists between the vertical and lateral

motions of a vehicle ...".

9.5 Rail Vehicle Design

Numerical results illustrated that compared with inertial and suspension (stiffness and damping) parameter sets, the geometric parameter set has the most significant effect on lateral stability, curving performance, and vertical quality. By means of the GA, the sampling distribution of each design variable can be investigated, important design variables can be identified, and a design variable's global performance and sensitivity over its whole feasible domain can be judged. In the design of rail vehicle curving performance, the parameter study showed that the combination of angle of attack and L/V (lateral to vertical contact forces) ratio is an effective curving performance design criterion. With the multidisciplinary, multicriteria, and multimodel design approach developed in the study, a clear picture of the trade-off relationship between the conflicting design criteria of the lateral stability and curving performance of a rail vehicle can be obtained. Numerical experiments showed that this design approach can be used to automate the process of selecting design variables for improving the compatibility of the fundamental conflicting design criteria.

9.6 Mechatronic Vehicle Suspensions

A novel design optimization approach using the A-i-O method to mechatronic vehicle suspensions was proposed, developed, and tested by numerical experiments. This design optimization approach is an application of the above design optimization methodology to mechatronic vehicle suspensions. The A-i-O multidisciplinary optimization method makes the dynamic vehicle model, the LQG controller, and the Kalman filter a synergistic whole. The GA is utilized as an optimization solver at system level to coordinate the above coupled analysis disciplines and find the optimized design variables including passive mechanical and active control variables.

Numerical results showed that:

- A sequential optimization method, i.e. optimizing the passive mechanical system first then, based on the optimized mechanical vehicle system, using the LQG to determine

optimal controller, can not achieve the results obtained by the proposed approach.

- The optimized vehicle system based on the proposed approach has better overall performance than that derived based on the LQG in all three aspects including ride comfort, suspension working spaces, and wheel dynamic loads.

- With the co-existence of passive and active components in vehicle suspensions and the design variables determined by using the proposed approach, the corresponding actuator forces can actively resist track disturbance much longer than the actuator forces based on the case where the corresponding suspensions have no passive elements and the design variables are determined by using the LQG.

The proposed design optimization approach is applicable to the design optimization of complex three-dimensional ground vehicle models with active suspensions.

9.7 Directions for Future Research

To improve the design optimization methodology (shown in the thesis) for dynamic multibody systems, extend the applications of the methodology, and make use of the results obtained in the research as guidelines, several directions for future research are recommended.

1. **Implemention in Parallel Computational Environment**. The current applications of the design optimization methodology and the corresponding results are based on the numerical simulations performed on the SGI workstation in the Systems Modelling and Simulation Lab at the University of Waterloo. As discussed previously in the framework of the methodology, a GA is applied as the optimizer at the system level. With the parallelism property of GAs, the methodology is suitable for applications using massively-parallel computers. If the current applications are implemented in a massively-parallel computer system, the computation time could easily be reduced approximately by a factor of the population size of the GA.

2. **Application to the Design Optimization of Road Vehicles with an Integrated Control System**. Conventionally, for road vehicles, the anti-lock brake

system (ABS) and anti-slip control (ASC+T, T means traction) system, four-wheel steering (4WS) system, and active suspension system are controlled individually. The three systems of ABS/ASC+T, 4WS, and active suspension are based on three different directions of road vehicle dynamics, i.e. longitudinal, lateral, and vertical, respectively. Today, road vehicle dynamics is developed to a stage where researchers are trying to find an effective method to coordinate the three control systems and derive an integrated control system [3, 44, 81, 89, 98, 121, 128]. The design optimization methodology proposed in the thesis has already been successfully applied to the design of rail vehicle suspensions using two lateral dynamic models (an stability model and a curving model) and a vertical dynamic model. Moreover, with the methodology, the mechanical system and control system can be optimized simultaneously. The design optimization methodology is readily applicable to the design optimization of road vehicles with an integrated control system.

3. **Development of Algorithms for Automatically Identifying Stability Limit Based on Nonlinear Analysis**. Since the equations of motion of a rail vehicle are nonlinear, it seems more realistic to analyze the lateral stability of the rail vehicle using a nonlinear dynamic model than using a linear model. A few researchers have reported their work in the areas of rail vehicle nonlinear stability in the past two decades [55, 64, 104, 133, 134, 135]. To optimize the hunting stability automatically, the algorithms for identifying the corresponding stability limit based on nonlinear analysis are necessary. The algorithms developed in the study are based on the linear stability analysis, but they could likely be modified to apply to the nonlinear case.

4. **Application to other Stability Problems**. The numerical experiments shown in the thesis has demonstrated the feasibility and efficacy of the algorithm using the SQP and DMT for automatically identifying the critical speed of rail vehicles. Since the governing equations (with an asymmetric stiffness matrix) similar to those of rail vehicles are found in rotor dynamics, wind turbine dynamics, aeronautics, and road vehicle dynamics [82], the algorithm can also be applied to these problems for identifying the corresponding stability criterion automatically. Furthermore, when

the algorithm is combined with a GA and a multibody dynamics software package, e.g. ADAMS, the resulting combined approach can be applied to these problems in searching the design variables for optimizing the corresponding stability.

5. **Variable Geometry Active Suspensions for Rail Vehicles**. The numerical results obtained in the study demonstrated that, compared with inertial and suspension (stiffness and damping) parameter sets, the geometric parameter set has the most significant effect on the lateral stability, curving performance, and vertical ride quality. For conventional rail vehicles, however, these geometric parameters are fixed once the vehicle is designed and manufactured and they can not be changed with the operating conditions. It seems natural to expect that by varying the relevant geometric parameters with operating conditions, the rail vehicle may achieve better performance. In recent years, Sharp and Watanabe [118, 137] have done pioneer research on investigating variable geometry active suspension systems for passenger cars and motorcycles. To control the leverage ratio between spring/damper unit and wheel for a road vehicle, Watanabe and Sharp [137] derived a control system based on a half-vehicle model. In developing the control system, both roll and jacking responses of the car body were considered. Simulation results showed that variable geometry suspensions have a capacity to give very good suspension performance without too much additional weight and with very modest power consumption. Moreover the control and mechanical implementation of the variable geometry active suspension system were reported to be practically feasible. These interesting results might encourage and motivate researchers in rail vehicle dynamics to perform research on this novel active suspension system for improving rail vehicle performance.

Appendix A

Rail Vehicle Dynamic System Parameters and Matrices

A.1 Wheel/Rail Contact Data for the 17 DOF Model

Table A.1 below presents the wheel/rail contact data for the 17 DOF model used in Chapter 4.

Table A.1: Wheel/rail contact data for the 17 DOF model

Normal load on a wheel, $W = 5.36 \cdot 10^4[N]$; Wheel rolling radius, $r_0 = 0.356[m]$; Wheel transverse radius, $r_w = 1.0 \cdot 10^{30}[m]$; Rail transverse radius, $r_r = 0.356[m]$;	Poisson's ratio (for both wheel and rail materials), $\sigma = 0.28$; Young's modulus (for both wheel and rail materials), $E = 2.0685 \cdot 10^{11}[N/m^2]$.
Longitudinal creep coefficient, $f_{11} = 8.6605 \cdot 10^6[N]$; Lateral/spin creep coefficient, $f_{23} = 1.5334 \cdot 10^4[N]$;	Lateral creep coefficient, $f_{22} = 7.5848 \cdot 10^6[N]$; Spin creep coefficient, $f_{33} = 61.560[N \cdot m^2]$.

A.2 Nominal Design Variables for the 17, 20, 21, and 36 DOF Models

Table A.2 below offers the nominal design variables for the 17 DOF model (in Chapters 4 and 7), 20 DOF model (in Chapter 5), 21 DOF model (in Chapters 6 and 7), and 36 DOF model (in Chapters 4 and 7).

Table A.2: Nominal design variables for the 17, 21, 20, and 36 DOF models [53].

(1) Inertial property parameters:	Longitudinal damping, $c_{2x} = 0.0[N/m/s]$;
Wheelset mass, $M_w = 1190[kg]$;	Lateral stiffness, $k_{2y} = 1.97 \cdot 10^5[N/m]$;
Wheelset yaw inertia, $I_{wz} = 408[kg \cdot m^2]$;	Lateral damping, $c_{2y} = 4.27 \cdot 10^4[N/m/s]$;
Wheelset spin inertia, $I_{wy} = 200[kg \cdot m^2]$;	Vertical stiffness, $k_{2z} = 6.87 \cdot 10^5[N/m]$;
Bogie mass, $M_b = 3072[kg]$;	Vertical damping, $c_{2z} = 4.27 \cdot 10^4[N/m/s]$.
Bogie yaw inertia, $I_{bz} = 1622[kg \cdot m^2]$;	
Bogie roll inertia, $I_{bx} = 1144[kg \cdot m^2]$;	(4) Geometric Parameters:
Bogie pitch inertia, $I_{by} = 1622[kg \cdot m^2]$;	Half of contact point space, $a = 0.756[m]$;
Carbody mass, $M_c = 3.282 \cdot 10^4[kg]$;	Wheel conicity, $\lambda = 0.1$;
Carbody yaw inertia, $I_{cz} = 1.443 \cdot 10^6[kg \cdot m^2]$;	Half of bogie wheelbase, $b = 1.042[m]$;
Carbody roll inertia, $I_{cx} = 5.317 \cdot 10^4[kg \cdot m^2]$;	Half of bogie space, $L_1 = 8.23[m]$;
Carbody pitch inertia,	Half of primary suspension space,
$I_{cy} = 1.443 \cdot 10^6[kg \cdot m^2]$.	$d = 0.586[m]$;
	Half of secondary suspension space,
(2) Primary Suspension Parameters:	$g = 0.813[m]$;
Longitudinal stiffness, $k_{1x} = 3.15 \cdot 10^7[N/m]$;	Vertical distance from bogie center of mass
Longitudinal damping, $c_{1x} = 666[N/m/s]$;	to primary suspension, $L_3 = 0.0[m]$;
Lateral stiffness, $k_{1y} = 3.96 \cdot 10^6[N/m]$;	Vertical distance from bogie center of mass to
Lateral damping, $c_{1y} = 5220[N/m/s]$;	secondary suspension, $L_2 = 0.305[m]$;
Vertical stiffness, $k_{1z} = 2.10 \cdot 10^6[N/m]$;	Vertical distance from carbody center of mass
Vertical damping, $c_{1z} = 9910[N/m/s]$.	to the original point, $L_5 = 1.97[m]$;
	Vertical distance from secondary suspension
(3) Secondary Suspension Parameters:	to the carbody center of mass, $L_4 = 0.815[m]$;
Longitudinal stiffness, $k_{2x} = 0.0[N/m]$;	Wheel nominal rolling radius, $r_0 = 0.356[m]$.

A.3 Nominal Design Variables for the 20 DOF Model

Table A.3 below presents the nominal design variables for the 20 DOF model used in Chapter 4.

Table A.3: Nominal design variables for the 20 DOF model [136].

(1) Inertial property parameters:	Longitudinal damping, $c_{2x} = 0.0[N/m/s]$;
Wheelset mass, $M_w = 1000[kg]$;	Lateral stiffness, $k_{2y} = 0.55 \cdot 10^6[N/m]$;
Wheelset yaw inertia, $I_{wz} = 350[kg \cdot m^2]$;	Lateral damping, $c_{2y} = 1.5 \cdot 10^4[N/m/s]$;
Wheelset spin inertia, $I_{wy} = 200[kg \cdot m^2]$;	Vertical stiffness, $k_{2z} = 0.55 \cdot 10^6[N/m]$;
Bogie mass, $M_b = 1200[kg]$;	Vertical damping, $c_{2z} = 4.0 \cdot 10^4[N/m/s]$.
Bogie yaw inertia, $I_{bz} = 550[kg \cdot m^2]$;	
Bogie roll inertia, $I_{bx} = 450[kg \cdot m^2]$;	(4) Geometric Parameters:
Bogie pitch inertia, $I_{by} = 500[kg \cdot m^2]$;	Half of contact point space, $a = 0.756[m]$;
Carbody mass, $M_c = 1.4 \cdot 10^4[kg]$;	Wheel conicity, $\lambda = 0.1$;
Carbody yaw inertia, $I_{cz} = 0.3 \cdot 10^6[kg \cdot m^2]$;	Half of bogie wheelbase, $b = 1.0[m]$;
Carbody roll inertia, $I_{cx} = 2.2 \cdot 10^4[kg \cdot m^2]$;	Half of bogie space, $L_1 = 5.0[m]$;
Carbody pitch inertia,	Half of primary suspension space,
$I_{cy} = 0.25 \cdot 10^6[kg \cdot m^2]$.	$d = 0.55[m]$;
	Half of secondary suspension space,
(2) Primary Suspension Parameters:	$g = 0.6[m]$;
Longitudinal stiffness, $k_{1x} = 0.9 \cdot 10^6[N/m]$;	Vertical distance from bogie center of mass
Longitudinal damping, $c_{1x} = 8500[N/m/s]$;	to primary suspension, $L_3 = 0.0[m]$;
Lateral stiffness, $k_{1y} = 0.45 \cdot 10^7[N/m]$;	Vertical distance from bogie center of mass to
Lateral damping, $c_{1y} = 11000[N/m/s]$;	secondary suspension, $L_2 = 0.25[m]$;
Vertical stiffness, $k_{1z} = 0.25 \cdot 10^7[N/m]$;	Vertical distance from carbody center of mass
Vertical damping, $c_{1z} = 8000[N/m/s]$.	to the original point, $L_5 = 1.2[m]$;
	Vertical distance from secondary suspension
(3) Secondary Suspension Parameters:	to the carbody center of mass, $L_4 = 0.85[m]$;
Longitudinal stiffness, $k_{2x} = 0.15 \cdot 10^6[N/m]$;	Wheel nominal rolling radius, $r_0 = 0.356[m]$.

A.4 The System Matrices for the 17 DOF Lateral Stability Model

Offered below are the mass matrix $\mathbf{M}_{17\times17}$, damping matrix $\mathbf{C}_{17\times17}$, and stiffness matrix $\mathbf{K}_{17\times17}$ used in Chapter 4.

A.4.1 The Nonzero Elements of the Mass Matrix $\mathbf{M}_{17\times17}$

$M_{1,1} = M_w$, $M_{2,2} = I_{wz}$, $M_{3,3} = M_b$, $M_{4,4} = I_{bz}$, $M_{5,5} = I_{bx}$, $M_{6,6} = M_w$, $M_{7,7} = I_{wz}$, $M_{8,8} = M_c$, $M_{9,9} = I_{cz}$, $M_{10,10} = I_{cx}$, $M_{11,11} = M_w$, $M_{12,12} = I_{wz}$, $M_{13,13} = M_b$, $M_{14,14} = I_{bz}$, $M_{15,15} = I_{bx}$, $M_{16,16} = M_w$, $M_{17,17} = I_{wz}$.

A.4.2 The Nonzero Elements of the Damping Matrix $\mathbf{C}_{17\times17}$

$C_{1,1} = 2(c_{1y} + f_{22}/V)$, $C_{1,3} = -2c_{1y}$, $C_{1,4} = -2bc_{1y}$, $C_{2,2} = 2(d^2c_{1x} + a^2f_{11}/V)$, $C_{2,4} = -2d^2c_{1x}$, $C_{3,1} = -2c_{1y}$, $C_{3,3} = 2(2c_{1y} + c_{2y})$, $C_{3,5} = -2L_2c_{2y}$, $C_{3,6} = -2c_{1y}$, $C_{3,8} = -2c_{2y}$, $C_{3,9} = -2L_1c_{2y}$, $C_{3,10} = 2L_4c_{2y}$, $C_{4,1} = -2bc_{1y}$, $C_{4,2} = -2d^2c_{1x}$, $C_{4,4} = 4d^2c_{1x} + 4b^2c_{1y} + 2g^2c_{2x}$, $C_{4,6} = 2bc_{1y}$, $C_{4,7} = -2d^2c_{1x}$, $C_{4,9} = -2g^2c_{2x}$, $C_{5,3} = -2L_2c_{2y}$, $C_{5,5} = 4d^2c_{1z} + 2g^2c_{2z} + 2L_2^2c_{2y}$, $C_{5,8} = 2L_2c_{2y}$, $C_{5,9} = 2L_1L_2c_{2y}$, $C_{5,10} = -2(g^2c_{2z} + L_2L_4c_{2y})$, $C_{6,3} = -2c_{1y}$, $C_{6,4} = 2bc_{1y}$, $C_{6,6} = 2(c_{1y}+f_{22}/V)$, $C_{7,4} = -2d^2c_{1x}$, $C_{7,7} = 2(d^2c_{1x}+a^2f_{11}/V)$, $C_{8,3} = -2c_{2y}$, $C_{8,5} = 2L_2c_{2y}$, $C_{8,8} = 4c_{2y}$, $C_{8,10} = -4L_4c_{2y}$, $C_{8,13} = -2c_{2y}$, $C_{8,15} = 2L_2c_{2y}$, $C_{9,3} = -2L_1c_{2y}$, $C_{9,4} = -2g^2c_{2x}$, $C_{9,5} = 2L_1L_2c_{2y}$, $C_{9,9} = 4(g^2c_{2x} + L_1^2c_{2y})$, $C_{9,13} = 2L_1c_{2y}$, $C_{9,14} = -2g^2c_{2x}$, $C_{9,15} = -2L_1L_2c_{2y}$, $C_{10,3} = 2L_4c_{2y}$, $C_{10,5} = -2(g^2c_{2z} + L_2L_4c_{2y})$, $C_{10,8} = -4L_4c_{2y}$, $C_{10,10} = 4(g^2c_{2z} + L_4^2c_{2y})$, $C_{10,13} = 2L_4c_{2y}$, $C_{10,15} = -2(g^2c_{2z} + L_2L_4c_{2y})$, $C_{11,11} = 2(c_{1y} + f_{22}/V)$, $C_{11,13} = -2c_{1y}$, $C_{11,14} = -2bc_{1y}$, $C_{12,12} = 2(d^2c_{1x} + a^2f_{11}/V)$, $C_{12,14} = -2d^2c_{1x}$, $C_{13,8} = -2c_{2y}$, $C_{13,9} = 2L_1c_{2y}$, $C_{13,10} = 2L_4c_{2y}$, $C_{13,11} = -2c_{1y}$, $C_{13,13} = 2(2c_{1y} + c_{2y})$, $C_{13,15} = -2L_2c_{2y}$, $C_{13,16} = -2c_{1y}$, $C_{14,9} = -2g^2c_{2x}$, $C_{14,11} = -2bc_{1y}$, $C_{14,12} = -2d^2c_{1x}$, $C_{14,14} = 4d^2c_{1x}+4b^2c_{1y}+2g^2c_{2x}$, $C_{14,16} = 2bc_{1y}$, $C_{14,17} = -2d^2c_{1x}$, $C_{15,8} = 2L_2c_{2y}$, $C_{15,9} = -2L_1L_2c_{2y}$, $C_{15,10} = -2(g^2c_{2z} + L_2L_4c_{2y})$, $C_{15,13} = -2L_2c_{2y}$, $C_{15,15} = 4d^2c_{1z} + 2g^2c_{2z} + 2L_2^2c_{2y}$, $C_{16,13} = -2c_{1y}$, $C_{16,14} = 2bc_{1y}$, $C_{16,16} = 2(c_{1y}+f_{22}/V)$, $C_{17,14} = -2d^2c_{1x}$, $C_{17,17} = 2(d^2c_{1x}+a^2f_{11}/V)$.

A.4.3 The Nonzero Elements of the Stiffness Matrix $\mathbf{K}_{17\times17}$

$K_{1,1} = 2k_{1y}$, $K_{1,2} = -2f_{22}$, $K_{1,3} = -2k_{1y}$, $K_{1,4} = -2bk_{1y}$, $K_{2,1} = 2\lambda af_{11}/r_0$, $K_{2,2} = 2(d^2k_{1x}$, $K_{2,4} = -2d^2k_{1x}$, $K_{3,1} = -2k_{1y}$, $K_{3,3} = 2(2k_{1y}+k_{2y})$, $k_{3,5} = -2L_2k_{2y}$, $K_{3,6} = -2k_{1y}$, $K_{3,8} = -2k_{2y}$, $K_{3,9} = -2L_1k_{2y}$, $K_{3,10} = 2L_4k_{2y}$, $K_{4,1} = -2bk_{1y}$, $K_{4,2} = -2d^2k_{1x}$, $K_{4,4} = 4d^2k_{1x} + 4b^2k_{1y} + 2g^2k_{2x}$, $K_{4,6} = 2bk_{1y}$, $K_{4,7} = -2d^2k_{1x}$, $K_{4,9} = -2g^2k_{2x}$, $K_{5,3} = -2L_2k_{2y}$, $K_{5,5} = 4d^2k_{1z} + 2g^2k_{2z} + 2L_2^2k_{2y}$, $K_{5,8} = 2L_2k_{2y}$, $K_{5,9} = 2L_1L_2k_{2y}$, $K_{5,10} = -2(g^2k_{2z} + L_2L_4k_{2y})$, $K_{6,3} = -2k_{1y}$, $K_{6,4} = 2bk_{1y}$, $K_{6,6} = 2k_{1y}$, $K_{6,7} = -2f_{22}$, $K_{7,4} = -2d^2k_{1x}$, $K_{7,6} = 2\lambda af_{11}/r_0$, $K_{7,7} = 2d^2k_{1x}$, $K_{8,3} = -2k_{2y}$, $K_{8,5} = 2L_2k_{2y}$, $K_{8,8} = 4k_{2y}$, $K_{8,10} = -4L_4k_{2y}$, $K_{8,13} = -2k_{2y}$, $K_{8,15} = 2L_2k_{2y}$, $K_{9,3} = -2L_1k_{2y}$, $K_{9,4} = -2g^2k_{2x}$, $K_{9,5} = 2L_1L_2k_{2y}$, $K_{9,9} = 4(g^2k_{2x} + L_1^2k_{2y})$, $K_{9,13} = 2L_1k_{2y}$, $K_{9,14} = -2g^2k_{2x}$, $K_{9,15} = -2L_1L_2k_{2y}$, $K_{10,3} = 2L_4k_{2y}$, $K_{10,5} = -2(g^2k_{2z} + L_2L_4k_{2y})$, $K_{10,8} = -4L_4k_{2y}$, $K_{10,10} = 4(g^2k_{2z} + L_4^2k_{2y})$, $K_{10,13} = 2L_4k_{2y}$, $K_{10,15} = -2(g^2k_{2z} + L_2L_4k_{2y})$, $K_{11,11} = 2k_{1y}$, $K_{11,13} = -2k_{1y}$, $K_{11,14} = -2bk_{1y}$, $K_{12,11} = 2\lambda af_{11}/r_0$, $K_{12,12} = 2d^2k_{1x}$, $K_{12,14} = -2d^2k_{1x}$, $K_{13,8} = -2k_{2y}$, $K_{13,9} = 2L_1k_{2y}$, $K_{13,10} = 2L_4k_{2y}$, $K_{13,11} = -2k_{1y}$, $K_{13,13} = 2(2k_{1y} + k_{2y})$, $K_{13,15} = -2L_2k_{2y}$, $K_{13,16} = -2k_{1y}$, $K_{14,9} = -2g^2k_{2x}$, $K_{14,11} = -2bk_{1y}$, $K_{14,12} = -2d^2k_{1x}$, $K_{14,14} = 4d^2k_{1x} + 4b^2k_{1y} + 2g^2k_{2x}$, $K_{14,16} = 2bk_{1y}$, $K_{14,17} = -2d^2k_{1x}$, $K_{15,8} = 2L_2k_{2y}$, $K_{15,9} = -2L_1L_2k_{2y}$, $K_{15,10} = -2(g^2k_{2z} + L_2L_4k_{2y})$, $K_{15,13} = -2L_2k_{2y}$, $K_{15,15} = 4d^2k_{1z} + 2g^2k_{2z} + 2L_2^2k_{2y}$, $K_{16,13} = -2k_{1y}$, $K_{16,14} = 2bk_{1y}$, $K_{16,16} = 2k_{1y}$, $K_{17,14} = -2d^2k_{1x}$, $K_{17,16} = 2\lambda af_{11}/r_0$, $K_{17,17} = 2d^2k_{1x}$.

Appendix B

Vehicle Dynamic System Parameters and Matrices

B.1 Half-Vehicle Model System Parameters Used in Chapter 8

The vehicle system parameters for the half-vehicle models with rigid vehicle body and flexible vehicle body are shown in the following tables.

Table B.1: Nominal vehicle system parameters for the half-vehicle model with rigid vehicle body [131].

Inertial property parameters:	Geometric parameters:	Primary suspension parameters:	Secondary suspension parameters:
$M = 505.1[kg]$	$l = 2.5654[m]$	$k_3 = 155.9[kN/m]$	$k_1 = 19.96[kN/m]$
$m_1 = 28.58[kg]$	$b_1 = 2.5654[m]$	$c_3 = 0.0[N/m/s]$	$c_1 = 2014.0[kN/m/s]$
$m_2 = 54.43[kg]$	$b_2 = 0.0[m]$	$k_4 = 155.9[kN/m]$	$k_2 = 22.59[kN/m]$
$I_c = 651.0[kg \times m^2]$	$a_1 = 1.0978[m]$	$c_4 = 0.0[N/m/s]$	$c_2 = 2082.0[kN/m/s]$
	$a_2 = 1.4676[m]$		

Table B.2: Nominal vehicle system parameters for the half-vehicle model with flexible vehicle body [60].

Inertial property parameters;	Geometric parameters;	Primary suspension parameters:	Secondary suspension parameters:
$M = 10^4[kg]$	$l = 12.0[m]$	$k_3 = 2000.0[kN/m]$	$k_1 = 200.0[kN/m]$
$m_1 = 10^3[kg]$	$b_1 = 2.0[m]$	$c_3 = 0.0[N/m/s]$	$c_1 = 20[kN/m/s]$
$m_2 = 10^3[kg]$	$b_2 = 2.0[m]$	$k_4 = 2000.0[kN/m]$	$k_2 = 200.0[kN/m]$
$I_c = 1.2 \times 10^5[kg \times m^2]$	$a_1 = 4.0[m]$	$c_4 = 0.0[N/m/s]$	$c_2 = 20.0[kN/m/s]$
$EI = 10^8[N \times m^2]$	$a_2 = 4.0[m]$		
$\rho A = 834.0[kg/m]$			

B.2 Half-Vehicle Model Dynamic System Matrices Used in Chapter 8

B.2.1 Rigid Vehicle Body Case

$$\mathbf{A} = \begin{bmatrix} 0 & 0 & 0 & 0 & 1 & 0 & 0 & 0 \\ 0 & 0 & 0 & 0 & 0 & 1 & 0 & 0 \\ 0 & 0 & 0 & 0 & 0 & 0 & 1 & 0 \\ 0 & 0 & 0 & 0 & 0 & 0 & 0 & 1 \\ -\frac{k_1+k_3}{m_1} & \frac{k_1}{m_1} & 0 & 0 & -\frac{c_1+c_3}{m_1} & \frac{c_1}{m_1} & 0 & 0 \\ \frac{k_1 M_{11}}{I_c M} & \frac{-k_1 M_{11}}{I_c M} & \frac{-k_2 M_{12}}{I_c M} & \frac{k_2 M_{12}}{I_c M} & \frac{c_1 M_{11}}{I_c M} & \frac{-c_1 M_{11}}{I_c M} & \frac{-c_2 M_{12}}{I_c M} & \frac{c_2 M_{12}}{I_c M} \\ 0 & 0 & -\frac{k_2+k_4}{m_2} & \frac{k_2}{m_2} & 0 & 0 & -\frac{c_2+c_4}{m_2} & \frac{c_2}{m_2} \\ \frac{-k_1 M_{12}}{I_c M} & \frac{k_1 M_{12}}{I_c M} & \frac{k_2 M_{22}}{I_c M} & \frac{-k_2 M_{22}}{I_c M} & \frac{-c_1 M_{12}}{I_c M} & \frac{c_1 M_{12}}{I_c M} & \frac{c_2 M_{22}}{I_c M} & \frac{-c_2 M_{22}}{I_c M} \end{bmatrix} \tag{B.1}$$

where $M_{11} = a_1^2 M + I_c$, $M_{12} = a_1 a_2 M - I_c$, $M_{22} = a_2^2 M + I_c$.

$$\mathbf{B} = \begin{bmatrix} 0 & 0 & 0 & 0 & -1/m_1 & 1/M + a_1^2/I_c & 0 & 1/M - a_1 a_2/I_c \\ 0 & 0 & 0 & 0 & 0 & 1/M - a_1 a_2/I_c & -1/m_2 & 1/M + a_2^2/I_c \end{bmatrix}^T \tag{B.2}$$

$$\mathbf{D} = \begin{bmatrix} -1 & -1 & 0 & 0 & c_3/m_1 & 0 & 0 & 0 \\ 0 & 0 & -1 & -1 & 0 & 0 & c_4/m_2 & 0 \end{bmatrix}^T \tag{B.3}$$

$$\mathbf{C} = \begin{bmatrix} 1 & 0 & 0 & 0 & 0 & 0 & 0 & 0 \\ 0 & 1 & 0 & 0 & 0 & 0 & 0 & 0 \\ 0 & 0 & 1 & 0 & 0 & 0 & 0 & 0 \\ 0 & 0 & 0 & 1 & 0 & 0 & 0 & 0 \end{bmatrix} \tag{B.4}$$

B.2.2 Flexible Vehicle Body Case

For convenience, it is assumed that the matrix $\mathbf{A}$ is divided into two sub-matrices $\mathbf{A}_1$ and $\mathbf{A}_2$ as follows

$$\mathbf{A} = \begin{bmatrix} \mathbf{A}_1 & \mathbf{A}_2 \end{bmatrix} \tag{B.5}$$

where sub-matrices $\mathbf{A}_1$ and $\mathbf{A}_2$ can be further expressed as:

$$\mathbf{A}_1 = \begin{bmatrix} 0 & 0 & A_{1,3} & A_{1,4} & 0 & A_{1,6} & 0 \\ 0 & 0 & A_{2,3} & A_{2,4} & 0 & 0 & 0 \\ A_{3,1} & A_{3,2} & A_{3,3} & A_{3,4} & 0 & A_{3,6} & 0 \\ A_{4,1} & A_{4,2} & A_{4,3} & A_{4,4} & 0 & A_{4,6} & 0 \\ 0 & 0 & 0 & 0 & 0 & A_{5,6} & 0 \\ A_{6,1} & 0 & A_{6,3} & A_{6,4} & A_{6,5} & A_{6,6} & 0 \\ 0 & 0 & 0 & 0 & 0 & 0 & 0 \\ 0 & A_{8,2} & A_{8,3} & A_{8,4} & 0 & 0 & A_{8,7} \\ 0 & 0 & 0 & 0 & 0 & 0 & 0 \\ A_{10,1} & A_{10,2} & A_{10,3} & A_{10,4} & 0 & A_{10,6} & 0 \\ 0 & 0 & 0 & 0 & 0 & 0 & 0 \\ A_{12,1} & A_{12,2} & A_{12,3} & A_{12,4} & 0 & A_{12,6} & 0 \\ 0 & 0 & 0 & 0 & 0 & 0 & 0 \\ A_{14,1} & A_{14,2} & A_{14,3} & A_{14,4} & 0 & A_{14,6} & 0 \end{bmatrix} \tag{B.6}$$

$$\mathbf{A}_2 = \begin{bmatrix} 0 & 0 & A_{1,10} & 0 & A_{1,12} & 0 & A_{1,14} \\ A_{2,8} & 0 & A_{2,10} & 0 & A_{2,12} & 0 & A_{2,14} \\ A_{3,8} & 0 & A_{3,10} & 0 & A_{3,12} & 0 & A_{3,14} \\ A_{4,8} & 0 & A_{4,10} & 0 & A_{4,12} & 0 & A_{4,14} \\ 0 & 0 & 0 & 0 & 0 & 0 & 0 \\ 0 & 0 & A_{6,10} & 0 & A_{6,12} & 0 & A_{6,14} \\ A_{7,8} & 0 & 0 & 0 & 0 & 0 & 0 \\ A_{8,8} & 0 & A_{8,10} & 0 & A_{8,12} & 0 & A_{8,14} \\ 0 & 0 & A_{9,10} & 0 & 0 & 0 & 0 \\ A_{10,8} & A_{10,9} & A_{10,10} & 0 & A_{10,12} & 0 & A_{10,14} \\ 0 & 0 & 0 & 0 & A_{11,12} & 0 & 0 \\ A_{12,8} & 0 & A_{12,10} & A_{12,11} & A_{12,12} & 0 & A_{12,14} \\ 0 & 0 & 0 & 0 & 0 & 0 & A_{13,14} \\ A_{14,8} & 0 & A_{14,10} & 0 & A_{14,12} & A_{14,13} & A_{14,14} \end{bmatrix} \tag{B.7}$$

where the elements of matrices $\mathbf{A}_1$ and $\mathbf{A}_2$ are given as: $A_{1,3} = 1$, $A_{1,4} = a_1$, $A_{1,6} = -1$, $A_{1,10} = Z_1(b_1)$, $A_{1,12} = Z_2(b_1)$, $A_{1,14} = Z_3(b_1)$, $A_{2,3} = 1$, $A_{2,4} = -a_2$, $A_{2,8} = -1$, $A_{2,10} = Z_1(b_2)$, $A_{2,12} = Z_2(b_2)$, $A_{2,14} = Z_3(b_2)$, $A_{3,1} = -k_1/M$, $A_{3,2} = -k_2/M$, $A_{3,3} = -(c_1 + c_2)/M$, $A_{3,4} = -(a_1c_1 - a_2c_2)/M$, $A_{3,6} = c_1/M$, $A_{3,8} = c_2/M$, $A_{3,10} = -(c_1Z_1(b_1) + c_2Z_1(b_2))/M$, $A_{3,12} = -(c_1Z_2(b_1) + c_2Z_2(b_2))/M$, $A_{3,14} = -(c_1Z_3(b_1) + c_2Z_3(b_2))/M$, $A_{4,1} = -a_1k_1/I_c$, $A_{4,2} = a_2k_2/I_c$, $A_{4,3} = -(a_1c_1 - a_2c_2)/I_c$, $A_{4,4} = -(a_1^2c_1 + a_2^2c_2)/I_c$, $A_{4,6} = a_1c_1/I_c$, $A_{4,8} = -a_2c_2/I_c$, $A_{4,10} = -(a_1c_1Z_1(b_1) - a_2c_2Z_1(b_2))/I_c$, $A_{4,12} = -(a_1c_1Z_2(b_1) - a_2c_2Z_2(b_2))/I_c$, $A_{4,14} = -(a_1c_1Z_3(b_1) - a_2c_2Z_3(b_2))/I_c$, $A_{5,6} = 1$, $A_{6,1} = k_1/m_1$, $A_{6,3} = c_1/m_1$, $A_{6,4} = a_1c_1/m_1$, $A_{6,5} = -k_3/m_1$, $A_{6,6} = -(c_1 + c_3)/m_1$, $A_{6,10} = c_1Z_1(b_1)/m_1$, $A_{6,12} = c_1Z_2(b_1)/m_1$, $A_{6,14} = c_1Z_3(b_1)/m_1$, $A_{7,8} = 1$, $A_{8,2} = k_2/m_2$, $A_{8,3} = c_2/m_2$, $A_{8,4} = -a_2c_2/m_2$, $A_{8,7} = -k_4/m_2$, $A_{8,8} = -(c_2 + c_4)/m_2$, $A_{8,10} = c_2Z_1(b_2)/m_2$, $A_{8,12} = c_2Z_2(b_2)/m_2$, $A_{8,14} = c_2Z_3(b_2)/m_2$, $A_{9,10} = 1$, $A_{10,1} = -k_1Z_1(b_1)/M_1$, $A_{10,2} = -k_2Z_1(b_2)/M_1$, $A_{10,3} = -(c_1Z_1(b_1) + c_2Z_1(b_2))/M_1$, $A_{10,4} = -(a_1c_1Z_1(b_1) - a_2c_2Z_1(b_2))/M_1$, $A_{10,6} = c_1Z_1(b_1)/M_1$, $A_{10,8} = c_2Z_1(b_2)/M_1$, $A_{10,9} = -\gamma_1/M_1$, $A_{10,10} = -(\vartheta\gamma_1 + c_1Z_1^2(b_1) + c_2Z_1^2(b_2))/M_1$, $A_{10,12} = -(c_1Z_1(b_1)Z_2(b_1) + c_2Z_1(b_2)Z_2(b_2))/M_1$, $A_{10,14} = -(c_1Z_1(b_1)Z_3(b_1) + c_2Z_1(b_2)Z_3(b_2))/M_1$, $A_{11,12} = 1$, $A_{12,1} = -k_1Z_2(b_1)/M_2$, $A_{12,2} = -k_2Z_2(b_2)/M_2$, $A_{12,3} =$

$-(c_1Z_2(b_1)+c_2Z_2(b_2))/M_2$, $A_{12,4}=-(a_1c_1Z_2(b_1)-a_2c_2Z_2(b_2))/M_2$, $A_{12,6}=c_1Z_2(b_1)/M_2$, $A_{12,8}=c_2Z_2(b_2)/M_2$, $A_{12,10}=-(c_1Z_1(b_1)Z_2(b_1)+c_2Z_1(b_2)Z_2(b_2))/M_2$, $A_{12,11}=-\gamma_2/M_2$, $A_{12,12}=-(\vartheta\gamma_2+c_1Z_2^2(b_1)+c_2Z_2^2(b_2))/M_2$, $A_{12,14}=-(c_1Z_2(b_1)Z_3(b_1)+c_2Z_2(b_2)Z_3(b_2))/M_2$, $A_{13,14}=1$, $A_{14,1}=-k_1Z_3(b_1)/M_3$, $A_{14,2}=-k_2Z_3(b_2)/M_3$, $A_{14,3}=-(c_1Z_3(b_1)+c_2Z_3(b_2))/M_3$, $A_{14,4}=-(a_1c_1Z_3(b_1)-a_2c_2Z_3(b_2))/M_3$, $A_{14,6}=c_1Z_3(b_1)/M_3$, $A_{14,8}=c_2Z_3(b_2)/M_3$, $A_{14,10}=-(c_1Z_1(b_1)Z_3(b_1)+c_2Z_1(b_2)Z_3(b_2))/M_3$, $A_{14,12}=-(c_1Z_2(b_1)Z_3(b_1)+c_2Z_2(b_2)Z_3(b_2))/M_3$, $A_{14,13}=-\gamma_3/M_3$, $A_{14,14}=-(\vartheta\gamma_3+c_1Z_3^2(b_1)+c_2Z_3^2(b_2))/M_3$.

Again it is assumed that the matrix B takes the following format

$$\mathbf{B}=\begin{bmatrix}\mathbf{B}_1 & \mathbf{B}_2\end{bmatrix}^T \tag{B.8}$$

where the matrices $\mathbf{B}_1$ and $\mathbf{B}_2$ are expressed as follows

$$\begin{cases}\mathbf{B}_1=\begin{bmatrix}0&0&1/M&a_1/I_c&0&-1/m_1&0\\0&0&1/M&-a_2/I_c&0&0&0\end{bmatrix}\\ \mathbf{B}_2=\begin{bmatrix}0&0&Z_1(b_1)/M_1&0&Z_2(b_1)/M_2&0&Z_3(b_1)/M_3\\-1/m_2&0&Z_1(b_2)/M_1&0&Z_2(b_2)/M_2&0&Z_3(b_2)/M_3\end{bmatrix}\end{cases} \tag{B.9}$$

The disturbance matrices $\mathbf{D}_1$ and $\mathbf{D}_2$ are of the following forms

$$\mathbf{D}_1=\begin{bmatrix}0&0&0&0&0&k_3/m_1&0&0&0&0&0&0&0&0\\0&0&0&0&0&0&0&k_4/m_2&0&0&0&0&0&0\end{bmatrix} \tag{B.10}$$

$$\mathbf{D}_2=\begin{bmatrix}0&0&0&0&0&c_3/m_1&0&0&0&0&0&0&0&0\\0&0&0&0&0&0&0&c_4/m_2&0&0&0&0&0&0\end{bmatrix} \tag{B.11}$$

Once 4 velocities are measured, the output matrix $\mathbf{C}_a$ takes the following form

$$\mathbf{C}_a=\begin{bmatrix}0&0&C_{1,3}&C_{1,4}&0&0&0&0&0&C_{1,10}&0&C_{1,12}&0&C_{1,14}&0&0\\0&0&C_{2,3}&C_{2,4}&0&0&0&0&0&C_{2,10}&0&C_{2,12}&0&C_{2,14}&0&0\\0&0&0&0&0&C_{3,6}&0&0&0&0&0&0&0&0&0&0\\0&0&0&0&0&0&0&C_{4,8}&0&0&0&0&0&0&0&0\end{bmatrix} \tag{B.12}$$

where $C_{1,3}=1$, $C_{1,4}=-(a_2+b_2)$, $C_{1,10}=Z_1(0)$, $C_{1,12}=Z_2(0)$, $C_{1,14}=Z_3(0)$, $C_{2,3}=1$, $C_{2,4}=l-a_2-b_2$, $C_{2,10}=Z_1(l)$, $C_{2,12}=Z_2(l)$, $C_{2,14}=Z_3(l)$, $C_{3,6}=1$, $C_{4,8}=1$.

However, if 5 velocities are measured, the output matrix $\mathbf{C}_a$ is offered as follows

$$\mathbf{C}_a = \begin{bmatrix} 0 & 0 & C_{1,3} & C_{1,4} & 0 & 0 & 0 & 0 & 0 & C_{1,10} & 0 & C_{1,12} & 0 & C_{1,14} & 0 & 0 \\ 0 & 0 & C_{2,3} & 0 & 0 & 0 & 0 & 0 & 0 & C_{2,10} & 0 & C_{2,12} & 0 & C_{2,14} & 0 & 0 \\ 0 & 0 & C_{3,3} & C_{3,4} & 0 & 0 & 0 & 0 & 0 & C_{3,10} & 0 & C_{3,12} & 0 & C_{3,14} & 0 & 0 \\ 0 & 0 & 0 & 0 & 0 & C_{4,6} & 0 & 0 & 0 & 0 & 0 & 0 & 0 & 0 & 0 & 0 \\ 0 & 0 & 0 & 0 & 0 & 0 & 0 & C_{5,8} & 0 & 0 & 0 & 0 & 0 & 0 & 0 & 0 \end{bmatrix} \tag{B.13}$$

where $C_{1,3} = 1$, $C_{1,4} = -(a_2 + b_2)$, $C_{1,10} = Z_1(0)$, $C_{1,12} = Z_2(0)$, $C_{1,14} = Z_3(0)$, $C_{2,3} = 1$, $C_{2,10} = Z_1(a_2 + b_2)$, $C_{2,12} = Z_2(a_2 + b_2)$, $C_{2,14} = Z_3(a_2 + b_2)$, $C_{3,3} = 1$, $C_{3,4} = l - a_2 - b_2$, $C_{3,10} = Z_1(l)$, $C_{3,12} = Z_2(l)$, $C_{3,14} = Z_3(l)$, $C_{4,6} = 1$, $C_{5,8} = 1$.

B.3 Weighting Matrices G, H, and N for Equation (8.51)

$$\mathbf{G} = \begin{bmatrix} G_{1,1} & G_{1,2} & G_{1,3} & G_{1,4} \\ G_{2,1} & G_{2,2} & G_{2,3} & G_{2,4} \\ G_{3,1} & G_{3,2} & G_{3,3} & G_{3,4} \\ G_{4,1} & G_{4,2} & G_{4,3} & G_{4,4} \end{bmatrix} \tag{B.14}$$

where $G_{1,1} = \rho_1 \nu^2 k_2^2 + \rho_2 k_2^2/m_2^2 + \rho_3 + \rho_4$, $G_{1,2} = G_{2,1} = (-2\rho_1 \nu^2 k_2^2 - 2\rho_2 k_2^2/m_2^2 - 2\rho_4)/2$, $G_{1,3} = G_{3,1} = (2\rho_1 \nu^2 c_2 k_2 + 2\rho_2 c_2 k_2/m_2^2)/2$, $G_{1,4} = G_{4,1} = (-2\rho_1 \nu^2 c_2 k_2 - 2\rho_2 c_2 k_2/m_2^2)/2$, $G_{2,2} = \rho_2 k_2^2/m_2^2 + \rho_1 \nu^2 k_2^2 + \rho_4$, $G_{2,3} = G_{3,2} = (-2\rho_1 \nu^2 c_2 k_2 - 2\rho_2 c_2 k_2/m_2^2)/2$, $G_{2,4} = G_{4,2} = (2\rho_1 \nu^2 c_2 k_2 + 2\rho_2 c_2 k_2/m_2^2)/2$, $G_{3,3} = \rho_2 c_2^2/m_2^2 + \rho_1 \nu^2 c_2^2$, $G_{3,4} = G_{4,3} = (-2\rho_1 \nu^2 c_2^2 - 2\rho_2 c_2^2/m_2^2)/2$, $G_{4,4} = \rho_2 c_2^2/m_2^2 + \rho_1 \nu^2 c_2^2$.

$$\mathbf{H} = \rho_2/m_2^2 + \rho_1 \tag{B.15}$$

$$\mathbf{N}^T = \begin{bmatrix} N_{1,1} & N_{2,1} & N_{3,1} & N_{4,1} \end{bmatrix} \tag{B.16}$$

where $N_{1,1} = (2\rho_1 \nu k_2 + 2\rho_2 k_2/m_2^2)/2$, $N_{2,1} = (-2\rho_1 \nu k_2 - 2\rho_2 k_2/m_2^2)/2$, $N_{3,1} = (2\rho_1 \nu c_2 + 2\rho_2 c_2/m_2^2)/2$, $N_{4,1} = (-2\rho_1 \nu c_2 - 2\rho_2 c_2/m_2^2)/2$.

B.4 Weighting Matrices G, H, and N for Equation (8.54)

$$\mathbf{G} = \begin{bmatrix} G_{1,1} & G_{1,2} & G_{1,3} & G_{1,4} & G_{1,5} \\ G_{2,1} & G_{2,2} & G_{2,3} & G_{2,4} & G_{2,5} \\ G_{3,1} & G_{3,2} & G_{3,3} & G_{3,4} & G_{3,5} \\ G_{4,1} & G_{4,2} & G_{4,3} & G_{4,4} & G_{4,5} \\ G_{5,1} & G_{5,2} & G_{5,3} & G_{5,4} & G_{5,5} \end{bmatrix} \tag{B.17}$$

where $G_{1,5} = -\rho_3$, $G_{2,5} = 0$, $G_{3,5} = 0$, $G_{4,5} = 0$, $G_{5,5} = \rho_3$. The other elements of the matrix are the same as the corresponding elements of the matrix shown in (B.14).

$$\mathbf{H} = \rho_2/m_2^2 + \rho_1 \tag{B.18}$$

$$\mathbf{N}^T = \begin{bmatrix} N_{1,1} & N_{2,1} & N_{3,1} & N_{4,1} & N_{5,1} \end{bmatrix} \tag{B.19}$$

where $N_{5,1} = 0$ and the other elements of the matrix are the same as the corresponding elements of the matrix shown in (B.16).

B.5 Weighting Matrices G, H, and N for Equation (8.55)

$$\mathbf{G} = \begin{bmatrix} G_{1,1} & G_{1,2} & G_{1,3} & G_{1,4} & G_{1,5} & G_{1,6} & G_{1,7} & G_{1,8} \\ G_{2,1} & G_{2,2} & G_{2,3} & G_{2,4} & G_{2,5} & G_{2,6} & G_{2,7} & G_{2,8} \\ G_{3,1} & G_{3,2} & G_{3,3} & G_{3,4} & G_{3,5} & G_{3,6} & G_{3,7} & G_{3,8} \\ G_{4,1} & G_{4,2} & G_{4,3} & G_{4,4} & G_{4,5} & G_{4,6} & G_{4,7} & G_{4,8} \\ G_{5,1} & G_{5,2} & G_{5,3} & G_{5,4} & G_{5,5} & G_{5,6} & G_{5,7} & G_{5,8} \\ G_{6,1} & G_{6,2} & G_{6,3} & G_{6,4} & G_{6,5} & G_{6,6} & G_{6,7} & G_{6,8} \\ G_{7,1} & G_{7,2} & G_{7,3} & G_{7,4} & G_{7,5} & G_{7,6} & G_{7,7} & G_{7,8} \\ G_{8,1} & G_{8,2} & G_{8,3} & G_{8,4} & G_{8,5} & G_{8,6} & G_{8,7} & G_{8,8} \end{bmatrix} \tag{B.20}$$

where $A_a = 1/M + a^2/I_c$, $B_b = 1/M + b^2/I_c$, $A_b = 1/M - ab/I_c$, $G_{1,1} = k_1^2\rho_1 A_a^2 + \rho_3 + k_1^2\rho_2 A_b^2 + \rho_5$; $G_{1,2} = -k_1^2(\rho_1 A_a^2 + \rho_5 + \rho_2 A_b^2)$, $G_{1,3} = k_1k_2(\rho_1 A_b A_a + \rho_2 B_b A_b)$, $G_{1,4} = -k_1k_2(\rho_1 A_b A_a + \rho_2 B_b A_b)$, $G_{1,5} = c_1k_1(\rho_1 A_a^2 + \rho_2 A_b^2)$, $G_{1,6} = -c_1k_1(\rho_1 A_a^2 + \rho_2 A_b^2)$, $G_{1,7} = c_2k_1(\rho_1 A_b A_a + \rho_2 B_b Ab)$, $G_{1,8} = -c_2k_1(\rho_1 A_b A_a + \rho_2 B_b A_b)$, $G_{2,1} = G_{1,2}$, $G_{2,2} = \rho_1 k_1^2 A_a^2 + \rho_2 k_1^2 A_b^2 + \rho_5$, $G_{2,}3 = -k_1k_2(\rho_1 A_b A_a + \rho_2 B_b A_b)$, $G_{2,4} = k_1k_2(\rho_1 A_b A_a + \rho_2 B_b A_b)$, $G_{2,5} = -c_1k_1(\rho_1 A_a^2 + \rho_2 A_b^2)$, $G_{2,6} = c_1k_1(\rho_1 A_a^2 + \rho_2 A_b^2)$, $G_{2,7} = -c_2k_1(\rho_1 A_b A_a + \rho_2 B_b A_b)$, $G_{2,8} = c_2k_1(\rho_1 A_b A_a + \rho_2 B_b A_b)$, $G_{3,1} = G_{1,3}$, $G_{3,2} = G_{2,3}$, $G_{3,3} = \rho_4 + \rho_2 k_2^2 B_b^2 + \rho_1 k_2^2 A_b^2 + \rho_6$, $G_{3,4} = -k_2^2(\rho_1 A_b^2 + \rho_6 + \rho_2 B_b^2)$, $G_{3,5} = c_1k_2(\rho_1 A_a A_b + \rho_2 A_b B_b)$, $G_{3,6} = -c_1k_2(\rho_1 A_a A_b + \rho_2 A_b B_b)$, $G_{3,7} = c_2k_2(\rho_1 A_b^2 + \rho_2 B_b^2)$, $G_{3,8} = -c_2k_2(\rho_1 A_b^2 + \rho_2 B_b^2)$, $G_{4,1} = G_{1,4}$, $G_{4,2} = G_{2,4}$, $G_{4,3} = G_{3,4}$, $G_{4,4} = k_2^2\rho 2B_b^2 + k_2^2\rho_1 A_b^2 + \rho_6$, $G_{4,5} = -c_1k_2(\rho_1 A_a A_b + \rho_2 A_b B_b)$, $G_{4,6} = c_1k_2(\rho_1 A_a A_b + \rho_2 A_b B_b)$, $G_{4,7} = -c_2k_2(\rho_1 A_b^2 + \rho_2 B_b^2)$, $G_{4,8} = c_2k_2(\rho_1 A_b^2 + \rho_2 B_b^2)$, $G(5,1) = G_{1,5}$, $G(5,2) = G_{2,5}$, $G(5,3) = G_{3,5}$, $G(5,4) = G_{4,5}$, $G(5,5) = c_1^2(\rho_1 A_a^2 + \rho_2 A_b^2)$, $G(5,6) = -c_1^2(\rho_1 A_a^2 + \rho_2 A_b^2)$, $G(5,7) = c_1c_2(\rho_1 A_b A_a + \rho_2 B_b A_b)$, $G(5,8) = -c_1c_2(\rho_1 A_b A_a + \rho_2 B_b A_b)$, $G_{6,1} = G_{1,6}$, $G_{6,2} = G_{2,6}$, $G_{6,3} = G_{3,6}$, $G_{6,4} = G_{4,6}$, $G_{6,5} = G_{5,6}$, $G_{6,6} = c_1^2(\rho_1 A_a^2 + \rho_2 A_b^2)$, $G_{6,7} = -c_1c_2(\rho_1 A_b A_a + \rho_2 B_b A_b)$, $G_{6,8} = c_1c_2(\rho_1 A_b A_a + \rho_2 B_b A_b)$, $G_{7,1} = G_{1,7}$, $G_{7,2} = G_{2,7}$, $G_{7,3} = G_{3,7}$, $G_{7,4} = G_{4,7}$, $G_{7,5} = G_{5,7}$, $G_{7,6} = G_{6,7}$, $G_{7,7} = c_2^2(\rho_1 A_b^2 + \rho_2 B_b^2)$, $G_{7,8} = -c_2^2(\rho_1 A_b^2 + \rho_2 B_b^2)$, $G_{8,1} = G_{1,8}$, $G_{8,2} = G_{2,8}$, $G_{8,3} = G_{3,8}$, $G_{8,4} = G_{4,8}$, $G_{8,5} = G_{5,8}$, $G_{8,6} = G_{6,8}$, $G_{8,7} = G_{7,8}$.

$$\mathbf{H} = \begin{bmatrix} \rho_1 A_a^2 + \rho_2 A_b^2 & \rho_1 A_b A_a + \rho_2 B_b A_b \\ \rho_1 A_b A_a + \rho_2 B_b A_b & \rho_1 A_b^2 + \rho_2 B_b^2 \end{bmatrix} \tag{B.21}$$

$$\mathbf{N}^T = \begin{bmatrix} N_{1,1} & N_{2,1} & N_{3,1} & N_{4,1} & N_{5,1} & N_{6,1} & N_{7,1} & N_{8,1} \\ N_{1,2} & N_{2,2} & N_{3,2} & N_{4,2} & N_{5,2} & N_{6,2} & N_{7,2} & N_{8,2} \end{bmatrix} \tag{B.22}$$

where $N_{1,1} = k_1(\rho_1 A_a^2 + \rho_2 A_b^2)$, $N_{1,2} = k_1(\rho_1 A_b A_a + \rho_2 B_b A_b)$, $N_{2,1} = -k_1(\rho_1 A_a^2 + \rho_2 A_b^2)$, $N_{2,2} = -k_1(\rho_1 A_b A_a + \rho_2 B_b A_b)$, $N_{3,1} = k_2(\rho_1 A_a A_b + \rho_2 A_b B_b)$, $N_{3,2} = k_2(\rho_1 A_b^2 + \rho_2 B_b^2)$, $N_{4,1} = -k_2(\rho_1 A_a A_b + \rho_2 A_b B_b)$, $N_{4,2} = -k_2(\rho_1 A_b^2 + \rho_2 B_b^2)$, $N_{5,1} = c_1(\rho_1 A_a^2 + \rho_2 A_b^2)$, $N_{5,2} = c_1(\rho_1 A_b A_a + \rho_2 B_b A_b)$, $N_{6,1} = -c_1(\rho_1 A_a^2 + \rho_2 A_b^2)$, $N_{6,2} = -c_1(\rho_1 A_b A_a + \rho_2 B_b A_b)$, $N_{7,1} = c_2(\rho_1 A_a A_b + \rho_2 A_b B_b)$, $N_{7,2} = c_2(\rho_1 A_b^2 + \rho_2 B_b^2)$, $N_{8,1} = -c_2(\rho_1 A_a A_b + \rho_2 A_b B_b)$, $N_{8,2} = -c_2(\rho_1 A_b^2 + \rho_2 B_b^2)$.

Bibliography

[1] ISO 2631/1. Evaluation of human exposure to whole-body vibration – part 1: General requirements. 1985.

[2] A. Alexandridis and T. Weber. Active vibration isolation of track cabs. In *1984 American Control Conference*, pages 1199–1208, San Diego, California, 1984.

[3] A. Alleyne. Improved vehicle performance using combined suspension and braking forces. *Vehicle System Dynamics*, 27:235–265, 1997.

[4] R. Anderson. A general multi-body approach to dynamic modelling of rail vehicles. In *Proceedings of ASME International Computers in Engineering Conference*, pages 223–228, Chicago, 1983.

[5] R. Anderson. A general, multi-body approach to dynamic modelling of rail vehicles. In *Proceedings of the* 3^{rd} *ASME International Computers in Engineering Conference*, pages 223–228, Chicago, U.S.A., 1983.

[6] R. Anderson. The *A'GEM* multibody dynamics package. *Vehicle System Dynamics*, 22:41–44, 1993.

[7] R. Anderson. Tracking dynamic modes of rail vehicles. In *Proceedings of the* 15^{th} *Canadian Congress of Applied Mechanics*, pages 330–331, University of Victoria, Canada, 1995.

[8] R. Anderson, J. Elkins, and B. Brickle. Rail vehicle dynamics for the 21^{th} century. In *Proceedings of ICTAM 2000*, Chicago, U.S.A., 2001.

[9] T. Apparao. Curving behavior of rail transit vehicles: a parametric study. In *The 5^{th} Symposium on Engineering Applications of Mechanics*, pages 271–276, Ottawa, Canada, 1980.

[10] A. Baumal. Automated design of mechanical systems through numerical optimization of dynamic behaviour. *Master's thesis, University of Waterloo, Canada*, 1997.

[11] A. Baumal and J. McPhee. On the use of numerical optimization to maximize the critical velocity of a simple rail vehicle. *to appear in CSME Transactions*, 2002 (accepted in 2002).

[12] A. Baumal, J. McPhee, and P. Calamai. Application of genetic algorithms to the optimization of an active vehicle suspension design. *Computer Methods in Applied Mechanics and Engineering*, 163:87–94, 1998.

[13] C. Bell, D. Horak, and J. Hedrick. Stability and curving mechanics of rail vehicles. *J. Dyn. Sys. Meas. Cont.*, 103:181–190, 1981.

[14] I. Besselink and F. Asperen. Numerical optimization of linear dynamic behavior of commercial vehicles. *Vehicle System Dynamics*, 23:53–70, 1994.

[15] D. Bestle. Optimization of automotive systems. In E.J. Haug, editor, *Concurrent Engineering: Tools and Technologies for Mechanical System Design*, pages 274–296. Springer–Verlag, 1994.

[16] D. Bestle and P. Eberhard. Analyzing and optimizing multibody systems. *Mechanics of Structures and Machines*, 20:67–92, 1992.

[17] D. Bestle and P. Eberhard. Dynamic system design via multicriteria optimization. In G. Fandel and T. Gal, editors, *Multiple Criteria Decision Making: Proceeding of the Twelfth International Conference on Multiple Criteria Decision Making*, pages 467–478. Springer–Verlag, 1995.

[18] D. Bestle and P. Eberhard. Multi–criteria multi–model design optimization. In D. Bestle and W. Schiehlen, editors, *Optimization of Mechanical Systems: Proceed-*

ings of the IUTAM Symposium on Optimization of Mechanical Systems, pages 467–478. Kluwer Academic Publishers, 1995.

[19] D. Bestle, P. Eberhard, and W. Schiehlen. Optimization of an actively controlled vehicle system. *Journal of Computer and Systems and Sciences International*, 33(3):7–15, 1995.

[20] D. Bestle and W. Schiehlen. *IUTAM Symposium on optimization of mechanical systems*. Kluwer Academic Publisher, 1996.

[21] M. Bhatti. *Practical Optimization Methods*. Springer, New York, 1998.

[22] D. Boocock. Steady-state motion of railway vehicles on curved track. *Journal of Mechanical Engineering Science*, 11(6):908–918, 1969.

[23] R. Braun and I. Kroo. Development and application of the collaborative optimization architecture in a multidisciplinary design environment. In N. Alexandrov and M. Hussaini, editors, *Multidisciplinary Design Optimization: State of the Art*. SIAM, 1997.

[24] A. Bryson and Y. Ho. *Applied Optimal Control, Optimization, Estimation and Control*. John Wiley and Sons, New York, 1975.

[25] J. Castillo, P. Pintado, and F. Benitez. Optimization for vehicle suspension ii: frequency domain. *Vehicle System Dynamics*, 19:331–352, 1990.

[26] I. Cech. A full-car roll model of a vehicle with controlled suspension. *Vehicle System Dynamics*, 23:467–480, 1994.

[27] G. Celniker and J. Hedrick. Rail vehicle active suspensions for lateral ride and stability improvement. *J. Dyn. Sys. Meas. Cont.*, 104:100–106, 1982.

[28] R. Chalasani. Ride performance potential of active suspension systems– part 2: comprehensive analysis based on a full-car model. In L. Segel, J. Wong, E. Law, and D. Hrovat, editors, *Symposium on Simulation and Control of Ground Vehicles and Transportation Systems*, pages 205–226, New York, 1986.

[29] N. Cooperrider, J. Cox, and J. Hedrick. Lateral dynamics optimization of a conventional railcar. *J. Dyn. Sys. Meas. Cont.*, 97:293–299, 1975.

[30] N. Cooperrider and Q. He. The influence of rail head geometry and cant angle variations on rail vehicle dynamics. In *Proceedings of the IUTAM Conference*, Cambridge, MA, U.S.A., 1983.

[31] N. Cooperrider and E. Law. The nonlinear dynamics of rail vehicles in curve entry and negotiation. In *Proceedings of* 7^{th} *IAVSD Symposium on the Dynamics of Vehicles on Roads and on Railway Tracks*, pages 357–370, 1982.

[32] J. Cox, J. Hedrick, and N. Cooperrider. Optimization of rail vehicle operating speed with practical constraints. *J. Dyn. Sys. Meas. Cont.*, 100:260–269, 1978.

[33] E. Cramer, J.Dennis, P. Frank, R. Lewis, and G. Shubin. Problem formulation for multidisciplinary design optimization. *SIAM Journal on Optimization*, 4(4):754–776, 1994.

[34] D. Crolla and M. Abdel-hady. Active suspension control: performance comparisons using control laws applied to a full vehicle model. *Vehicle System Dynamics*, 20:107–120, 1991.

[35] R. Curmi. Urban rail vehicle running gear: a state of the art review. In *Ontario Ministry of Transportation and Communications Publication*, pages 1–46, 1977.

[36] S. Datoussaid, R. Hadjit, O. Verlinden, and C. Conti. Optimization design of multibody systems by using genetic algorithms. *Vehicle System Dynamics*, 28:704–710, 1998.

[37] M. Demic. Optimization of the characteristics of the elasto-damping elements of a passenger car by means of a modified nedler-mead method. *Int. J. of Vehicle Design*, 10(2):136–152, 1989.

[38] M. Demic. Optimization of the characteristics of the elasto-damping elements of cars from the aspect of comfort and handling. *Int. J. of Vehicle Design*, 13(1):29–46, 1992.

[39] J. Dennis and V. Torczon. Direct search methods on parallel machines. *SIAM J. Optimiz.*, 1:448–474, 1991.

[40] R. Dukkipati and J. Amyot. *Computer-aided simulation in railway dynamics*. Marcel Dekker, Inc., New York, 1988.

[41] R. Dukkipati and S. Swamy. Non-linear steady-state curving analysis of some unconventional rail trucks. *Mechanism and Machine Theory*, 36:507–521, 2001.

[42] P. Eberhard, W. Schiehlen, and D. Bestle. Some advantages of stochastic methods in multicriteria optimization of multibody systems. *Archive of Applied Mechanics*, 69:543–554, 1999.

[43] B. Eickhoff, J. Evans, and A. Minnis. A review of modelling for railway vehicle suspension components. *Vehicle System Dynamics*, 24:469–496, 1995.

[44] E. Elbeheiry, D. Karnopp, M. Elaraby, and A. Abdelraaouf. Advanced ground vehicle suspension systems - a classified bibliography. *Vehicle System Dynamics*, 24:231–258, 1995.

[45] E. Elbeheiry, D. Karnopp, M. Elaraby, and A. Abdelraaouf. Suboptimal control design of active and passive suspensions based on a full car model. *Vehicle System Dynamics*, 26:197–222, 1996.

[46] J. Elkins and R. Gostling. A general quasi-static curving theory for railway vehicles. In *Proceedings of the* 5^{th} *IAVSD Symposium on the Dynamics of Vehicles on Roads and on Railway Tracks*, pages 388–406, Amsterdam, 1977.

[47] M. Elmadany. Stochastic optimal control of highway tractors with active suspensions. *Vehicle System Dynamics*, 17:193–210, 1988.

[48] W. Elmaraghy. Ride quality and dynamics of rail vehicle models for microcomputers. *Vehicle System Dynamics*, 16:193–211, 1987.

[49] I. Esat. Genetic algorithm–based optimization of a vehicle suspension system. *Int. J. Vehicle Design*, 21(2/3):148–160, 1999.

[50] E. Esmailzadeh and F. Fahimi. Optimal adaptive active suspensions for a full car model. *Vehicle System Dynamics*, 27:89–107, 1997.

[51] J. Evans. Rail vehicle dynamic simulations using VAMPIRE. *Vehicle System Dynamics*, Supplement, 31:119–140, 1999.

[52] E. Foo and R. Goodall. Active suspension control of flexible-bodied railway vehicles using electro-hydraulic and electro-magnetic actuators. *Control Engineering Practice*, 8:507–518, 2000.

[53] C. Fortin. Dynamic curving simulation of forced-steering rail vehicles. *Ph.D thesis, Queen's University, Canada*, 1984.

[54] V. Garg and R. Dukkipati. *Dynamics of railway vehicle systems.* Academic Press, Toronto, 1984.

[55] R. Gasch, D. Moelle, and K. Knothe. The effect of nonlinearities on the limit cycles of railway vehicles. In *Proceedings of the* 8^{th} *IAVSD Symposium*, pages 207–224, Cambridge, MA, U.S.A., 1984.

[56] P. Gill, W. Murray, and W. Wright. *Practical Optimization.* Academic Press, London and New York, 1981.

[57] D. Goldberg. *Genetic Algorithms in Search, Optimization, and Machine Learning.* Addison–Wesley, Reading, Massachusetts, 1989.

[58] R. Goodall and W. Kortum. Active controls in ground transportation - a review of the state-of-the-art and future potential. *Vehicle System Dynamics*, 12:225–257, 1983.

[59] A. Hac. Suspension optimization of a 2-DOF vehicle model using stochastic optimal control technique . *Journal of Sound and Vibration*, 100(3):343–357, 1985.

[60] A. Hac. Stochastic optimal control of vehicles with elastic body and active suspension. *ASME, Journal of Dynamic Systems, Measurement and Control*, 108:106–110, 1986.

[61] M. Hady and D. Crolla. Active suspension control algorithms for a four-wheel vehicle model. *Int. J. Veh. Design*, 13(2):144–158, 1992.

[62] P. Hajela and J. Lee. Genetic algorithms in multidisciplinary rotor blade design. In *Proceedings of the* 36^{th} *AIAA/ASME/AHS/ASC Structures, Structural Dynamics, and Materials*, number AIAA–1995–1144, New Orleans, 1995.

[63] D. Hannebrink, H. Lee, and et al. Influence of axle load, track gage, and wheel profile on rail vehicle hunting. *ASME paper No. 76-WA/RT-3*, 1976.

[64] X. He and R. Huilgol. Application of hopf bifurcation at infinity to hunting vibrations of rail vehicle trucks. In *Proceedings of the* 12^{th} *IAVSD Symposium*, pages 240–253, 1991.

[65] Y. He and J. McPhee. Comparative study of optimization algorithms used in ground vehicle suspension design. In 6^{th} *U.S. National Congress on Computational Mechanics*, pages 660–660, Dearborn, Michigan, U.S.A., 2001.

[66] Y. He and J. McPhee. Design optimization of rail vehicles with passive and active suspensions: a combined approach using genetic algorithms and multibody dynamics. In *Proceedings of the 17th IAVSD Symposium*, Copenhagen, Denmark, 2001.

[67] Y. He and J. McPhee. An integrated approach using genetic algorithms, multibody dynamics, and LQG control strategy for design optimization of ground vehicles with active suspensions. In *Proceedings of CSME Forum*, Queen's University, Kingston, Ontario, Canada, May 2002.

[68] Y. He and J. McPhee. Application of SQP and dynamic mode tracking to the identification of the critical speed of rail vehicles. *Submitted to the Journal of Sound and Vibration*, 2002.

[69] Y. He and J. McPhee. Optimization of the lateral stability of rail vehicles. *to appear in Vehicle System Dynamics*, 2002 (accepted in March 2002).

[70] K. Heal, M. Hansen, and K. Rickard. *Maple V learning guide*. Springer, New York, 1998.

[71] J. Hedrick. Railway vehicle active suspensions. *Vehicle System Dynamics*, 10:267–283, 1981.

[72] J. Hedrick, G. Billington, and D. Dreesbach. Analysis, design, and optimization of high speed vehicle suspensions using state variable techniques. *J. Dyn. Sys. Meas. Cont.*, pages 193–203, 1974.

[73] J. Hedrick and H. Firouztash. The covariance propagation equation including time-delayed inputs. *IEEE Trans. on Automatic Control*, AC–19(4):587–589, 1974.

[74] J. Hedrick, D. Wormley, and A. Kar. Performance limits of rail passenger vehicles: evaluation and optimization. In *Technical Report Prepared under U.S. Department of Transportation, Contract DOT–OS–70052*, 1978.

[75] D. Horak, C. Bell, and J. Hedrick. A comparison of the stability and curving performance of radial and conventional rail vehicle trucks. *J. Dyn. Sys. Meas. Cont.*, 103:191–200, 1981.

[76] R. Huston. *Multibody dynamics*. Butterworth-Heinemann, Boston, London, Singapore, Sydney, Toronto, Wellington, 1990.

[77] S. Iwnicki. The results of the Manchester benchmarks. *Vehicle System Dynamics Supplement*, 31:2–12, 1999.

[78] J. Kalker. Survey of wheel-rail rolling contact theory. *Vehicle System Dynamics*, 5:317–358, 1979.

[79] D. Karnopp. Design principles for vibration control systems using semi-active dampers. *J. Dyn. Sys. Meas. Cont.*, 112:448–455, 1990.

[80] D. Karnopp, M. Crosby, and R. Harwood. Vibration control using semi-active force generators. *Trans. ASME, J. Eng. Ind.*, pages 619–626, 1974.

[81] K. Kitajima and H. Peng. H_∞ control for integrated side-slip, roll and yaw controls for ground vehicles. In *Proceedings of the* 5^{th} *International Symposium on Advanced Vehicle Control*, pages 187–194, University of Michigan, Michigan, U.S.A., 2000.

[82] K. Knothe and F. Bohm. History of stability of railway and road vehicles. *Vehicle System Dynamics*, 31:283–323, 1999.

[83] K. Knothe and S. Stichel. Direct covariance analysis for the calculation of creepages and creep-forces for various bogies on straight track with random irregularities. *Vehicle System Dynamics*, 23:237–251, 1994.

[84] S. Kodiyalam and J. Sobieski. Bi-level integrated system synthesis with response surfaces. *AIAA Journal*, 38(8), 2000.

[85] S. Kodiyalam and J. Sobieszczanki-Sobieski. Multidisciplinary design optimization – some formal methods, framework requirements, and application to vehicle design. *Int. J. Vehicle Design (Special Issue)*, 25(1/2):3–22, 2001.

[86] W. Kortum. Review of multibody computer codes for vehicle system dynamics. *Vehicle System Dynamics*, Supplement, 22:3–26, 1993.

[87] W. Kortum, W. Schiehlen, and M. Hoffmann. Progress in integrated system analysis and design software for controlled vehicles. *Vehicle System Dynamics*, Supplement, 23:274–296, 1994.

[88] B. Kuo. *Automatic control systems.* Prentice Hall, Englewood Cliffs, New Jersey, 1991.

[89] M. Lakehal-ayat, S. Diop, E. Fenaux, F. Lamnabhi-Lagarrigue, and F. Zarka. On global chassis control: combined braking and cornering, and yaw rate control. In *Proceedings of the* 5^{th} *International Symposium on Advanced Vehicle Control*, pages 197–203, University of Michigan, Michigan, U.S.A., 2000.

[90] R. Langlois. Preview control algorithms for the active suspension of an off-road vehicle. *Master's thesis, Queen's University, Canada*, 1991.

[91] R. Langlois, D. Hanna, and R. Anderson. Implementing preview control on an off-road vehicle with active suspension. *Vehicle System Dynamics*, Supplement, 20:340–353, 1991.

[92] E. Law and J. Clark. Investigation of the truck hunting instability of high speed trains. *ASME paper No. 67-TRAN-17*, 1967.

[93] T. Li and Y. Kuo. Evolutionary algorithms for passive suspension systems. *JSME International Journal*, 43(3):537–554, 2000.

[94] Y. Lin and Y. Zhang. Suspension optimization by a frequency domain equivalent optimal control algorithm. *Journal of Sound and Vibration*, 133(2):239–249, 1989.

[95] W. Liu and S. Meng. *Optimization of mechanical design.* Tsinghua University, Beijing, China, (in Chinese), 1986.

[96] N. Louam, D. Wilson, and R. Sparp. Optimal control of a vehicle suspension incorporating the time delay between front and rear wheel inputs. *Vehicle System Dynamics*, 17:317–336, 1988.

[97] C. MacNaughton. Suspension and structure design for the modification of an urban transit vehicle. *Master's Project Report, Queen's University, Canada*, 1996.

[98] W. Manning, D. Crolla, M. Brown, and M. Selby. Co-ordination of chassis control systems for vehicle motion control. In *Proceedings of the* 5^{th} *International Symposium on Advanced Vehicle Control*, pages 313–319, University of Michigan, Michigan, U.S.A., 2000.

[99] D. Margolis and D. Edeal. Modeling and control of large flexible frame vehicles using bond graphs. *SAE Paper No. 892488*, 1989.

[100] J. McPhee and R. Anderson. Model reduction procedure for the dynamic analysis of rail vehicles subjected to linear creep forces. *Vehicle System Dynamics*, 25:349–367, 1996.

[101] T. Mei and R. Goodall. LQG and GA solution for active steering of railway vehicles. *IEE Proc. -Control Theory Appl.*, 147(1):111–117, 2000.

[102] T. Mei and R. Goodall. Modal controllers for active steering of railway vehicles with solid axle wheelsets. *Vehicle System Dynamics*, 34:25–41, 2000.

[103] P. Michelberger, L. Palkovics, and J. Bokor. Robust design of active suspension systems. *Int. J. of Vehicle Design*, 14:145–165, 1993.

[104] D. Moelle and R. Gasch. Nonlinear bogie hunting. In *Proceedings of the* 7^{th} *IAVSD Symposium*, pages 455–467, 1981.

[105] D. Newland. Steering a flexible railway truck on curved track. *Journal of Engineering for Industry*, pages 908–918, 1969.

[106] D. Newland. *An introduction to random vibrations, spectral and wavelet analysis.* Longman Scientific and Technical, Harlow, England, 1993.

[107] M. No and J. Hedrick. High speed stability for rail vehicles considering varying conicity and creep coefficients. *Vehicle System Dynamics*, 13:299–313, 1984.

[108] N. Orlandea, M. Chace, and D. Calahan. A sparsity oriented approach to the dynamic analysis and design of mechanical systems. *Journal of Engineering for Industry*, 99:773–784, 1977.

[109] A. Pil and H. Asada. Integrated structure/control design of mechatronic systems using a recursive experimental optimization method. *IEEE/ASME Transactions on Mechatronics*, 1(3):191–203, 1996.

[110] K. Reckdahl. Working model technical note: modeling uniform flexible bodies in working model. *Part 1: Numerical Integration Basics*, Doc No.: WMTN13:1–9, 1994.

[111] J. Renaud and G. Gabriele. Improved coordination in non-hierarchic system optimization. *AIAA Journal*, 31(12):2367–2373, 1993.

[112] J. Renders and S. Flasse. Hybrid methods using genetic algorithms for global optimization. *IEEE Transactions on Systems, Man, and Cybernetics-Part B: Cybernetics*, 26(2):243–258, 1996.

[113] R. Ryan. Adams–mechanical system simulation software. *Vehicle System Dynamics*, 22:144–148, 1993.

[114] W. Schiehlen. Modelling of complex vehicle systems. In *Proceedings of the* 8^{th} *IAVSD Symposium*, pages 584–563, Cambridge, MA, U.S.A., 1984.

[115] W. Schiehlen. *Multibody Systems Handbook*. Springer-Verlag, Berlin, 1990.

[116] W. Schiehlen. Symbolic computations in multibody systems. In M. Pereira and J. Ambrosio, editors, *Computer-Aided Analysis of Rigid and Flexible Mechanical Systems*, pages 101–136. Kluwer Academic Publishers, 1994.

[117] R. Sharp. Multi-body dynamics applications in vehicle engineering. *IMechE Conference Transactions*, C553/045:215–228, 1998.

[118] R. Sharp. Variable geometry active rear suspension for motorcycles. In *Proceedings of the* 5^{th} *International Symposium on Advanced Vehicle Control*, pages 389–395, University of Michigan, Michigan, U.S.A., 2000.

[119] R. Sharp and D. Crolla. Road vehicle suspension system design - a review. *Vehicle System Dynamics*, 16:167–192, 1987.

[120] P. Sinha, D. Wormley, and J. Hedrick. Rail passenger vehicle lateral dynamic performance through active control. *J. Dyn. Sys. Meas. Cont.*, 100:270–283, 1978.

[121] H. Smakman. Functional integration of active suspension with slip control for improved lateral vehicle dynamics. In *Proceedings of the* 5^{th} *International Symposium on Advanced Vehicle Control*, pages 397–404, University of Michigan, Michigan, U.S.A., 2000.

[122] R. Smith and R. Anderson. Characteristics of guided-steering railway trucks. *Vehicle System Dynamics*, 17:1–36, 1988.

[123] J. Sobieszczanki-Sobieski and R. Haftka. Multidisciplinary aerospace design optimization: survey of recent developments. *Structural Optimization*, 14(1):1–23, 1997.

[124] J. Sobieszczanski-Sobieski, J. Kodiyalam, and R. Yang. Optimization of car body for noise, vibration and harshness (nvh) and crash. In *Proceedings of the* 41^{st} *AIAA/ASME/AHS/ASC, Structures, Structural Dynamics, and Materials*, number AIAA–2001–1273, Atlanta, 2000.

[125] Y. Suda. Improvement of high speed stability and curving performance by parameter control of trucks for rail vehicles considering independently rotating wheelsets and unsymmetric structure. *JSME International Journal*, 33(2):176–182, 1990.

[126] S. Suzuki and N. Kawamura. Simultaneous optimization of sailplane design and its flight trajectory. *Journal of Aircraft*, 33:567–571, 1996.

[127] S. Swamy, R. Dukkipati, and M. Osman. Analysis of modified railway passenger truck designs to improve lateral stability/curving behaviour compatibility. In *Proceedings of IMechE*, volume 209, pages 49–59, 1995.

[128] S. Taheri. An investigation of the use of a new non-linear control strategy for integration of active suspension and anti-lock braking systems. *SAE Paper No. 980248*, 1998.

[129] A. Thompson. An active suspension with optimal linear state feedback. *Vehicle System Dynamics*, 5:187–203, 1976.

[130] A. Thompson. Suspension design for optimum road-holding. *SAE Paper No. 830663*, 1983.

[131] A. Thompson and C.Pearce. An optimal suspension for an automobile on a random road. *SAE Paper No. 790478*, 1979.

[132] V. Torczon. On the convergence of pattern search methods. In *Rice University Technical Report TR93–10*, 1993.

[133] H. True. Does a critical speed for a railroad vehicle exist? In K. Hawthorne and R. Hill, editors, *Proceedings of the 1994 ASME/IEE Joint Railroad Conference*, pages 125–131, Chicago, Illinois, 1994.

[134] H. True and J. Jenson. Parameter study of hunting and chaos in railway vehicle dynamics. In *Proceedings of the* 13^{th} *IAVSD Symposium*, pages 508–521, 1993.

[135] H. True and C. Kaas-Petersen. A bifurcation analysis of nonlinear oscillations in railway vehicles. In *Proceedings of the* 8^{th} *IAVSD Symposium*, pages 655–665, Cambridge, MA, U.S.A., 1984.

[136] A'GEM user's manual. R. Anderson Engineering Analysis. Kingston, Canada, 1994.

[137] Y. Watanabe and R. Sharp. Mechanical control design of a variable geometry active suspension system. *Vehicle System Dynamics*, 32:217–235, 1999.

[138] D. Whitley. The genetic algorithm and selection pressure: why rank-based allocation of reproduction trials is best. In J. Schaffer, editor, *Proceedings of the Third International Conference on Genetic Algorithms*, pages 116–121. Morgan Kaufmann Publishers, 1989.

[139] A. Wickens. The dynamic stability of a simplified four-wheeled railway vehicle having profiled wheels. *International Journal of Solids and Structures*, 1:385–406, 1965.

[140] A. Wickens. The dynamic stability of railway vehicle wheelsets and bogies having profiled wheels. *International Journal of Solids and Structures*, 1:319–341, 1965.

[141] A. Wickens. Steering and dynamic stability of railway vehicles. *Vehicle System Dynamics*, 5:15–46, 1975.

[142] A. Wickens. Steering and stability of the bogie: vehicle dynamics and suspension design. In *Proceedings of IMechE Conference*, volume 205, pages 109–122, 1991.

[143] D. Wilson, R. Sharp, and S. Hussan. Application of linear optimal control theory to the design of automobile suspensions. *Vehicle System Dynamics*, 15:103–118, 1986.

[144] J. Wong and K. Goheen. Review of the state-of-the-art and applications of active suspensions to rail vehicles. *Vehicle Systems Development Corporation, Nepean, Ontario*, 1991.

[145] R. Yang, L. Gu, C. Tho, and J. Sobieski. Multidisciplinary design optimization of a full vehicle with high performance computing. In *Proceedings of the* 42^{nd} *AIAA/ASME/AHS/ASC, Structures, Structural Dynamics, and Materials*, number AIAA–2001–1273, Seattle, Washington, 2001.

[146] R. Yang, L. Tseng, L. Nagy, and J. Cheng. Feasibility study of crash optimization. *ASME, Journal of Mechanical Design*, 69–2:549–556, 1994.

[147] T. Yoshimura, K. Nakaminami, M. Kurimoto, and J. Hino. Active suspension of passenger cars using linear and fuzzy-logic controls. *Control Engineering Practice*, 7:41–48, 1999.

[148] Z. Yu. *Theory of Automobiles*. Publishing House of the Mechanical Industry, Beijing, China, (in Chinese), 1989.